UNIVERSITY OF CALIFORNIA
SANTA CRUZ

HYDROGENETIC FERROMANGANESE CRUSTS OF THE CALIFORNIA CONTINENTAL MARGIN

A dissertation submitted in partial satisfaction
of the requirements of the degree of

DOCTOR OF PHILOSOPHY

in

EARTH SCIENCES

by

Tracey A. Conrad

June 2017

This dissertation of Tracey A. Conrad
is approved:

_____
Professor James C. Zachos, Chair

_____
Professor Quentin Williams

_____
Adina Paytan, Ph.D. (UCSC)

_____
James R. Hein, Ph.D. (USGS)

_____
Tyrus Miller
Vice Provost and Dean of Graduate Studies

TABLE OF CONTENTS

Supplemental Files

LIST OF FIGURES AND TABLES

ABSTRACT

Hydrogenetic Ferromanganese Crusts of the California Continental Margin

Tracey A. Conrad

Hydrogenetic Ferromanganese (Fe-Mn) crusts grow from seawater and in doing so sequester elements of economic interest and serve as archives of past seawater chemistry. Ferromanganese crusts have been extensively studied in open-ocean environments. However, few studies have examined continent-proximal Fe-Mn crusts especially from the northeast Pacific. This thesis addresses Fe-Mn crusts within the northeast Pacific California continental margin (CCM), which is a dynamic geological and oceanographic environment. In the first of three studies, I analyzed the chemical and mineralogical composition of Fe-Mn crusts and show that continental-proximal processes greatly influence the chemistry and mineralogy of CCM Fe-Mn crusts. When compared to global open-ocean Fe-Mn crusts, CCM crusts have higher concentrations of iron, silica, and thorium with lower concentrations of many elements of economic interest including manganese, cobalt, and tellurium, among other elements. The mineralogy of CCM Fe-Mn crusts is also unique with more birnessite and todorokite present than found in open-ocean samples. Unlike open-ocean Fe-Mn crusts, carbonate-fluorapatite is not present in CCM crusts. This lack of phosphatization makes CCM Fe-Mn crusts excellent candidates for robust paleoceanography records. The second and third studies in this thesis use isotope

geochemistry on select CCM Fe-Mn crusts from four seamounts in the CCM to study past terrestrial inputs into the CCM and sources and behavior of Pb and Nd isotopes over the past 7 million years along the northeast Pacific margin. The second study focuses on riverine inputs into the Monterey Submarine Canyon System and sources of the continental material. Osmium isotopes in the crusts are compared to the Cenozoic Os seawater curve to develop an age model for the samples that show the crusts range in age of initiation of crust growth from approximately 20 to 6 Myr. Lead and neodymium isotopes measured in select Fe-Mn crusts show that large amounts of terrestrial material entered the CCM via the Monterey Canyon from prior to 6.8±0.5 until 4.5 ±0.5 Myr ago. These data combined with reconstructions of the paleo-coastline indicate that incision of the modern Monterey Canyon started around 7 Myr ago. Isotope plots of potential source regions indicate that the source of the material is the border of the southern Sierra Nevada and western Basin and Range. This answers a long-standing and fundamental question about the timing and formation of the Monterey Canyon, the dominant feature of the Monterey Bay. The third study presented here uses the differences in lead and neodymium isotopic values in CCM Fe-Mn crusts over time compared to open-ocean Pacific, North Pacific, and Arctic Ocean Fe-Mn crusts to identify regional time-series trends and sources for these important oceanographic tracers. I found that sediment fluxes and inputs of terrestrial material from North American rivers effects the lead and neodymium isotope composition of regional seawater.

ACKNOWLEDGEMENTS AND DEDICATION

I would like to thank my advisers James R. Hein and Adina Paytan for their support, and encouragement throughout my graduate studies. I am grateful to members of my committee: James Zachos and Quentin Williams for their thoughtful feedback that improved this work. I am grateful to the Pacific Costal and Marine Science Center of the USGS for funding, laboratory space, and support, particularly the Marine Minerals Team. I am also grateful to members of the Woods Hole Oceanographic Institute who provided laboratory space, equipment, a great deal of support, and were extremely generous with their time and expertise. I am grateful to Dustin Winslow for assistance with Python coding that proved integral during the lead isotope analysis.

In dedication to my parents

Sue and Fred Conrad

For their unwavering support and encouragement

INTRODUCTION

This thesis focuses on hydrogenetic ferromanganese (Fe-Mn) crusts from an active continental margin environment along the eastern boundary of the North Pacific Subtropical Gyre, the California continental margin (CCM). Ferromanganese crusts from the CCM are used to study local and regional inputs and processes that characterize the boundary region. Many processes affect the CCM. Upwelling of nutrient-rich water and terrestrial inputs result in high primary productivity in surface waters and lead to a well-developed oxygen minimum zone [Biller and Bruland, 2014]. Redox cycling occurs in sediments on the continental shelf and slope which, releases elements into the water column under low-oxygen conditions. [Biller and Bruland, 2014]. The CCM is also tectonically active with primarily right-lateral strike slip movement dominated by the San Andreas Fault system and to a lesser degree by the Palo-Colorado San Gregorio Fault zone [Amina, et al., 2002]. One of North America's largest submarine canyons, the Monterey Canyon, also occurs in this region within the Monterey Bay National Marine Sanctuary. Despite rivaling the Grand Canyon in scale, the age of formation of the Monterey Canyon is not well constrained.

Hydrogenetic Fe-Mn crusts are found in the global ocean at water depths of 400 to 7000 meters [Hein et al., 2000]. These rocks grow by precipitation and accretion of iron and manganese oxides from seawater onto elevated seafloor rock surfaces where sediment accumulation is not present or is insignificant. The slow

growth rates of Fe-Mn crusts (1 to 5 mm/Myr) high porosity (mean 60%) and extremely high surface area (mean 325 m^2/g) allow for the sorption of many elements from seawater [Hein et al., 2000]. Redox reactions on the surface of the negatively charged manganese oxide and positively charged iron oxyhydroxide minerals result in further enrichment of many elements [Koschinsky and Hein, 2003]. These processes make Fe-Mn crusts important sinks for many elements in the ocean. There is interest, particularly internationally, in Fe-Mn crusts for their potential economic value, as Fe-Mn crusts have high concentrations of heavy rare earth elements, tellurium, and cobalt, among other elements [Hein et al., 2013].

Ferromanganese crusts can also be used as archives for paleo seawater chemistry [Frank, 2002]. Due to the extremely slow growth rates, Fe-Mn crusts are most useful as paleo-archives when studying long-term trends that occur over hundred-thousand to million-year time scales. Ferromanganese crusts have been used as paleoceanographic records to study global ocean circulation, water mass mixing, terrestrial inputs and other sources and sinks of elements in the global ocean [Frank, 2002]. This dissertation focuses on three isotope systems in the Fe-Mn crusts that do not re-equilibrate with seawater once the crust is formed; osmium, lead, and neodymium. Osmium remains in seawater for thousands to around 50 thousand years and is generally well-mixed in the global ocean, but can show isotope variations due to strong regional inputs with very different isotope signatures than seawater [Levasseur et al., 2004; Paquay and Ravizza, 2012]. Lead is scavenged in seawater by sinking particles and in sediments. This scavenging results in its removal from

seawater over 80 to 100 years, which is rapid relative to the ~1000 years it takes for global circulation of seawater to travel from the North Atlantic, where deep water forms, to the northeast Pacific [Frank, 2002].

Neodymium isotopes are currently of great interest in oceanography and have been designated as a "key parameter" of the international GEOTRACES program [van de Flierdt et al., 2016]. Neodymium has a residence time in seawater of 400 to 950 years with isotope values that vary between ocean basins [Frank, 2002]. In the past, neodymium isotopes were used to trace different water masses in seawater [van de Flierdt et al., 2016]. However, additional studies have shown that there are multiple sources of neodymium in the oceans that are poorly constrained. These sources include fluxes from seafloor sediment, exchange along continental margins between terrestrial particles and seawater, submarine groundwater discharge, and river and dust inputs of terrestrial material [van de Flierdt et al., 2016]. Without knowing the neodymium isotopic signature and concentration for all sources and sinks within a region, neodymium cannot be used as a conservative tracer of water mass mixing [van de Flierdt et al., 2016]. Many of the sources of neodymium and lead to seawater are particularly important in a near-shore environment, such as the CCM.

The first chapter in this dissertation addresses the chemical and mineralogical composition of the CCM Fe-Mn crusts. It explores how upwelling, high primary productivity in surface waters, the presence of a well-developed oxygen minimum zone and proximity to continental shelf and slope sediments influence the formation

of Fe-Mn crusts. Samples were collected from within the United States 200 nautical mile Exclusive Economic Zone and the potential of these samples as a future economic resource is evaluated. This provides essential information to inform policy makers and regulations. The paleoceanographic potential of these Fe-Mn crusts are also assessed and a select group of these samples are used for additional work in later chapters. This chapter provides an extensive dataset of Fe-Mn crust chemistry and mineralogy for a large number of Fe-Mn crusts from sixteen seamounts across the CCM, a region that has not previously been well studied. Further, it shows that existing data from the Pacific Ocean cannot be unequivocally extrapolated or inferred for the study region or for other similar continental-margin sites. These data significantly add to our knowledge of how near-shore processes in a region of high biological productivity, effect long-term seawater chemistry and ultimately the formation of Fe-Mn crusts.

The second and third studies use CCM Fe-Mn crusts as paleoceanographic archives by analyzing the osmium, neodymium, and lead isotopes recorded in the samples. The second chapter in this thesis focuses on constraining the initiation of Monterey Canyon incision and identifying the continental sources of inputs during canyon incision. Ferromanganese crusts from near the base of the Monterey Canyon Submarine Fan and farther off shore were selected based on analyses from Chapter 1. Osmium measurements from select CCM Fe-Mn crusts are used to create an age model which is then applied to high-resolution neodymium and lead isotope records

and used to study local inputs that markedly affect seawater chemistry recorded in Fe-Mn crusts closest to the base of the Monterey Canyon.

In the third study, lead and neodymium isotopes from the northeast Pacific are put in a regional and global context through comparison of time-series data from around the North Pacific and Arctic oceans. This study focuses on the behavior of neodymium and lead in the northeast Pacific margin over the past 7 Myr. Fluvial input from North American rivers is shown to be an important source of lead over the past 6 Myr. This study also improves our understanding of neodymium sources within the marine environment by showing the importance of sediment pore-water flux as a long-term source of neodymium to bottom and intermediate waters, which are recorded in the Fe-Mn crusts. Chapter 3 also shows that river input transporting old continental material from the interior of western North America into the northeastern Pacific is a significant source of unradiogenic neodymium that has affected the neodymium isotopic composition of seawater in the northeast Pacific and parts of the central Pacific over the past 3 Myr. The comparison presented in this section helps to improve our understanding of neodymium sources into the North Pacific and suggests an unradiogenic neodymium end member that was not identified in previous studies that focused on the central Pacific.

Each chapter in this thesis contributes to our understanding of the processes that effect the northeast Pacific CCM with applications for other near-shore regions of the global ocean. Each of these studies explores unique research questions that are

connected in terms of the study region and type of samples used to further our understanding of continental-margin processes.

References

Amina, R. J., Eitreim, S. L., Edwards, B. D., and Stevenson, A. J. (2002), Nearshore morphology and late Quaternary geologic framework of the northern Monterey Bay Marine Sanctuary, California, *Mar. Geol.*, *181*.

Biller, D. V., and K. W. Bruland (2014), The central California Current transition zone: A broad region exhibiting evidence for iron limitation, *Prog. Oceanogr.*, *120*, 370–382, doi:10.1016/j.pocean.2013.11.002.

van de Flierdt, T., A. M. Griffiths, M. Lambelet, S. H. Little, T. Stichel, and D. J. Wilson (2016), Neodymium in the oceans: a global database, a regional comparison and implications for palaeoceanographic research, *Phil Trans R Soc A*, *374*(2081), 20150293, doi:10.1098/rsta.2015.0293.

Frank, M. (2002), Radiogenic Isotopes: Tracers of Past Ocean Circulation and Erosional Input, *Rev. Geophys.*, *40*(1), 1–1, doi:10.1029/2000RG000094.

Hein, J. R., A. Koschinsky, M. Bau, F. T. Manheim, J.-K. Kang, and L. Roberts (2000), Cobalt-rich ferromanganese crusts in the Pacific: Chapter 9, in *Handbook of marine mineral deposits*, pp. 239–279, CRC Press, Boca Raton, Florida.

Hein, J. R., K. Mizell, A. Koschinsky, and T. A. Conrad (2013), Deep-ocean mineral deposits as a source of critical metals for high- and green-technology applications: Comparison with land-based resources, *Ore Geol. Rev.*, *51*, 1–14, doi:10.1016/j.oregeorev.2012.12.001.

Koschinsky, A., and J. R. Hein (2003), Uptake of elements from seawater by ferromanganese crusts: solid-phase associations and seawater speciation, *Mar. Geol.*, *198*(3–4), 331–351, doi:10.1016/S0025-3227(03)00122-1.

Levasseur, S., M. Frank, J. R. Hein, and A. N. Halliday (2004), The global variation in the iron isotope composition of marine hydrogenetic ferromanganese deposits: implications for seawater chemistry?, *Earth Planet. Sci. Lett.*, *224*(1–2), 91–105, doi:10.1016/j.epsl.2004.05.010.

Paquay, F. S., and G. Ravizza (2012), Heterogeneous seawater $^{187}Os/^{188}Os$ during the Late Pleistocene glaciations, *Earth Planet. Sci. Lett.*, *349–350*, 126–138, doi:10.1016/j.epsl.2012.06.051.

Chapter 1. Formation of Fe-Mn crusts within a continental margin environment

Tracey A. Conrad[a]*, James R. Hein[b], Adina Paytan[a], David A. Clague[c]

[a] University California Santa Cruz, 1156 High Street, Santa Cruz, CA 95060, USA

[b] U.S. Geological Survey, PCMSC, 2885 Mission St., Santa Cruz, CA, 95060, USA

[c] Monterey Bay Aquarium Research Institute, 7700 Sandholdt Rd. Moss Landing, CA 95039, USA

*Corresponding Author: Tracey A. Conrad

Available online September 9, 2016; In Press: Conrad, T. A., Hein, J. R., Paytan, A., Clague, D. A. (2017) Formation of Fee-Mn crusts within a continental margin environment, *Ore Geology Reviews*, doi.org/10.1016/j.oregeorev.2016.09.010

=

Ore Geology Reviews 87 (2017) 25–40

Contents lists available at ScienceDirect

Ore Geology Reviews

journal homepage: www.elsevier.com/locate/oregeorev

Formation of Fe-Mn crusts within a continental margin environment

Tracey Conrad [a,*], James R. Hein [b], Adina Paytan [a], David A. Clague [c]

[a] University California Santa Cruz, 1156 High Street, Santa Cruz, CA 95060, USA
[b] U.S. Geological Survey, PCMSC, 2885 Mission St., Santa Cruz, CA 95060, USA
[c] Monterey Bay Aquarium Research Institute, 7700 Sandholdt Rd., Moss Landing, CA 95039, USA

ARTICLE INFO

Article history:
Received 7 April 2016
Accepted 8 September 2016
Available online 9 September 2016

Keywords:
Ferromanganese crusts
Eastern Pacific
California margin
Strategic metals
Marine mineral resources

ABSTRACT

This study examines Fe-Mn crusts that form on seamounts along the California continental-margin (CCM), within the United States 200 nautical mile exclusive economic zone. The study area extends from approximately 30° to 38° North latitudes and from 117° to 126° West longitudes. The area of study is a tectonically active northeast Pacific plate boundary region and is also part of the North Pacific Subtropical Gyre with currents dominated by the California Current System. Upwelling of nutrient-rich water results in high primary productivity that produces a pronounced oxygen minimum zone. Hydrogenetic Fe-Mn crusts forming along the CCM show distinct chemical and mineral compositions compared to open-ocean crusts. On average, CCM crusts contain more Fe relative to Mn than open-ocean Pacific crusts. The continental shelf and slope release both Fe and Mn under low-oxygen conditions. Silica is also enriched relative to Al compared to open-ocean crusts. This is due to the North Pacific silica plume and enrichment of Si along the path of deep-water circulation, resulting in Si enrichment in bottom and intermediate waters of the eastern Pacific.

The CCM Fe-Mn crusts have a higher percentage of birnessite than open-ocean crusts, reflecting lower dissolved seawater oxygen that results from the intense coastal upwelling and proximity to zones of continental slope pore-water anoxia. Carbonate fluorapatite (CFA) is not present and CCM crusts do not show evidence of phosphatization, even in the older sections. The mineralogy indicates a suboxic environment under which birnessite forms, but in which pH is not high enough to facilitate CFA deposition. Growth rates of CCM crusts generally increase with increasing water depth, likely due to deep-water Fe sources mobilized from reduced shelf and slope sediments.

Many elements of economic interest including Mn, Co, Ni, Cu, W, and Te have slightly or significantly lower concentrations in CCM crusts relative to crusts from the Pacific Prime Crust Zone and other open-ocean basins. However, concentrations of total rare earth elements and yttrium average only slightly lower contents and in the future may be a strategic resource for the U.S.

1. Introduction

Hydrogenetic ferromanganese (Fe-Mn) crusts and nodules precipitate from seawater on elevated seafloor features devoid of sediment. Fe-Mn crusts have growth rates typically ranging from 1–5 mm/Myr (75% of analyzed open-ocean samples), with very high mean porosity of 60%, and extremely high mean specific surface area of 325 m^2/g (Hein et al., 2000). Fe-Mn crusts up to 26 cm thick that accumulated over 80 Ma have been found in the central Pacific Ocean (Hein et al., 2000; Hein and Koschinsky, 2014). The main manganese mineral in Fe-Mn crusts is vernadite (δ-MnO_2), which has a negative surface charge in seawater that can sorb positively charged ions from seawater (Koschinsky and Halbach, 1995; Koschinsky and Hein, 2003). The main iron mineral is Fe oxyhydroxide (FeO(OH)) that has a slight positive surface charge in seawater that is conducive to sorption of negatively charged ions and neutral complexes from seawater (Koschinsky and Hein, 2003). These properties of Fe-Mn crusts result in their enrichment in many elements relative to the Earth's crustal abundance (Hein et al., 2000, 2010a; Koschinsky and Hein, 2003). The most notable of these are Te, Co, Mo, Bi, Pt, Nb, W, Zr, and rare earth elements plus yttrium (REY) (Hein et al., 2000; Hein and Koschinsky, 2014).

Much of the research on Fe-Mn crusts has focused on open-ocean crusts from the equatorial Pacific (Hein et al., 2009). Fe-Mn crusts from the Pacific prime crust zone (PCZ) in the north-equatorial Pacific have the greatest economic potential and four exploration contracts

Abbreviations: Fe-Mn, ferromanganese; CCM, California continental margin; EEZ, exclusive economic zone; CCS, California Current System; NPIW, North Pacific Intermediate Water; CFA, carbonate fluorapatite; OMZ, oxygen minimum zone; PCZ, Pacific prime crust zone; CCZ, Clarion Clipperton Zone; PGE, platinum group elements; ppb, parts per billion; ppm, parts per million; REE, rare earth elements; REY, rare earth elements plus yttrium; HREY, heavy REY; CL, confidence level; ROV, remotely operated vehicle; PAAS, post-Archean Australian Shale.

* Corresponding author.
E-mail address: tconrad@ucsc.edu (T. Conrad).

http://dx.doi.org/10.1016/j.oregeorev.2016.09.010
0169-1368/

have been signed through the International Seabed Authority in that region (Hein et al., 2013, 2016). One exploration contract for Fe-Mn crusts from the Rio Grande Rise in the Atlantic Ocean has also been signed. There are fewer detailed studies of Fe-Mn crusts from the Atlantic and Indian Oceans with the exception of the northeast and northwest Atlantic Ocean (Koschinsky and Halbach, 1995; Muiños et al., 2013) and the Indian Ocean Afanasiy-Nikitin seamount complex (Banakar et al., 2007; Rajani et al., 2005) and Ninetyeast Ridge (Hein et al., 2016). Only a few studies have focused solely on continent-proximal Fe-Mn crusts from the east Pacific off southern California and within the Borderland (Hein et al., 2005, 2010a).

The California continental margin (CCM) is subject to relatively large terrestrial inputs, metal fluxes from continental shelf and slope hypoxic sediments, seasonal upwelling, high primary productivity, and a well-developed oxygen minimum zone (OMZ) (Hein et al., 2000). All of these CCM characteristics influence the formation of Fe-Mn crusts. This study looks at Fe-Mn crusts within the 200 nmi U.S. EEZ from central to southern California along the CCM (Fig. 1). Samples were collected on USGS cruises F6-87-NC, F7-87-SC, and MBARI cruises in 2000, 2003, 2004, and 2010 from the following edifices: Adam, Hoss, Ben, Little Joe, San Marcos, San Juan, Rodriguez, Davidson, Guide, Pioneer, Gumdrop, and Taney (A–D) seamounts and Northeast Bank, Patton Escarpment, and Santa Lucia Escarpment. USGS Open File Report 2010-1069 (Hein et al., 2010b), provides sample data from USGS cruise F7-87-SC for six of the fifteen seamounts and includes 64 of the samples encompassed in this study. Four of the five samples from the Santa Lucia Escarpment, USGS cruise F6-87-NC, are presented by Gibbs et al. (1993). Data from crusts collected on MBARI 2003 and 2004 cruises were included in the mean CA margin data presented in Hein et al. (2013) and Hein and Koschinsky (2014). Fe-Mn crust data from the Taney Seamounts, MBARI cruises 2000 and 2010, have not been previously published.

2. Setting

The CCM is a tectonically active area with movement currently dominated by the San Andreas Fault system, a series of right lateral strike-slip faults that separate the Pacific and North American plates. The San

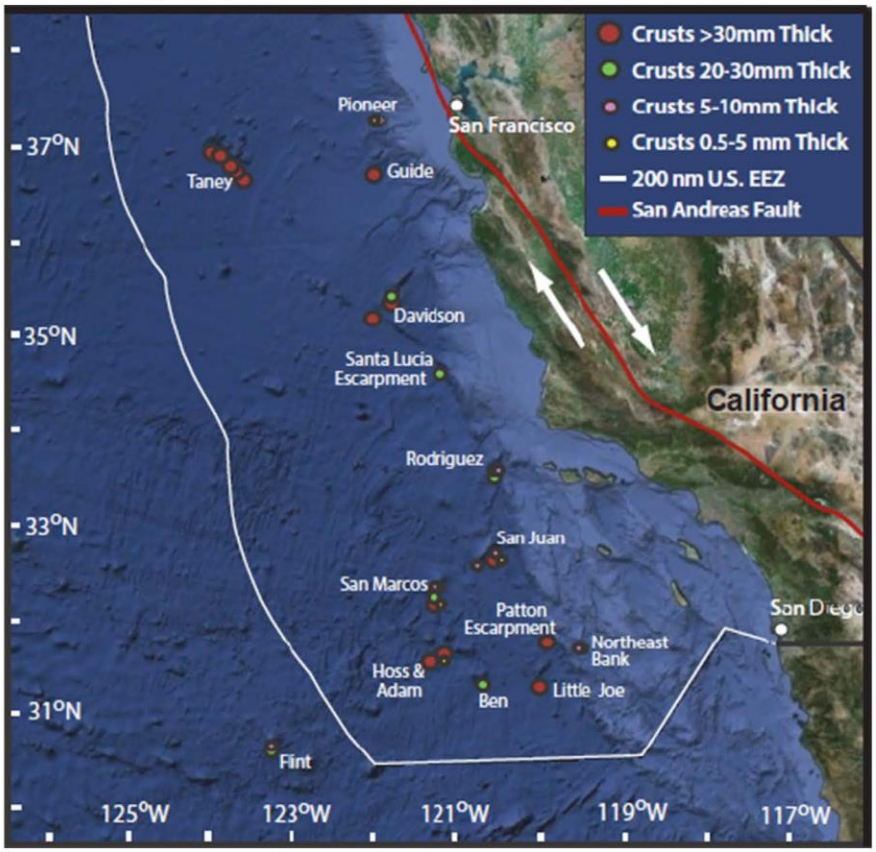

Fig. 1. Map of the sample area with seamounts labeled and mean thicknesses indicated.
(Google Earth 2015, U.S. EEZ from https://maritimeboundaries.noaa.gov/arcgis/rest/services/MaritimeBoundaries/US_Maritime_Limits_Boundaries/MapServer/3, 2/2016).

Andreas is currently moving at a rate of approximately 35 mm/yr (Powell and Weldon, 1992). The total movement northward of the Pacific Plate relative to the North American Plate is approximately 600 km over 20 Ma (Powell and Weldon, 1992). Basin and Range extension began around 17 Ma and continues today. Paleo-tectonic events include the opening of the Gulf of California between 7.7 and 5.8 Ma, and uplift of the Coast Ranges and Sierra Nevada approximately 5 Ma (Holt et al., 2000; Oskin and Stock, 2003). The oceanic crust age for the sampled region ranges from approximately 30 to 20 Ma based on magnetic anomalies (Atwater and Severinghaus, 1989; Cande and Kent, 1995; Davis et al., 2002).

The California Current System (CCS) is the eastern boundary region of the North Pacific Subtropical Gyre and exhibits strong upwelling of cold, nutrient-rich water with upwelling velocities between 10 and 20 m d^{-1} during the spring and summer seasons due to northwesterly winds and Ekman transport (Biller and Bruland, 2013; Carr, 2001; Checkley and Barth, 2009). Increasing element concentrations along the path of deep-water circulation are controlled by biogeochemical cycles and residence times and enrichment from continental margin sediments to the benthic boundary layer. Upwelled water contains high concentrations of macronutrients (nitrate, phosphate, silicic acid) and micronutrients (Fe, Mn, Co, Ni, Cu, Zn, Cd) promoting phytoplankton growth (Biller and Bruland, 2013). The upwelled water is transported off shore and nutrient distributions are affected by mixing, biologic drawdown, and particulate scavenging (Biller and Bruland, 2013).

The dominant water masses along the CCM are the North Pacific Intermediate Water (NPIW) (~300–600 m), Antarctic Intermediate Water mixed with NPIW (~600–1300 m), Pacific Deep Water mixed with Upper Circumpolar Deep Water (~1300–3800 m), and Lower Circumpolar deep Water (below 3800 m) (Conway and John, 2015; Talley, 2008). A pronounced OMZ is present in waters of the CCM, the depth of which varies seasonally but averages ~550–2000 m with oxygen concentrations <75 nmol kg^{-1} (Conway and John, 2015).

Seamounts and escarpments along the CCM are primarily composed of basalt and frequently show pillow structures. Edifice summits range from 516 m (NE Bank) to over 3700 m (Taney D) (Supplemental Table S1). The basement age for the sample region ranges from ~30 to 20 Ma based on magnetic stratigraphy with seamounts ranging in age from ~20 to 7 Ma (Atwater and Severinghaus, 1989; Cande and Kent, 1995; Davis et al., 2002).

The Taney Seamount chain consists of five submarine volcanoes (A through E from north to south) and is 53 km long (Clague et al., 2000; Coumans et al., 2015). Remotely operated vehicle (ROV) and dredge samples collected from Taney Seamounts consist of enriched mid-ocean ridge basalt and slightly alkalic and tholeiitic (Taney A) basalts and have high Al_2O_3 and low SiO_2 contents; with some pillow structures indicating emplacement in a submarine environment (Clague et al., 2000; Coumans et al., 2015). Submarine imaging surveys found little sediment accumulation, making the Taney Seamounts an ideal location for Fe-Mn crust formation (Clague et al., 2000). The Taney Seamount chain has several edifices with very flat tops resulting from caldera collapse and infilling of earlier large calderas, rather than wave erosion from subsidence after subaerial exposure (Clague et al., 2000; Coumans et al., 2015).

Pioneer, Gumdrop, Guide, and Davidson Seamounts are composed of similar rock types, ranging from alkalic basalts to trachyte and have the northeast-southwest orientation that is common in this region (Davis et al., 2002, 2010). These seamounts consist of a series of parallel ridges and aligned cones separated by sediment filled troughs and lack summit craters or calderas (Davis et al., 2002). The most common rocks on all of these seamounts are alkali basalt, hawaiite, and mugearite (Davis et al., 2002). Davidson and Guide Seamounts formed above a fossil spreading center and Davidson is intersected at its southwest end by a fossil transform fault, the Morro Fracture Zone (Clague et al., 2009; Davis et al., 2002, 2010). Davidson Seamount is part of the Monterey Bay National Marine Sanctuary and is considered a pristine habitat for a variety of species including deep sea corals.

Rodriguez, San Juan, and North East Bank all have features consistent with subaerial exposure including graded sand, gravel, and cobble beds (Paduan et al., 2009). They also have volcanic glass with lower sulfur concentrations than found on other CCM seamounts; this is consistent with subaerial degassing of the lava (Paduan et al., 2009). Lavas from the summits of these three seamounts do not have pillow structures or glassy rinds, which also indicate subaerial flows (Paduan et al., 2009). The shallowest pillow structures on Rodriguez, San Juan, and North East Bank were found at 925, 1282, and 560 m below sea level respectively (Paduan et al., 2009). These seamounts are thought to have subsided due to thermal contraction of the oceanic crust from 11 to 7 Ma (Paduan et al., 2009). Based on the modern water depths of the seamount summits and the extent of terrestrial deposits, Paduan et al. (2009) proposed that Rodriguez and San Juan subsided approximately 700 m while North East Bank subsided 500 m since their formation.

The Patton Escarpment is a relict accretionary wedge that lies at the edge of the continental shelf (Marsaglia et al., 2006). It is thought that a trench-ridge-trench triple junction was present at the Patton Escarpment 18 to 16 Ma (Marsaglia et al., 2006). The Santa Lucia Escarpment lies near the intersection of the continental shelf and the Morro Fracture Zone, south-east of Davidson Seamount (Gibbs et al., 1993). Spreading centers were active near the Santa Lucia Escarpment in the early Miocene (Gibbs et al., 1993).

Adam and Hoss Seamounts are small adjacent edifices with Fe-Mn encrustations on most dredge samples recovered. On USGS cruise F7-87-SC, fewer than 15% of samples collected by dredging on San Marcos Seamount were coated with Fe-Mn crusts (Hein et al., 2010b). All of the samples collected from Little Joe had some Fe-Mn encrustation, most of moderate thickness, from 10 to 35 mm, with some crusts up to 65 mm thick (Hein et al., 2010b). Ben Seamount has little sediment cover, but sediment deposits exist next to the north flank (Hein et al., 2010b).

3. Methods

Fe-Mn crust samples were selected for chemical analysis based on location. A range of water depths and sample thicknesses were selected to represent the different sites, if possible. Samples influenced by hydrothermal inputs, identifiable by chemical signatures, were excluded. Hydrogenetic samples are considered to be those with Fe/Mn ratios between 0.5 and 3.0 (Hein et al., 1993). The concentrations of minor elements were also considered in sample selection; samples with Co, Ni, and Cu concentrations multiplied by 10 that are less than 5% are considered to be hydrothermal based on the traditional discrimination ternary diagram (Bonatti et al., 1972; Hein et al., 1993) and excluded from comparisons.

Chemical analyses of major and minor elements in the crusts were performed by SGS Canada analytical laboratory. Analyses of major elements were run using borate-fused disk X-ray florescence as oxides. Minor elements were analyzed by inductively coupled plasma mass spectrometry (ICP-MS) after a 4-acid (HCl, HF, HNO_3, and $HClO_4$) digest, the resulting solution was dried and dissolved in 1 ml aqua regia and diluted to 10 g with 1% HNO_3. Rare earth elements plus yttrium (REY) were analyzed using Li-metaborate fused disk dissolved in weak HNO_3 and analyzed by ICP-MS. Tellurium and Se concentrations were determined following the same 4-acid digest and hydride generation with a modified flow-injection and analyzed using atomic absorption spectroscopy. Analytical precision is 1.5% or better for all elements. Sorbed (hygroscopic) water was measured by heating the sample to 110 °C for one hour and calculating the difference in wet vs dry sample weight to determine the water weight. Samples were measured dry within 10 min of removal from oven. Platinum group elements (PGE) were analyzed by Intertek Genalysis, Australia, using nickel sulfide fire assay and run on an ICP-MS with analytical precision better than 10%. Procedural blanks are less than 1 ppb for Au, Ru, Rh, Pd, Re, and Pt, 0.1 ppb for Ir,

and 3 ppb for Os. Chemical data are water normalized to 0% hygroscopic water (0% H_2O^-) so that minor elements can be more accurately compared. This is consistent with open-ocean data reported previously (Hein and Koschinsky, 2014).

Selected crusts were split into layers based on visually distinct textural or compositional differences. Compositional differences were identified based on color variations reflecting greater Mn (black) or Fe (red-brown) layers. All depths within Fe-Mn crusts are provided in mm from the top of the crust (the surface that was in contact with seawater).

The age and growth rates of Fe-Mn crusts were calculated using the cobalt chronometer, an empirically derived formula where growth rate $(GR) = 0.68 / (Co^n)^{1.67}$, $Co^n = Co \times (50 / Fe + Mn)$, with metals in wt.% (Manheim and Lane-Bostwick, 1988). The growth rate model assumes a constant flux of Co into the crusts of at least one order of magnitude over the growth rate (Halbach et al., 1983). This formula does not account for growth hiatuses, erosional or dissolution events, and is considered a minimum age estimate (Klemm et al., 2005). It is also not possible to exclude changes in growth rate within a bulk sample or on a scale finer than the chemically analyzed layers.

Mineralogical compositions were determined by X-ray diffraction (XRD) using a Philips diffractometer with Cu Kα radiation and a graphite monochromator. PANalytical software packages and inorganic minerals data base were used to interpret the XRD spectra.

Plots of REY were normalized to Post-Archean Australian Shale (PAAS) values (Bau, 1996; Bau et al., 2014; McLennan, 1989). Discrimination plots used PAAS normalized REY data with $Ce_{sn}^* = 0.5La_{sn} + 0.5Pr_{sn}$ or if Pr data were unavailable $Ce^* = 0.67La + 0.33Nd$; plots are Ce_{sn}/Ce_{sn}^* vs Nd and Ce_{sn}/Ce_{sn}^* vs Y_{sn}/Ho_{sn} (Bau et al., 2014) to further confirm that the samples used for comparison are hydrogenetic. This plot did not exclude any additional samples.

The Pearson product correlation coefficient was used to calculate correlation coefficient matrices for the chemical data. The presented matrix included 141 bulk and 17 mean bulk crust samples, collected by ROV on MBARI cruises for which exact location and water depths are known (Supplemental Table S2). Mean bulk samples are the weighted percent averages of two to five continuous layers collected through a crust. The 158 samples used for the correlation matrix were also used in a Q-mode factor analysis to determine groupings of elements (Hein et al., 2012; Klovan and Imbrie, 1971). Q-mode factor analysis calculations were run in MatLab (Pisias et al., 2013). These groupings (factors) are interpreted so that each factor represents a particular mineral or mineral group in which elements associated with the factor are contained. This interpretation uses the mineralogy data and element correlations linking the mineralogy related to environmental conditions to element concentrations that represent sources.

4. Results

4.1. Samples

Samples from USGS cruises F7-87-SC and F6-87-NC were collected by chain-bag dredge and have only approximate water depths based on the length of the dredge line, tensiometer readings, and wire angle. Samples collected on MBARI cruises were obtained by ROV and have precise water depths and locations. Samples collected on the MBARI 2003, 2004, and 2010 cruises have accompanying seawater data, such as oxygen probe measurements. Unpublished water-normalized bulk and mean bulk crust data used in this study are presented in Supplemental Table S3 and statistics of the data by seamount are presented in Supplemental Table S4.

Over the entire study area, water depths of samples ranged from 570.5 m (Patton Escarpment) to 3934 m (Taney D). Water depth ranges on individual seamounts are much more limited (Supplemental Table S1). A wide range of crust thicknesses was observed ranging from a very thin <0.1 mm patina to 84 mm. Surface textures are variable and include large botryoids, microbotryoids, granular to micro-granular (dendritic), with abraded and polished areas on some of the crust surfaces. The microbotryoidal to granular surface texture was the most common. Thick CCM Fe-Mn crusts can be massive, laminar, columnar, or botryoidal laminar. Some of the thick crusts contain visually distinct layers while others do not. Thin dendritic layers also occur in some of the crust samples. Detrital grains generally from fine silt to course sand size, including some embedded cobbles are present in some of the CCM Fe-Mn crust samples, particularly those close to shore. Many of the Fe-Mn crusts had encrusted worm tubes on their upper surface with a few also having sea sponge encrustations. A few hydrogenetic seamount nodules were also found on Santa Lucia Escarpment and Adam seamount.

4.2. Mineralogy

XRD analysis of CCM Fe-Mn crusts show δ-MnO_2 to be the dominant mineral along with an X-ray amorphous FeO(OH) which crystallized to goethite in about 9% of the crusts (Supplemental Table S7; Hein et al., 2010b). While δ-MnO_2 is common in open-ocean crusts, goethite is less common and has been recorded in the oldest sections of only 6% of open-ocean Pacific crusts (Hein et al., 2000). Todorokite is present in approximately 35% of CCM Fe-Mn crusts and is slightly more common in the southern section of the sample region. Birnessite is present in approximately 5% of CCM samples; this is significant as todorokite and birnessite occur in less than 2% of open-ocean crusts if all CCM crust are excluded (Hein et al., 2000, 2010b). Detrital quartz, plagioclase, and K-feldspar are common minor minerals, and phillipsite, smectite, and illite are present in some samples. Some CCM crust samples, particularly those with very high Ba, contain minor barite. Carbonate-fluorapatite (CFA) was not detected in the CCM crusts (Supplemental Table S7; Hein et al., 2010b).

4.3. Chemistry

One hundred and fifty-five bulk Fe-Mn crust samples and 22 mean bulk samples (compiled as weighted averages from layer data) were analyzed for major and minor elements and REY (Supplemental Table S3). Layers with 2–4 subsamples per curst were also analyzed for 32 Fe-Mn crusts totaling 74 subsamples (Supplemental Table S5). Surface scrapes of the upper 0.5 to 1 mm were analyzed for an additional 63 samples (Supplemental Table S6). When a bulk crust has a thickness of 1 mm or less it was reported in the bulk data table and not in the surface scrape table. In crusts where a surface scrape was used for the upper layer of a sample, that subsample is recorded in both the layer and the surface scrape data tables with a note added in the layer table; this occurs for 6 crusts. The new bulk and mean bulk data were added to the published data from Hein et al. (2010a,b) and Gibbs et al. (1993) to calculate the CCM mean for comparison to open-ocean samples (Table 1) and to determine statistics for each seamount (Supplemental Table S4). All data are presented on a hygroscopic water-free basis (0% H_2O^-).

4.4. Comparison to open-ocean Fe-Mn crust chemistry

When comparing bulk and mean bulk CCM Fe-Mn crusts to open-ocean crusts, Si is enriched in CCM crusts with an average concentration of 10.8% (n = 225) compared to 5.21% (n = 43), 6.82% (n = 23), and 4.05% (n = 303) for Atlantic Ocean, Indian Ocean, and PCZ crusts, respectively (Table 1). The Si/Al ratio is also higher for CCM Fe-Mn crusts (6.18) than in Fe-Mn crust samples from open-ocean locations; the PCZ has the second highest Si/Al ratio (4.00). Elements typically hosted in the aluminosilicate phase of crusts, K and Na are also higher in CCM Fe-Mn crusts (0.85%, 1.97%, respectively, n = 225) compared to PCZ crusts, 0.55% and 1.64%, respectively (n = 303). The Indian Ocean crusts average 0.63% K (n = 23). The mean K and Na concentrations in CCM

Table 1
Compiled mean composition of Fe-Mn crusts and nodules from the global ocean modified from Hein et al. (2000) and Hein and Koschinsky (2014); CCM updated with data presented in this paper.

	Atlantic Ocean		Indian Ocean		Prime Crust Zone		South Pacific Ocean		CA margin		CCZ nodules	
Element	Mean	N	Mean	N	Mean	N	Mean	N	Mean	N	Mean	N
Fe (wt.%)	20.9	43	22.3	23	16.9	362	18.1	286	23.8	225	6.16	66
Mn	14.5	43	17.0	23	22.8	362	21.7	321	19.5	225	28.4	66
Fe/Mn	1.44	43	1.31	23	0.74	362	0.83	286	1.33	225	–	0
Si	5.21	43	6.82	23	4.05	303	4.75	255	10.8	225	6.55	12
Al	2.20	43	1.83	23	1.01	351	1.28	241	1.79	225	2.36	65
Si/Al	2.37	43	3.73	23	4.00	303	3.72	241	6.18	225	–	0
Mg	1.58	43	1.25	23	1.10	328	1.32	192	1.26	225	1.89	66
Ca	4.03	43	2.27	23	4.03	328	3.53	256	2.25	225	1.70	66
Na	1.26	43	1.55	23	1.64	303	1.52	88	1.97	225	1.99	66
K	0.54	43	0.63	23	0.55	303	0.63	156	0.85	225	0.99	66
Ti	0.92	43	0.88	23	1.16	345	1.12	230	0.67	225	0.32	66
P	0.75	43	0.38	23	0.96	328	0.78	265	0.57	225	0.21	66
Cl	>0.74	31	>1.00	19	0.92	43	>1.08	40	0.74	14	0.27	12
LOI	26.0	43	26.6	23	32.0	185	18.5	55	16.4	172	26.5	12
H_2O^-	10.6	43	14.1	23	19.5	303	19.8	53	18.3	224	11.6	12
H_2O^+	–	0	–	0	7.99	263	10.2	7	–	0	8.80	7
CO_2	–	0	–	0	0.74	263	0.83	7	–	0	–	0
S_T	0.25	31	0.15	9	0.26	43	0.12	40	0.01	40	0.17	12
Ag (ppm)	0.20	18	0.37	9	–	0	0.97	13	0.90	169	0.17	12
As	308	42	207	19	393	328	287	84	257	225	67	12
B (ppm)	257	13	287	10	178	43	197	40	235	13	–	0
Ba	1556	43	1533	23	1934	328	1705	143	1838	225	3500	66
Be	8.98	43	6.93	23	6.07	43	5.38	59	3.99	181	1.9	12
Bi	19.3	38	30.2	22	42.9	34	22.4	46	16.2	182	8.8	12
Br	36.5	10	54.0	6	28.1	34	29.5	72	34.3	14	–	–
Cd	4.07	34	3.47	18	3.59	285	4.14	62	3.70	223	16	12
Co	3608	43	3291	23	6662	362	6167	321	3131	223	2098	66
Cr	46.8	40	22.3	18	27.9	272	35.0	79	51.9	225	17	12
Cs	–	0	5.00	1	3.71	1	1.90	18	0.66	155	1.5	61
Cu	861	43	1105	23	976	362	1082	321	383	223	10714	66
Ga	15.5	39	16.2	23	18.8	33	28.5	27	18.2	97	36	12
Ge	0.66	18	0.64	9	0.0	0	2.40	11	0.87	149	–	0
Hf	8.71	30	9.78	15	9.43	43	9.15	81	6.12	184	4.7	66
In	0.18	19	0.26	10	0.62	1	0.87	6	0.14	170	0.27	12
Li	33.1	42	8.34	22	2.92	33	3.46	36	16.6	33	131	66
Mo	409	43	392	23	461	328	418	67	385	223	590	66
Nb (ppm)	50.9	43	61.3	23	51.6	43	59.2	46	31.5	184	22	66
Ni	2581	43	2563	23	4209	362	4643	321	2269	223	13002	66
Pb	1238	43	1371	23	1641	326	1057	113	1565	223	338	66
Rb	15.0	24	15.8	17	17.0	12	10.6	27	14.6	184	23	66
Sb	51.1	30	39.9	15	39.3	43	35.4	73	36.9	184	41	12
Sc	16.4	43	12.5	23	6.55	43	9.29	82	9.36	182	11	66
Se	0.44	10	1.73	10	14.8	1	5.06	14	2.00	175	0.72	12
Sn	8.34	28	9.68	17	10.0	10	10.91	34	4.27	171	5.3	12
Sr	1262	43	1201	23	1510	303	1483	67	1302	202	645	66
Ta	1.34	17	0.91	10	2.36	2	1.23	47	0.59	176	0.33	66
Te	43	37	31	22	60	43	38	38	13	184	3.6	66
Tl	104	38	95.4	22	155	34	154	46	49	182	199	12
Th	52	42	56	18	11	40	15	67	48	177	15	66
U	10.9	35	10.3	18	12.4	38	12.0	67	11.7	177	4.2	66
V	849	43	634	23	641	328	660	177	628	223	445	66
W	79	35	80	18	89	36	97	56	66	184	62	66
Y	181	43	178	23	221	294	177	49	172	223	96	66
Zn	614	43	531	23	668	325	698	181	554	223	1366	66
Zr	362	38	535	22	548	43	754	46	464	184	307	66
La	272	42	290	21	339	83	204	75	270	187	114	66
Ce	1392	42	1469	21	1322	83	818	75	1264	223	284	66
Pr	63.8	20	66.2	12	61.3	83	40.8	31	60.3	187	33.4	66
Nd	243	42	259	21	258	83	184	67	253	187	140	66
Sm	55.5	20	60.8	12	51.5	83	38.1	67	53.5	187	34	66
Eu	11.5	42	12.5	21	12.5	83	17.5	75	12.7	187	8.03	66
Gd	57.9	20	67.2	12	56.2	83	43.9	31	55.5	187	31.8	66
Tb	9.17	20	9.99	12	8.79	82	5.98	53	8.92	187	4.98	66
Dy	47.1	20	55.6	12	60.0	83	40.7	30	49.6	187	28.5	66
Ho	9.61	41	10.6	13	10.9	82	8.45	17	10.0	187	5.35	66
Er	28.0	20	29.3	12	31.0	83	26.5	31	27.9	187	14.6	66
Tm	3.91	20	4.03	12	4.55	82	3.6	17	3.9	187	2.11	66
Yb	23.9	42	24.8	21	28.5	83	21.9	75	25.3	187	13.7	66
Lu	3.74	20	4.05	12	4.29	40	3.33	75	3.81	186	2.05	66
Au (ppb)	5.99	2	20.7	2	99.7	7	33.1	38	7.8	17	4.5	9
Hg	85.9	37	37.8	18	9.28	12	31.8	33	11.4	161	18	3

(continued on next page)

Table 1 (*continued*)

Element	Atlantic Ocean		Indian Ocean		Prime Crust Zone		South Pacific Ocean		CA margin		CCZ nodules	
	Mean	N	Mean	N	Mean	N	Mean	N	Mean	N	Mean	N
Ir	4.8	2	6.8	5	13	56	2.5	3	1.8	9	2	11
Os	2.4	1	4.0	3	2.4	4	2.5	1	3.5	11	–	0
Pd	6.0	2	15	6	3.8	54	7.0	14	4.1	28	8	12
Pt	567	2	211	6	470	60	465	15	70	30	128	12
Rh	37	2	20	6	23	59	33	15	6	29	9	12
Ru	18	2	20	6	17	58	13	6	9	15	12	12

Fe-Mn crusts approximate those of the Clarion Clipperton Zone (CCZ) nodules at 0.99 (n = 66) and 1.99% (n = 66), respectively. Rubidium is also hosted in the aluminosilicate minerals but has a slightly lower concentration in CCM crusts with a mean of 14.6 ppm (n = 184) compared to 15.0 ppm (n = 24), 15.8 ppm (n = 17), 17.0 ppm (n = 12) for the Atlantic Ocean, Indian Ocean, PCZ respectively.

Iron is enriched in CCM Fe-Mn crusts relative to open-ocean samples with a mean concentration of 23.8% (n = 225), which is 1.5% (n = 23) greater than Indian Ocean crusts which have the second highest concentration and 6.9% (n = 362) more than PCZ crusts which have the lowest mean concentration. Iron enrichment is also apparent in the ternary diagram where the plotted bulk CCM data trend towards Fe from the hydrogenetic field defined by open-ocean Fe-Mn crust samples (Fig. 2). The mean Mn concentration in CCM Fe-Mn crusts 19.5% (n = 225) is slightly lower than in crusts from the PCZ 22.8% (n = 362) and S. Pacific 21.7% (n = 321), and slightly higher than in crusts from the Atlantic 14.5 (n = 43) and Indian 17.0 (n = 23) Oceans. The mean Fe/Mn ratio is higher in CCM crusts 1.33 (n = 225) than in the PCZ 0.74 (n = 362) and S. Pacific 0.83 (n = 286), and is more comparable to the Fe/Mn ratios of the Atlantic and Indian Ocean crusts, 1.44 (n = 43) and 1.31 (n = 23), respectively (Hein and Koschinsky, 2014).

Thorium has a higher mean concentration in CCM crusts 48 ppm (n = 177) than in PCZ or S. Pacific Fe-Mn crusts which have concentrations of 11 ppm (n = 40) and 15 ppm (n = 67) respectively. Like Fe, the mean Th concentration in CCM Fe-Mn crusts is more comparable to the Indian and Atlantic Fe-Mn crust means, 56 ppm (n = 18) and 52 ppm (n = 42) respectively. Chromium is enriched in CCM Fe-Mn crusts 52 ppm (n = 225) compared to open-ocean samples: 47 (n = 40), 22 ppm (n = 18), 28 ppm (n = 272) for the Atlantic, Indian, and PCZ, respectively.

Other elements of potential economic interest in Fe-Mn crusts including Te, Co, Cu, Mo, Ni, W, and Pt, all have a lower mean concentration in CCM Fe-Mn crusts than in open-ocean Fe-Mn crusts from all of the other study regions. Tellurium has a significantly lower mean concentration of 13 ppm (n = 184) in CCM crusts while the Atlantic Ocean, Indian Ocean, PCZ, and S. Pacific have mean concentrations of 43 ppm (n = 37), 31 ppm (n = 22), 60 ppm (n = 43), 38 ppm (n = 38), respectively. Cobalt has a mean concentration of 3131 ppm (n = 223) in CCM crusts with the second lowest mean concentration occurring in Indian Ocean crusts, 3291 ppm (n = 23), while the PCZ has the highest, 6662 ppm (n = 362). Copper in CCM Fe-Mn crusts has a mean of 383 ppm (n = 223) with the next lowest in Atlantic Ocean crusts, 861 ppm (n = 43) and the highest in Indian Ocean crusts 1105 (n = 23). Platinum has significantly lower mean concentrations in CCM crusts, 70 ppb (n = 30), with 567 (n = 2), 211 (n = 6), 470 (n = 60), and 465 (n = 15) for the Atlantic Ocean, Indian Ocean, PCZ, and S. Pacific crusts, respectively.

4.5. Rare-earth elements in CCM Fe-Mn crusts

Hydrogenetic Fe-Mn crusts from the CCM have concentrations of REY comparable to open-ocean Fe-Mn crusts for both light (La, Ce, Pr, Nd, Sm) and heavy (Eu, Gd, Tb, Dy, Y, Ho, Er, Tm, Yb, Lu) REY. Plots of

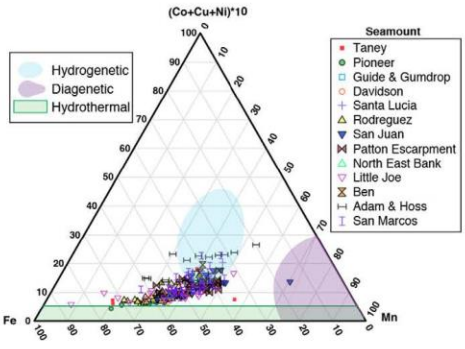

Fig. 2. Ternary diagram showing the criteria for exclusion of crust samples with samples plotted by seamount. The bottom, outlined region demarcates the hydrothermal region, the shaded Mn corner is the diagenetic field, and the light oval is the open-ocean hydrogenetic crust field (n = 300). California continental crusts trend from the hydrogenetic region towards Fe enrichment (Bonatti et al., 1972; Hein et al., 1993).

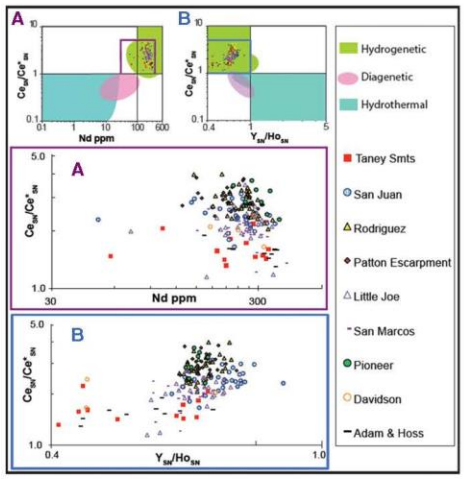

Fig. 3. Rare earth element discrimination plots after Bau et al. (2014). California continental margin Fe-Mn crusts plot in the hydrogenetic field.

the CCM Fe-Mn crust REY data normalized to PAAS are consistent with typical hydrogenetic Fe-Mn crust plots (Bau et al., 2014; McLennan, 1989). This characteristic hydrogenetic pattern shows a large positive Ce and negative Y anomaly with some samples showing smaller positive anomalies for Eu, La, and Gd (Bau et al., 2014). The REY pattern can be used to differentiate between hydrothermal Mn deposits, diagenetic Fe-Mn nodules, hydrogenetic Fe-Mn nodules and crusts (Bau et al., 2014). Patterns from 191 CCM Fe-Mn crust samples with REY data are generally consistent with hydrogenetic Fe-Mn crust profiles, with one sample each from Little Joe (T668-R13A) and San Juan Seamounts (T665-R17A) less REY enriched relative to PAAS, consistent with diagenetic Fe-Mn nodules (Bau et al., 2014; Taylor and McLennan, 1985) (Supplemental Fig. S1). San Juan Fe-Mn crust sample (T665-R17A) also plots in the diagenetic region of the ternary discrimination diagram. Those samples might have a diagenetic influence from a localized seamount sediment deposit. Hydrothermal Mn samples would also be less REY enriched relative to PAAS than typical crusts, but would have a very different profile with a negative Ce anomaly and positive Y anomaly (Bau et al., 2014), which are not observed in these two samples. The CCM Fe-Mn crusts also plot in the hydrogenetic region on PAAS normalized Ce/Ce* vs Nd (ppm) and Ce/Ce* vs Y/Ho REY discrimination plots (Bau et al., 2014) (Fig. 3).

4.6. Comparison within the CCM

Santa Lucia Escarpment Fe-Mn crusts have the highest mean Si concentration 13.9% (n = 5) and Davidson Seamount crusts have the highest mean Al concentration 2.36% (n = 3). Fe-Mn crusts from Ben Seamount have the lowest mean Si and Al concentrations at 6.41% and 1.11% respectively (n = 6) (Supplemental Table S4). The Fe-Mn crust with the highest Fe concentration is T627-R7 from the Pioneer Seamount with 33.2%. Pioneer Seamount also has the highest mean Fe concentration out of the CCM seamounts at 30.2% (n = 6). The lowest mean Fe and Mn concentrations are found on the Santa Lucia Escarpment at 16.5% and 13.7% (n = 5), respectively (Supplemental Table S4). The highest mean Mn concentration is from the Patton Escarpment at 25.1% (n = 24). The crust with the lowest Fe and Mn concentration is D6-1A from San Marcos Seamount with concentrations of 10.3% and 4.40%; that crust also has the highest Si and Al concentrations out of all CCM Fe-Mn crust samples at 25.0% and 4.89%, respectively.

Element concentrations in Fe-Mn crusts from seamounts in the northern sector of the study region, Pioneer (near shore, n = 11) and Taney Seamount Chain (off shore, n = 14) were compared to seamounts from the southern end of the study region; North East Bank and Patton Escarpment (near shore, n = 24) and Adam and Hoss Seamounts (off shore, n = 25) (Fig. 1). The near shore samples have higher Fe concentrations although the trend is slightly less apparent in crusts from the southern seamounts. When comparing the near shore samples, the northern crusts from Pioneer Seamount have higher Fe concentrations than all but three of the southern samples. There is no distinct difference in Mn, Si, Al, or K concentrations between near shore and off shore or northern and southern Fe-Mn crusts. Both P and Pb show higher concentrations in near shore crusts with slightly more overlap in Pb concentrations in the southern samples (Supplemental Table S4). Thorium also shows higher concentrations in near shore crusts for the northern sample region; there is insufficient data for southern off shore samples to make a determination. Copper shows the opposite trend with near shore data clustering below 400 ppm while the off shore data ranges up to 2088 ppm; only six of the off shore crusts have concentrations below 400 ppm.

Barium concentrations show no noticeable differences with latitude for off-shore or near-shore crusts. Off-shore Fe-Mn crust samples show a wide range of Ba from 1183 to 24323 ppm. The highest concentration of 24323 ppm (D10-4A) is an outlier with the next highest concentration at 9458 (D10-6) and the third highest is 6780 (D11-11A) all from Hoss Seamount (Hein et al., 2010b). The highest Ba concentrations measured in crusts from Taney and Adam seamounts are 6367 and 5536 ppm, respectively (Supplemental Table S4). While the lowest Ba concentrations measured in crusts from off shore seamounts are 1715, 1235, and 1183 ppm for Hoss, Adam, and Taney Seamounts, respectively. The near shore samples have a narrower range of concentrations with the highest Ba concentration of 5211 ppm on the Patton Escarpment and 1299 ppm from North East Bank and lowest concentrations on those edifices of 920 ppm and 993 ppm, respectively.

Layer and surface scrape data were used to evaluate older layers from the northern seamounts compared to the youngest layers of the southern seamounts to determine if element concentrations in Fe-Mn crusts have changed as the Pacific Plate moved northward relative to the North American Plate. Off shore seamounts Taney, San Marcos, Adam, and Hoss and near shore edifices Santa Lucia Escarpment, Rodriguez Seamount, Patton Escarpment, and Little Joe Seamount were evaluated as two separate groups. Neither group showed obvious trends for Fe, Mn, Si, Al, or P. The limited number of older layer samples from the northern edifices Taney (n = 4) and Santa Lucia Escarpment (n = 5) did not provide sufficient data for robust analysis (Supplemental Table S5).

4.7. Element correlations and associations in CCM crusts

A Pearson's product correlation coefficient matrix was used to evaluate element trends in 158 bulk Fe-Mn crust samples with known water depth, latitude and longitude, and dissolved oxygen and temperature measurements at the time of collection. The most interesting statistically significant (at the 99% confidence level (CL), p = 0.01) positive correlations are: Fe: Ag, Be, Nb, Pb, Ta, Th, Zr, and all REE; Mn: Mg, Ba, Cd, Co, Cu, Ni, W, Zn, and Te; both Fe and Mn: Ca, P, Ti, Bi, U, V, and HREE not including Eu and Gd; Si and Al both correlate with Na, K, Cr, Rb, and Sc; Si also correlates with Hf while Al correlates with Zr (Supplemental Table S2). A separate correlation coefficient matrix of 160 samples shows similar correlations and included distance from the coast, age, and growth rate. Iron increases towards shore and with decreasing water depth, while Mn only increases with decreasing water depth. Phosphorus, As, Cr, Pb, V, and Ce contents also increase towards shore. In addition to Fe and Mn, Ca, Mg, P, As, Bi, Co, Cr, Mo, Pb, Te, U, V, W, and Ce contents increase with decreasing water depth. Copper contents show the opposite trend, increasing in deeper water.

Manganese in the CCM Fe-Mn crusts shows a negative correlation with latitude at the 99% CL for both the entire data set and when evaluating only near-shore samples. Many of the elements enriched in CCM Fe-Mn crusts relative to open-ocean Pacific Fe-Mn crusts including Si, Na, K, Th, and Cr have a negative correlation with Mn at the 99% CL (Supplemental Table S2). Elements with a strong positive correlation with Mn including Ni, Te, Co, Ti, Cd, Cu, Mo, Ca, and Tl have lower mean concentrations in CCM Fe-Mn crusts than Central Pacific crusts (Supplemental Table S2 and Table 1). Element correlations with Fe are less likely to predict element enrichment or depletion in CCM crusts relative to open-ocean samples. This is likely due to the distribution of Fe in all of the major Fe-Mn crust phases.

Q-mode statistical analysis was run for three factors on the same data set, which accounted for 95.2% of variance. The three factors are interpreted to be hydrogenetic Mn; detrital Si, K, Al and Fe; and more reduced Mn phases. The third factor is thought to be birnessite- and todorokite-hosted Mn due to the high correlation coefficients with Cu, Ni, and Zn but that does not completely account for the correlation with Ba, K, and Al.

4.8. Growth rates of CCM crusts

The empirical Co-chronometer of Manheim and Lane-Bostwick (1988) was used to calculate growth rates for bulk hydrogenetic CCM Fe-Mn crust samples with seamount ages used to constrain the maximum ages (Fig. 4). CCM Fe-Mn crusts show a mean growth rate for all

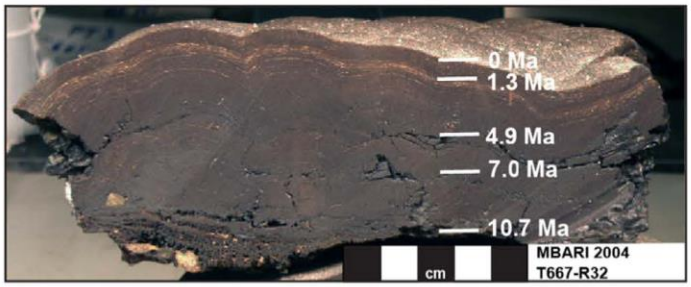

Fig. 4. Photo of hydrogenetic Fe-Mn crust T667-R32 collected from the Patton Escarpment at 1337 m water depth. White lines demark intervals sampled for stratigraphic layers with the approximate age for that depth in the crust calculated using the Co-chronometer (Manheim and Lane-Bostwick, 1988).

samples (n = 210) of 4.92 mm/Myr. The fastest growth rate is 21.9 mm/Myr from Taney D (T121-R6A). The crusts with the four fastest growth rates were all from Taney D, ranging from 17.1 to 21.9 mm/Myr with one crust from that seamount showing a more typical growth rate of 4.7 mm/Myr. Guide seamount has the next fastest growth rate of 19.7 mm/Myr (T123-R5A). Several other samples from Taney D, C, Guide, and Gumdrop have growth rates greater than 10 mm/Myr. When the seven samples with the fastest growth rates are excluded from the data set the mean growth rate drops to 4.51 mm/Myr (n = 203), all of the remaining samples have growth rates from 1 to 10 mm/Myr. This is slightly faster than growth rates for crusts from the global open-ocean, 75% of which range from 1-5 mm/Myr (Hein et al., 2000). The slowest growth rate is 1.0 mm/Myr (D17-6B) from Ben seamount. The oldest sample is from Hoss seamount (D11-11) at 27.7 Ma with the second oldest from Taney A (D176-R12) at 21.5 Ma.

A subset of 144 samples collected by ROV with exact water depth data was used to determine mean growth rate for 250 m water depth intervals and shows that growth rate increases with water depth (Fig. 5). A disproportionately large number of crust samples analyzed were collected from 1320 to 2570 m water depths.

Surface scrapes and thin bulk Fe-Mn crust samples between 0.5 and 1.0 mm thick from 67 crusts with exact water depth, temperature, and dissolved oxygen data measured in situ at the time of crust collection are used to show growth rate trends for individual seamounts (Fig. 6). Data from San Juan, Rodriguez, and combined data (all) show growth rates increasing with water depth. That trend is statistically significant at the 99% CL for San Juan and the combined data, while Rodriguez is statistically significant at the 95% CL. Little Joe, the Patton Escarpment, and Pioneer only have 6, 9, and 5 samples respectively, not enough for statistical analysis.

While growth rate does show a general increase with increasing dissolved oxygen at greater water depth that trend is only statistically significant at the 95% CL in samples from Rodriguez. Growth rate also increases with decreasing temperature, which is statistically significant for the combined data at the 99% CL and for samples from Rodriguez at the 95% CL. The difference in time scales between Fe-Mn crust growth rates and temperature and dissolved oxygen measurements must be kept in mind while evaluating trends in the data. Growth rates in this subset of data range from 1.11 to 9.13 mm/Myr and sample ages range from 0.05 Ma to 0.87 Ma, whereas O_2 and T data are for a single point in time.

5. Discussion

5.1. Mineralogy

The todorokite and birnessite present in CCM crusts could be interpreted to indicate a suboxic diagenetic input into CCM crusts. However, this interpretation is not consistent with the ternary or REY discrimination plots (Figs. 2 and 3). It is more likely that lower oxidation potential seawater conditions under which CCM crusts formed allowed for the precipitation of these Mn minerals that are less oxic than δ-MnO_2, the mineral that typifies open-ocean crusts.

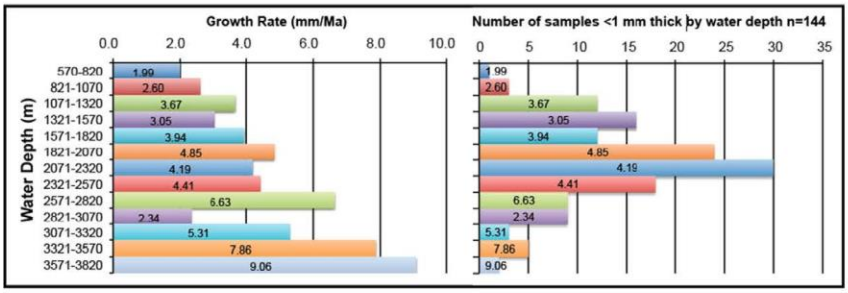

Fig. 5. Left panel: Co-chronometer growth rates and water depths for 144 California continental margin Fe-Mn crusts. Right panel: Number of samples collected at each water depth with growth rate indicated (Manheim and Lane-Bostwick, 1988).

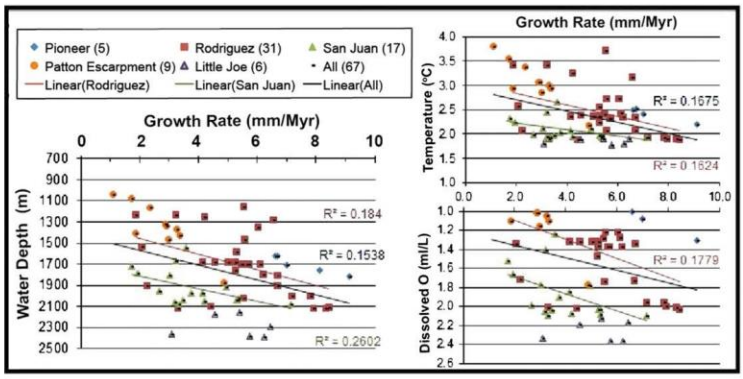

Fig. 6. Co-chronometer growth rates relative to water depth (A), dissolved oxygen (B), and temperature (C) for the upper 0.5 to 1.0 mm of 67 Fe-Mn crust samples collected by MBARI ROV.

Open-ocean Fe-Mn crusts are phosphatized by carbonate fluorapatite (CFA) impregnation of the older layers (Hein et al., 1993; Koschinsky et al., 1997). CFA deposition occurs by preferential replacement of calcium carbonate and partial replacement of Fe oxyhydroxides by CFA, and precipitation of CFA in pore space (Hein et al., 1993; Hyeong et al., 2013; Koschinsky et al., 1997; Puteanus and Halbach, 1988). In phosphatized Fe-Mn crusts Si, Fe, Al, Ti, Co, Mn, and Pb are depleted in that order with Si in particular showing up to a 45% decrease, whereas Ni, Cu, Zn, and REY are enriched, with Ni showing up to a 30% increase (Koschinsky et al., 1997). Phosphatization occurred in suboxic environments from nutrient-rich water in extended and intensified OMZs (Halbach et al., 1989; Hein et al., 1993; Koschinsky et al., 1997). Phosphate could also be supplied by upwelling into the OMZ of phosphate enriched deep water, where nutrients accumulated during stable climatic times (Hein et al., 1993). Open-ocean Fe-Mn crusts from the central Pacific show that two major phases of phosphatization occurred during climatic transitions at the Eocene/Oligocene (39–34 Ma), and the Oligocene/Miocene boundaries (27–21 Ma) (Hein et al., 1993). A minor phase of phosphatization may have occurred during the middle Miocene (Hein et al., 1993). Open-ocean Pacific crusts do not show evidence of phosphatization past the middle Miocene.

Fe-Mn crusts from CCM seamounts do not contain detectable CFA and show no evidence of phosphatization. The paucity of phosphatization in CCM Fe-Mn crusts is curious, as there are extensive formations of authigenic CFA phosphorites on the shelf, slope, and banks adjacent to CCM low-oxygen basins (Berndmeyer et al., 2012; Filippelli et al., 1994; Laurent et al., 2015). The Miocene Monterey Formation is one of the best-studied examples of CCM phosphate deposition, which outcrops along the CCM between San Francisco and Los Angeles. Phosphate occurs as a phosphate-rich carbonaceous member deposited from 14.5 to 14.1 Ma (during a period of cooling climate) and interstratified phosphatic laminae and lenses deposited from 11.05 to 7.85 Ma (Berndmeyer et al., 2012; Laurent et al., 2015). Based on the occurrence of phosphatized layers in open-ocean Fe-Mn crusts as recent as 10 Ma and phosphorite deposition in the study area along the CCM up to 7.85 Ma, the lack of phosphatization in CCM Fe-Mn crusts is unexpected. Approximately 19% of CCM bulk crusts and crust layers are older than 7.85 Ma and the older sections of those samples do not show element trends consistent with phosphatization. In addition, calcium carbonate minerals are scarce in CCM Fe-Mn crusts eliminating the possibility of phosphatization through the replacement of carbonates.

Suboxic environments have occurred around the CCM seamounts during much of their history, as evidenced by the Mn mineralogy. However, the seawater around the offshore seamounts may not have been depleted enough in oxygen and consequently enriched enough in phosphate to form CFA in these Fe-Mn crusts. Fluorine is also a necessary component in CFA but as a conservative element in seawater, F depletion sufficient to hinder CFA deposition is unlikely. More likely, primary productivity due to upwelling may not have been intense enough above the seamounts to provide the organic matter, and associated phosphorous, necessary to establish phosphatization. Despite the occurrence of the OMZ, upwelling and primary productivity were likely not intense enough to form organic matter-rich sediments leading to organic matter-poor depositional environments since the middle Miocene.

5.2. Sources and distribution of Fe and Mn

Flux of Fe and Mn were calculated for 62 Fe-Mn crust surface samples up to 1 mm thick with exact water depth and location data (Supplemental Table S6). The equation used to calculate flux is (F (μg cm^{-2} kyr^{-1}) $= C_e GrD$) where F is flux (μg cm^{-2} kyr^{-1}), C_e is the dry elemental concentration, Gr (mm/Myr) is growth rate (calculated from the cobalt chronometer), and D (1.3 g/cm^{-3}) is dry bulk density (Hein et al., 2009; Halbach et al., 1983). Since cobalt chronometer growth rates were used in the calculation Fe and Mn fluxes are not completely independent. Iron flux ranges from 31 to 575 (μg cm^{-2} kyr^{-1}), while Mn flux ranges from 47 to 285 (μg cm^{-2} kyr^{-1}). Pioneer Seamount had the largest Fe and Mn fluxes while the smallest Fe flux was from San Juan and Mn flux was from the Patton Escarpment (Supplemental Table S6). The flux of Fe in CCM Fe-Mn crusts is much greater than the Mn flux and shows greater variation, which is consistent with the complex nature of Fe in a continental-margin environment.

Terrestrial sources deliver trace metals to the surface ocean, specifically fluvial particulate matter delivered during winter precipitation is a significant source of Fe, Mn, and other trace metals to the continental shelf (Biller and Bruland, 2013). Eolian sources also contribute to the trace metal budget of the surface ocean (Mackey et al., 2002). In addition to aeolian and fluvial input of Fe into the surface waters, remobilization from shelf/slope sediments, and input of hydrothermal vents can also release Fe into intermediate and deep-water masses (Horner et al., 2015). Earth's continental crust contains more Fe (~4%) than Mn (~0.08%) (Rudnick and Gao, 2014), but has a lower Fe/Mn ratio than

the average oceanic crust (Fe/Mn 69.8) (White and Klein, 2014), mid-ocean ridge basalt (Fe/Mn = 54) (Qin and Humayun, 2008), and Hawaii ocean island basalt (Fe/Mn = 67) (Humayun, 2004). These ratios are not reflected in seawater, where Fe has a nutrient-type profile with low surface water concentrations of about 0.05 nmol Fe/L due to assimilation by primary producers in surface waters (Boyd and Ellwood, 2010). Iron is then regenerated with a maximum concentration at around 1000 m of approximately 0.7 nmol Fe/L, before being scavenged at depth with slight seawater concentration decrease (Biller and Bruland, 2013; Boyd and Ellwood, 2010; Bruland and Lohan, 2003). Conversely, Mn has a scavenged seawater profile; with higher surface water concentrations and decreasing concentrations with depth (Biller and Bruland, 2013).

Remobilization of shelf sediment provides a significant source for scavenged and hybrid type elements including Fe and Mn (Biller and Bruland, 2013). Iron is a critical trace metal used in photosynthesis and nitrate assimilation and regions along the CCM show evidence for Fe limitation (Biller et al., 2013; Morel et al., 2014). Leachable particulate and dissolved Fe along the CCS is related to both upwelling intensity and the width of continental shelf mud belts between 50-90 m isobaths (Biller et al., 2013). Leachable particulate Fe concentrations are highest in coastal areas with the widest mid-self-mud belts and with a hypoxic benthic boundary layer; this has a greater influence on Fe concentrations than the overall shelf width (Biller et al., 2013). Iron isotopes from open-ocean Pacific crust CD29-2 from 20 Myr to the present show that seawater ($\delta^{56/54}$Fe ~ +0.4‰) is offset from dust end members ($\delta^{56/54}$Fe ~ +0.7‰) by −0.3‰ (Horner et al., 2015). The secondary source of Fe is isotopically light and is likely due to reductive sediment mobilization of metals (Horner et al., 2015). Under low-oxygen conditions, such as those associated with the high primary productivity along the CCM, reduced, bioavailable, isotopically light Fe is released from shelf sediments (Horner et al., 2015). Seawater measurements have shown that isotopically light dissolved δ^{56}Fe from reduced shelf sediments is laterally transported at least 1900 km off shore from the California Margin between ~550 and 2000 m water depths in the OMZ (Conway and John, 2015).

Further support for continental shelf and slope sediments as a source of Fe can be gleaned by comparison of Fe-Mn crusts from near shore (Pioneer and Gumdrop Seamounts) and offshore (Taney Seamounts) in the northern sector, and offshore (Adam and Hoss Seamounts) and near shore (Patton Escarpment and Northeast Bank) in the southern sector shows that Fe is typically higher in samples closer to the continental margin (Supplemental Table S4). Iron is consistently higher near shore when comparing Fe-Mn crust samples off a narrower shelf in the northern sector where Fe is over 29.2% in all samples from Pioneer and Grumdrop Seamounts (n = 7) and under 20.2% from all Taney Seamount Chain crusts (n = 14). In the southern sector, Patton Escarpment and Northeast Bank (n = 27) are much closer to the coast than Adam and Hoss seamounts (n = 22) and typically have higher Fe concentrations, with a few exceptions. When comparing the northern and southern seamounts, Pioneer, the seamount closest to shore, has the highest Fe concentration. No difference in Fe concentration exists between crust samples from the Taney Seamount Chain compared to the Adam and Hoss seamounts when reviewing Fe concentrations off shore and parallel to the coastline from the northern and southern ends of the study area. This shows that Fe released from continental shelf/slope sediments is the most likely source of Fe to CCM Fe-Mn crusts, and proximity to that source accounts for the Fe enrichment in CCM Fe-Mn crusts

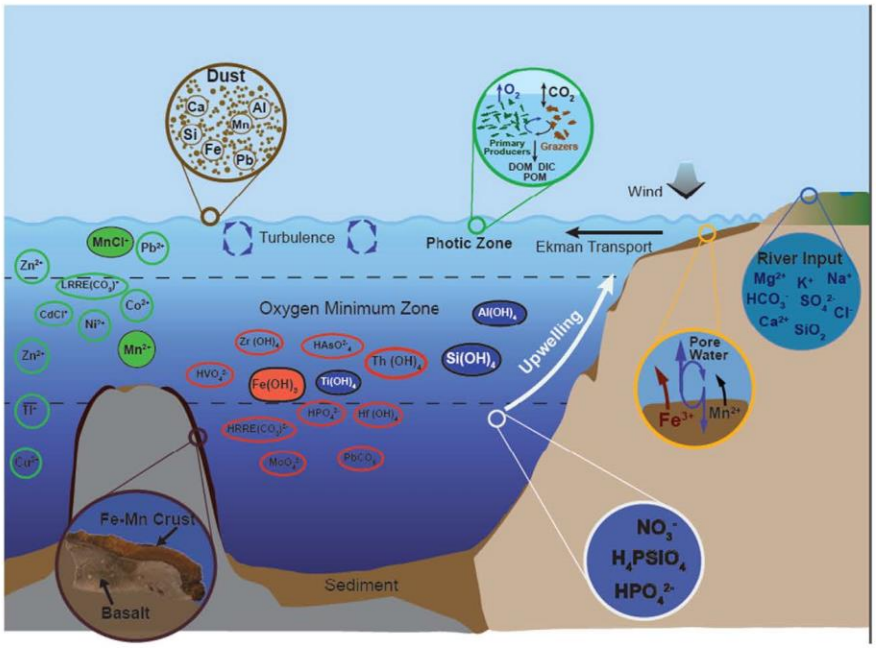

Fig. 7. Genetic model showing sources of elements into the CCM and regional influences on Fe-Mn crust formation. DOM = dissolved organic matter, DIC = dissolved inorganic carbon, POM = particulate organic matter.

relative to open-ocean crusts. A simplified genetic model showing sources and regional influences on seawater and therefore CCM Fe-Mn crusts is presented in Fig. 7.

Manganese is also influenced by these processes and reduced Mn is remobilized from shelf sediments (McManus et al., 2012). However, unlike Fe, Mn in CCM crusts does not show a concentration increase towards the continental shelf. Manganese does show a negative correlation with increasing water depth as expected since dissolved Mn is enriched in seawater in the OMZ. Mn concentrations in Fe-Mn crusts are controlled by the redox potential of seawater from which the crust formed.

5.3. 4.3 Thorium enrichment

The most common Th isotope in seawater is ^{232}Th, typically hosted by detrital material from aeolian sources; ^{232}Th has a conservative distribution in seawater down to the benthic boundary layer where there is a concentration increase (Chen et al., 1986; Hsieh et al., 2011). Dissolved and particulate ^{230}Th have profiles with a linear concentration increase with water depth and that show concentration increases along the path of circumpolar deep-water circulation (Mangini and Key, 1983; Roy-Barman et al., 1996). Decay of ^{238}U produces ^{234}Th, which has a short half-life of 24.1 days and is generally in equilibrium with its parent with a conservative seawater profile (Coale and Bruland, 1987). However, in surface water with high particulate organic carbon, ^{234}Th is scavenged and removed to the sediments at a faster rate than ^{238}U (Coale and Bruland, 1987).

Thorium is enriched in CCM Fe-Mn crusts relative to open-ocean Pacific crusts, with contents comparable to crusts from the Atlantic and Indian Oceans. The enrichment of ^{230}Th in older water masses, and increased input of ^{232}Th due to proximity to the continental margin is the most likely cause of Th enrichment in CCM Fe-Mn crusts. Dissolved Th has a residence time in seawater of < 100 years because it is very particle reactive (Hein et al., 2012; Nozaki et al., 1987). Thorium positively correlates with Fe and Si and negatively correlates with Mn at the 99% CL in CCM crusts indicating that the higher Fe concentration may also help to account for the increased Th concentration observed in CCM Fe-Mn crusts relative to open-ocean crusts. Dissolution of biogenic silica is thought to be an additional seabed source for Th, as is biogenic calcite, both of which adsorb Th from the water column (Hein et al., 2012). There is also no correlation between Th and water depth in CCM crusts, unlike samples from Shatsky Rise in the NW Pacific and the Ninetyeast Ridge in the Indian Ocean where Th correlates with increasing water depth (Hein et al., 2012, 2016).

5.4. Element relationships with primary productivity

The Si/Al ratio is significantly higher in CCM crust samples, 6.2 for n = 225 relative to a mean value of 3.7 n = 610 for all other global open-ocean deposits (Hein and Koschinsky, 2014). In CCM crusts neither Si nor Al show an increase towards the continental shelf, when comparing concentrations from off shore and near shore seamounts. If the Si enrichment in CCM crusts was due to terrestrial input, or dissolved biosilica from surface water diatom primary productivity, Si contents in CCM Fe-Mn crusts would be expected to increase towards shore. Since this relationship is not found, the high Si concentrations in CCM crusts is likely due to the high Si concentrations in NE Pacific seawater. Dissolved Si in seawater ranges from 10 to 40 μmol/kg in the Atlantic, and up to 180 μmol/kg in the NE Pacific (Johnson et al., 2006; Talley and Joyce, 1992). Evidence of the high Si in the waters along the CCM area is also present in several basins along the California borderland; this is shown in the Monterey Formation, which has an increase in biosilica from ~9.3 Ma onwards (Laurent et al., 2015).

The high concentration of dissolved Si in the Pacific is due in part to the North Pacific silica plume. The North Pacific silica plume originates in the NE Pacific, extends across the North Pacific from 50°N to 20°N, and is centered around 2300 m water depth (Johnson et al., 2006; Talley and Joyce, 1992 and references therein). The maximum concentrations of Si in the plume reach approximately 164 Tmol above the average background of 165 μmol/L (Johnson et al., 2006). Possible sources of dissolved silica in the North Pacific silica plume include; hydrothermal venting, remineralization of biosilica in the water column from surface diatoms, dissolution of bottom sediments, and accumulation of bottom water silica along the path of deep water circulation (Talley and Joyce, 1992). Additionally sediment compression and thermal advection through faults during the formation of the accretionary margin might provide an additional source of Si to the region (Johnson et al., 2006).

Other trace metals, Ni, Zn, and Cd with nutrient-type seawater profiles also show enrichment in bottom-waters along the path of deep-water circulation (Bruland and Lohan, 2003). However, these elements are not noticeably enriched in CCM crusts relative to open-ocean crusts. Barium and P both have nutrient-type profiles in seawater and can be used as tracers of primary productivity (Broecker et al., 1982; Chan et al., 1976; Paytan and Griffith, 2007). However, Ba and P are also not enriched in CCM Fe-Mn crusts relative to open-ocean crusts. With the exception of a few outliers, P shows higher concentrations in near shore CCM crusts relative to off shore samples, which probably reflects the strong upwelling and primary productivity.

CCM crust samples with high Ba contain minor barite, this is observed on Hoss Seamount (D10-3 and D10-4A) and Little Joe Seamount (D13-2C) (Hein et al., 2010b). However, overall CCM Fe-Mn crusts have somewhat lower Ba concentrations than crusts from the PCZ, 1838 ppm (n = 225) and 1934 ppm (n = 328), respectively. In contrast, the CCM crusts do have higher Ba concentrations than the Fe-Mn crust mean from the Atlantic and Indian Oceans, 1556 ppm (n = 43) and 1533 ppm (n = 23), respectively. Barium in near shore CCM Fe-Mn crusts partially overlaps with the lower concentration in off shore samples. That indicates that Ba is not consistently higher in crusts closer to the shelf or continental margin.

Marine barite can form in a number of ways, for example authigenic processes occurring in sulfate reducing sediments during diagenesis, cold-seep fluids along the seafloor, low-temperature hydrothermal fluids < 120 °C, intermediate-temperature fluids (150–250 °C), and precipitation in the water column typically in the presence of organic matter (Hein et al., 2007; Paytan et al., 2002). Fe-Mn crust samples with Ba concentrations significantly higher than the regional Fe-Mn crust mean may have been exposed to localized cold-seep or low temperature, diffuse-flow hydrothermal fluids, despite the overall hydrogenetic origin of the crusts.

5.5. Growth rate

Increasing growth rate with increasing water depth is an expected trend and is likely due to increasing dissolved oxygen concentrations in seawater below the oxygen minimum zone (Halbach et al., 1983; Hein et al., 2016). The correlation of Fe-Mn crust growth rate and water depth is not due to a relationship between Fe or Mn concentrations with water depth. Plots of these elements in Fe-Mn crusts versus water depth for the same data set do not show a significant correlation. The trend is also not due to continental proximity as growth rates continue to trend with water depth in Fe-Mn crusts from individual seamounts. Dissolved Mn concentrations in seawater correlates with the strength of the OMZ which provides a reservoir of dissolved Mn; with advective and diffusive transport Mn moves out of the OMZ and is oxidized (Dickens and Owen, 1994; Halbach and Puteanus, 1984; Hein et al., 2016). It is significant that CCM crusts continue to grow in a region with a well-developed OMZ, and that growth rates are slower in the OMZ than below the OMZ. This correlation has not yet been determined elsewhere in the global ocean and needs to be resolved for open-ocean settings where the OMZ is weaker. However, this does assume that the OMZ has been present since crust formation began. It also assumes that sufficient supplies of Fe and Mn, with residence times in seawater of around

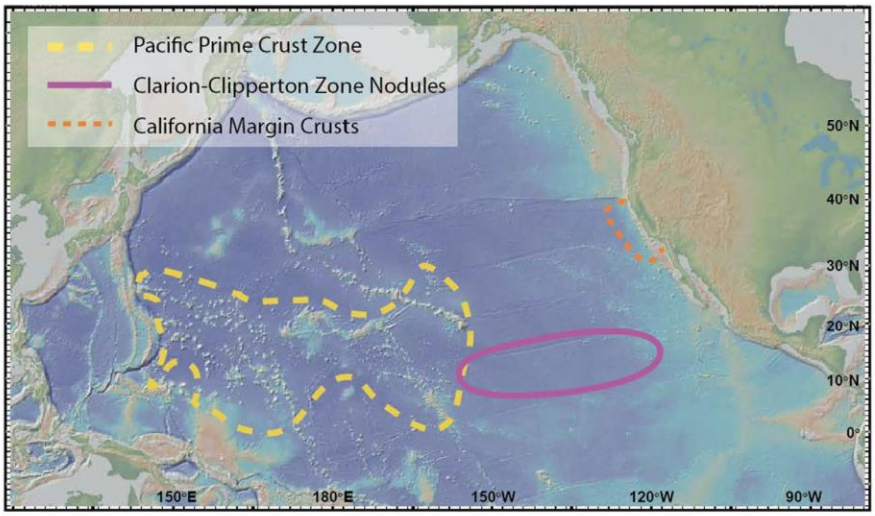

Fig. 8. Map of the North Pacific Ocean showing areas within which marine mineral samples were collected and discussed in this paper (http://www.geomapapp.org; Ryan et al., 2009). (Modified from Hein and Koschinsky, 2014).

500 years and 100 years respectively, have been available for Fe-Mn crust formation (Johnson et al., 1996, 1997). Alternatively, the increased growth rate with water depth observed in CCM Fe-Mn crusts may indicate deep-water sources of Fe and Mn influencing Fe-Mn crust formation.

5.6. Resource potential of CCM crusts

Elements of economic interest in Fe-Mn crusts include Mn, Ni, Co, Ti, Te, Th, W, Bi, REY and PGE (Hein et al., 2013). Co and

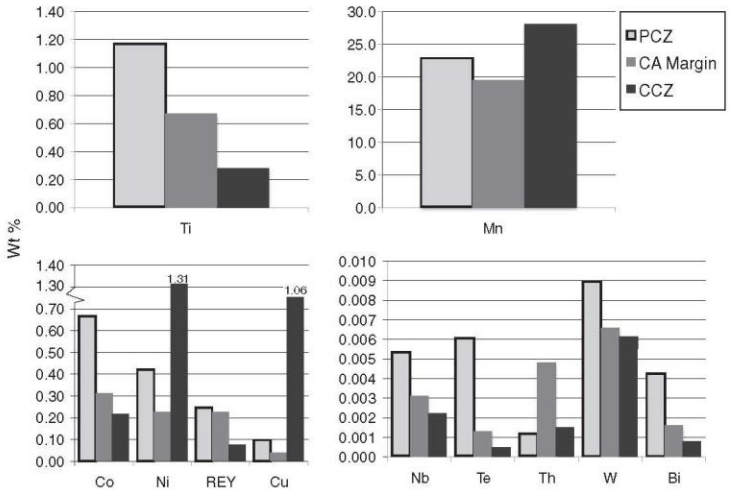

Fig. 9. Concentrations of elements of economic interest in Fe-Mn crusts from the Prime Crust Zone (PCZ) in the NW Pacific and the California continental margin and diagenetic Fe-Mn nodules from the Clarion-Clipperton Fracture Zone (CCZ) in the central-east Pacific (Hein and Koschinsky, 2014).

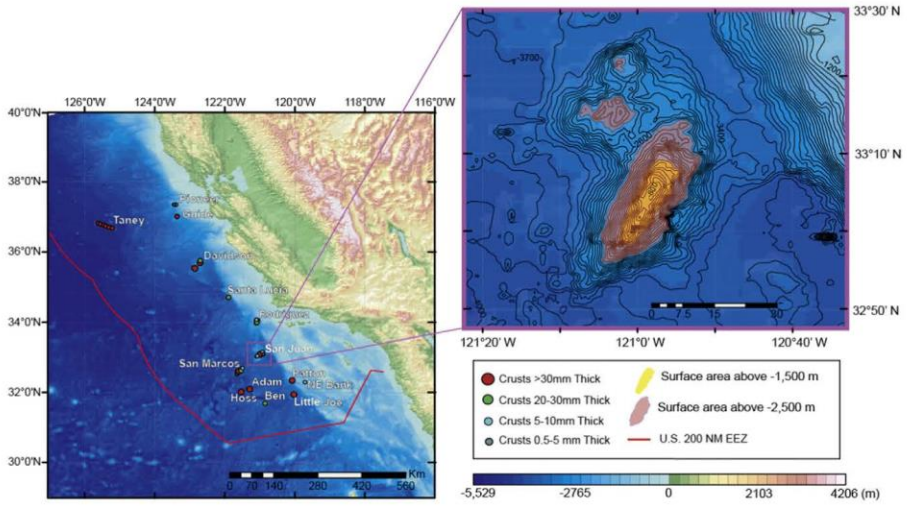

Fig. 10. Bathymetric image of San Juan Seamount showing surface area above 2500 m (white) and 1500 m (dark grey) water depths (Google Earth 2015; GEBCO, 2014; ESRI, 2011).

then Ni and Mn have traditionally been considered to have the most economic potential (Hein et al., 2013). However, increased demand for critical metals including Te and the REY may change the economic outlook of mining these deposits. There is also an increasing economic demand for Cu and while it would not be economically viable to mine crusts solely for Cu, as the grade is much lower than that of CCZ nodules and some seafloor massive sulfide deposits, the amount of Cu in crusts is of interest as a byproduct of mining (Hein et al., 2013).

The two main regions in which the most data for Fe-Mn marine minerals are available are the PCZ, which hosts hydrogenetic Fe-Mn crusts, and the CCZ, which contains diagenetic-hydrogenetic Fe-Mn nodules (Fig. 8). Other regions of the global oceans are currently being explored for both ferromanganese and non-ferromanganese deposits such as seafloor massive sulfides. Approximately 2,200,000 km^2 of seabed are under contract for marine mineral exploration and 12,000 km^2 of that area is for Fe-Mn crust exploration (Hein et al., 2013). The Council and Assembly of the International Seabed Authority passed regulations governing Fe-Mn crust exploration in July 2012 and the first contracts for the exploration of Fe-Mn crusts were granted in July of 2013 (Hein et al., 2013).

Comparison of grades between CCM crusts and PCZ crusts and CCZ nodules are presented for select elements of economic interest (Fig. 9). Cu is included although Cu grades in Fe-Mn crust samples are lower than terrestrial mines, which currently have Cu grades of approximately 0.5% for porphyry copper from which about 50% of terrestrial Cu is produced. Seafloor massive sulfide deposits have small tonnages, but Cu grades can be up to 12 wt.% (Hein et al., 2013). CCM crusts have total REY concentrations of 0.227 wt.%, with the heavy REY (HREY) complement comprising 15.5% of total REY. CCM crusts have a lower grade for total REY than the large carbonatite terrestrial mines, but a much higher percentage of HREY, which are <1% in carbonatite deposits (Hein et al., 2013). Other elements of economic interest, Mn, Ni, Co, Ti, Nb, Te, W, and Bi have slightly lower grades in CCM crusts than in crusts from the PCZ. Concentrations for Mo, Zr, and total HREY are roughly comparable between the PCZ and the CCM. Th is higher in CCM crusts than in crusts from the PCZ, but is still much lower than in terrestrial REE deposits where radioactive Th in mine waste is an environmental concern (Hein et al., 2013).

To evaluate the tonnage of elements of economic interest, total surface area above 2500 m water depth was calculated for CCM edifices using General Bathymetric Chart of the Oceans (GEBCO) 2014 base map and ArcGIS. The total surface area was reduced to account for the Monterey Bay National Marine Sanctuary, which includes Davidson seamount and by 5% for prohibitively steep slopes, followed by 10% for sediment cover, and then 25% for biologic corridors (Hein et al., 2009). In the CCM, San Juan Seamount has the greatest surface area above 2500 m with a flat summit and low sediment cover (Fig. 10). The surface area likely to contain Fe-Mn crusts in the CCM is significantly less than that of the PCZ, which has large relatively flat plateaus and guyots (flat topped seamounts) (Table 2). Crusts in the CCM are also thinner than those of the PCZ. A mean crust thickness of 1.6 cm was used based on mean CCM sample thicknesses. The crust thickness is conservative as the majority of cruises had sampling bias that strongly favored collection of basalts with little to no crust cover. Tonnage calculations are based on an average of 1.3 g/cm^3 dry bulk density for Fe-Mn crusts (Hein et al., 2009; Hein and Koschinsky, 2014). Tonnages of dry crust for the CCM and San Juan

Table 2
Surface area calculations for CCM and San Juan Seamount and dry tonnages.

	PCZ	CCZ	CCM (total)	CCM (reduced)	San Juan (total)	San Juan (reduced)
SA (km^2) ≤2500 m	–	–	1461	681	425	273
Dry tons	7.53×10^9	2.11×10^{10}	3.04×10^7	1.54×10^7	8.85×10^6	5.67×10^6

Table 3
Dry tons of in place metals of economic interest $\times 10^6$ for the CCM and San Juan Seamount.

		Mn	Ti	Co	Ni	Cu	Mo	Zr	W	Th	Te	Total REY	HREE
CA margin	tons $\times 10^6$	301	10.3	4.83	3.50	0.60	0.59	0.72	0.10	0.07	0.02	3.50	0.31
	wt.%	19.5	0.67	0.31	0.23	0.04	0.04	0.05	0.007	0.005	0.001	0.227	0.020
San Juan Smt	tons $\times 10^6$	137	4.31	2.16	1.32	0.15	0.25	0.28	0.04	0.03	0.009	1.28	0.18
	wt.%	24.2	0.76	0.38	0.23	0.03	0.044	0.049	0.008	0.005	0.002	0.225	0.032

Seamount above 2500 m water depth are presented in Table 3. While it is more likely to be economic to exploit Fe-Mn deposits in the central Pacific than along the CCM, there are advantages to CCM Fe-Mn crusts. The absence of CFA in CCM crusts and lower concentrations of P are preferred for smelting, potentially decreasing processing costs. The proximity of CCM Fe-Mn crusts to California could also reduce transportation time and expenses.

5.7. Environmental considerations

The potential environmental impacts associated with exploitation of Fe-Mn crusts along the CCM must be considered at all steps of the evaluation process. While there is no overburden to remove when collecting Fe-Mn crusts and the risk of large-scale sediment resuspension is much lower than with Fe-Mn nodules, any form of mining impact needs to be evaluated. Selecting sites down current from preserved areas with nearby seamounts and continental slope habitats that have depth ranges comparable to those on the seamounts of interest, and preserving biologic corridors on the edifice would allow for dispersal of species to the area by current transport, stepping stones, and active dispersal that would aid in recolonization. In the CCM, the CCS and nearby continental slope should enable redistribution of species. CCM seamounts are not island habitats with highly endemic faunas but rather have species compositions similar to other regional deep-sea habitats (Rowden et al., 2010). However, the CCM is a region of high primary productivity that hosts 28 cetacean, 6 pinniped, and 2 fissiped marine mammal species, and large commercial fisheries valued at over $230 million in 2012 (Lundsten et al., 2009). Sport fishing and tourism are also significant stakeholder industries in the region. Any mining activities must weigh the economic potential against possible environmental impact and the needs of other stakeholders. As crusts contain Fe and other potentially limiting nutrients, as well as potentially toxic trace metals, the effect of even a small amount of re-suspended crust on benthic and pelagic species requires further investigation. The process of mining crusts will remove non-mobile species in the impacted area. Collecting crusts on areas previously fished by trawling, where such damage has already been inflicted would limit further reduction of these species. Since only sections on seamounts with the thickest, metal-rich crusts would be considered for extraction; mining of Fe-Mn crusts would impact a much smaller portion of a seamount than trawling fisheries.

6. Conclusions

Fe-Mn crusts along the CCM have distinct chemical and mineralogical compositions relative to open-ocean samples. A number of factors may influence the formation of CCM crusts, especially their close proximity to terrestrial sources of dissolved and particulate material transported to the ocean, remobilization of Fe and Mn from sediment on the continental shelf and slope, upwelling and high primary productivity, and older deep water masses along the CCM enriched in elements with long residence times (Fig. 7). Iron is higher in CCM Fe-Mn crusts than in those from the open ocean, resulting in a higher Fe/Mn ratio. The Fe enrichment is due to the remobilization of continental shelf and slope sediments. The CCM Fe-Mn crusts show increasing Fe concentrations with proximity to the continental shelf. Thorium is also enriched in CCM Fe-Mn crusts compared to samples from the PCZ and S. Pacific, with values approaching concentrations of crusts from the Atlantic and Indian Oceans. The enrichment of Th in CCM crusts may reflect proximity to the continental shelf, aeolian sources, and the dissolution of biogenic Si. Further work is needed to determine the most prominent source.

Silica is significantly higher in CCM Fe-Mn crusts than in open-ocean samples as is the Si/Al ratio. This is likely due to the high Si concentrations in the North Pacific silica plume. Enrichment of Si in bottom waters along the path of deep-water circulation, also contributes to the high seawater concentrations of Si along the CCM. Phosphorous is another element associated with primary productivity but is not enriched in CCM Fe-Mn crusts. CCM crusts do not contain CFA or show evidence of phosphatization, which may explain why P concentrations are lower than in crusts from the central Pacific, many of which are phosphatized in the older layers. Todorokite, which is only found in 2% open-ocean crusts (Hein et al., 2000), is found in 35% CCM crusts and is not associated with phosphatization. It is thought that seawater around CCM seamounts did not become suboxic enough to encourage phosphatization in the crusts. Birnessite is a common accessory mineral and occurs in 5% of CCM Fe-Mn crusts; in contrast to open-ocean hydrogenetic crusts where it has not been detected.

Growth rates calculated by Co chronometer show increasing growth rates with increasing water depth both for the study area as a whole and to a greater extent for individual seamounts. This increase in growth rate with water depth is due to the increased supply of deeply sourced remobilized Fe and to a lesser extent Mn from continental shelf and slope sediments. This is the first study to document this water depth-growth rate relationship.

Elements of economic interest in Fe-Mn crusts are generally not as enriched in CCM samples as those from the PCZ crusts. Environmental concerns associated with extraction of crusts in a highly dynamic and productive environment need to be evaluated using best practices and the precautionary approach, as is true for all areas of the deep-ocean being considered for extraction of mineral resources.

Supplementary data to this article can be found online at http://dx.doi.org/10.1016/j.oregeorev.2016.09.010.

Acknowledgements

We would like to thank the Monterey Bay Aquarium Research Institute (MBARI) for providing samples and the opportunity to participate on research cruises to the study area. We thank the crew of the R.V. *Western Flyer* and the operators of the ROV *Doc Ricketts*. We would also like to thank Jenny Paduan, for help in sampling and data retrieval. We are also grateful to UCSC student Kristina Tu for her assistance with Arc GIS and sample preparation and UCSC student Natalie Zimdahl for her assistance with sample preparation. We would also like to thank Dr. Xiangwen, Dr. Katz Suzuki, and Mariah Mikesell for their thoughtful reviews.

References

Atwater, T., Severinghaus, J., 1989. Tectonic maps of the northeast Pacific, in the eastern Pacific Ocean and Hawaii. In: Winterer, E.L., Hussong, D.M., Decker, R.W. (Eds.), The Geology of North America – An Overview. Geological Society of America, Boulder, Colorado, pp. 265–297.

Banakar, V.K., Hein, J.R., Rajani, R.P., Chodankar, A.R., 2007. Platinum group elements and gold in ferromanganese crusts from Afanasiy-Nikitin seamount, equatorial Indian Ocean: sources and fractionation.

Bau, M., 1996. Controls on the fractionation of isovalent trace elements in magmatic and aqueous systems: evidence from Y/Ho, Zr/Hf, and lanthanide tetrad effect. Contrib. Mineral. Petrol. 123, 323–333. http://dx.doi.org/10.1007/s004100050159.

Bau, M., Schmidt, K., Koschinsky, A., Hein, J., Kuhn, T., Usui, A., 2014. Discriminating between different genetic types of marine ferro-manganese crusts and nodules based on rare earth elements and yttrium. Chem. Geol. 381, 1–9. http://dx.doi.org/10.1016/j.chemgeo.2014.05.004.

Berndmeyer, C., Birgel, D., Brunner, B., Wehrmann, L.M., Jöns, N., Bach, W., Arning, E.T., Föllmi, K.B., Peckmann, J., 2012. The influence of bacterial activity on phosphorite formation in the Miocene Monterey Formation. California. Palaeogeogr. Palaeoclimatol. Palaeoecol. 317–318, 171–181. http://dx.doi.org/10.1016/j.palaeo.2012.01.004.

Biller, D.V., Bruland, K.W., 2013. Sources and distributions of Mn, Fe, Co, Ni, Cu, Zn, and Cd relative to macronutrients along the central California coast during the spring and summer upwelling season. Mar. Chem. 155, 50–70. http://dx.doi.org/10.1016/j.marchem.2013.06.003.

Biller, D.V., Coale, T.H., Till, R.C., Smith, G.J., Bruland, K.W., 2013. Coastal iron and nitrate distributions during the spring and summer upwelling season in the central California Current upwelling regime. Cont. Shelf Res. 66, 58–72. http://dx.doi.org/10.1016/j.csr.2013.07.003.

Bonatti, E., Kraemer, T., Abdulla, H.A.N., 1972. Classification and genesis of submarine iron-manganese deposits. In: Horn, D.R. (Ed.), Ferromanganese Deposits on the Ocean Floor. National Science Foundation, Washington, D.C. USA, pp. 149–166.

Boyd, P.W., Ellwood, M.J., 2010. The biogeochemical cycle of iron in the ocean. Nat. Geosci. 3, 675–682. http://dx.doi.org/10.1038/ngeo964.

Broecker, W.S., Peng, T., Lamont-Doherty Geological Observatory, 1982. Tracers in the Sea. Eldigio Press, Palisades, N.Y.

Bruland, K.W., Lohan, M.C., 2003. Controls of trace metals in seawater. Treatise on Geochemistry. Elsevier, pp. 23–47.

Cande, S.C., Kent, D.V., 1995. Revised calibration of the geomagnetic polarity timescale for the Late Cretaceous and Cenozoic. J. Geophys. Res Solid Earth 100, 6093–6095. http://dx.doi.org/10.1029/94JB03098.

Carr, M.-E., 2001. Estimation of potential productivity in Eastern Boundary Currents using remote sensing. Deep Sea Res. Part II Top. Stud. Oceanogr. 49, 59–80. http://dx.doi.org/10.1016/S0967-0645(01)00094-7.

Chan, L.H., Edmond, J.M., Stallard, R.F., Broecker, W.S., Chung, Y.C., Weiss, R.F., Ku, T.L., 1976. Radium and barium at GEOSECS stations in the Atlantic and Pacific. Earth Planet. Sci. Lett. 32, 258–267. http://dx.doi.org/10.1016/0012-821X(76)90066-2.

Checkley, D.M., Barth, J.A., 2009. Patterns and processes in the California Current System. Prog. Oceanogr. 83, 49–64. http://dx.doi.org/10.1016/j.pocean.2009.07.028.

Chen, J.H., Lawrence Edwards, R., Wasserburg, G.J., 1986. ^{238}U, ^{234}U and ^{232}Th in seawater. Earth Planet. Sci. Lett. 80, 241–251. http://dx.doi.org/10.1016/0012-821X(86)90108-1.

Clague, D.A., Reynolds, J.R., Davis, A.S., 2000. Near-ridge seamount chains in the northeastern Pacific Ocean. J. Geophys. Res. Solid Earth 105, 16541–16561.

Clague, D.A., Paduan, J.B., Duncan, R.A., Huard, J.J., Davis, A.S., Castillo, P.R., Lonsdale, P., DeVogelaere, A., 2009. Five million years of compositionally diverse, episodic volcanism: construction of Davidson Seamount atop an abandoned spreading center: Davidson Seamount ages and glass chemistry. Geochem. Geophys. Geosyst. 10. http://dx.doi.org/10.1029/2009GC002665 n/a-n/a.

Coale, K.H., Bruland, K.W., 1987. Oceanic stratified euphotic zone as elucidated by ^{234}Th:^{238}U disequilibria. Limnol. Oceanogr. 32, 189–200. http://dx.doi.org/10.4319/lo.1987.32.1.0189.

Conway, T.M., John, S.G., 2015. The cycling of iron, zinc and cadmium in the North East Pacific Ocean – insights from stable isotopes. Geochim. Cosmochim. Acta 164, 262–283. http://dx.doi.org/10.1016/j.gca.2015.05.023.

Coumans, J.P., Stix, J., Clague, D.A., Minarik, W.G., 2015. The magmatic architecture of Taney Seamount-A, NE Pacific Ocean. J. Petrol. 56, 1037–1067. http://dx.doi.org/10.1093/petrology/egv027.

Davis, A.S., Gray, L.B., Clague, D.A., Hein, J.R., 2002. The Line Islands revisited: new $^{40}Ar/^{39}Ar$ geochronologic evidence for episodes of volcanism due to lithospheric extension: Line Islands revisited. Geochem. Geophys. Geosystems 3, 1–28. http://dx.doi.org/10.1029/2001GC000190.

Davis, A.S., Clague, D.A., Paduan, J.B., Cousens, B.L., Huard, J., 2010. Origin of volcanic seamounts at the continental margin of California related to changes in plate margins: origin of seamounts offshore California. Geochem. Geophys. Geosyst. 11. http://dx.doi.org/10.1029/2010GC003064 n/a-n/a.

Dickens, G.R., Owen, R.M., 1994. Late Miocene-Early Pliocene manganese redirection in the central Indian Ocean: Expansion of the Intermediate Water oxygen minimum zone. Paleoceanography 9, 169–181. http://dx.doi.org/10.1029/93PA02699.

ESRI 2011. ArcGIS Desktop: Release 10. Environmental Systems Research Institute, Redlands, CA.

Filippelli, G.M., Delaney, M.L., Garrison, R.E., Omarzai, S.K., Behl, R.J., 1994. Phosphorus accumulation rates in a Miocene low oxygen basin: the Monterey Formation (Pismo Basin), California. Mar. Geol. 116, 419–430. http://dx.doi.org/10.1016/0025-3227(94)90055-8.

GEBCO, 2014. The GEBCO 2014 Grid, version 20150318. www.gebco.net.

Gibbs, A.E., Hein, J.R., Lewis, S.D., McCulloch, D.S., 1993. Hydrothermal palygorskite and ferromanganese mineralization at a central California margin fracture zone. Mar. Geol. 115, 19.

Halbach, P., Puteanus, D., 1984. The influence of the carbonate dissolution rate on the growth and composition of Co-rich ferromanganese crusts from Central Pacific seamount areas. Earth Planet. Sci. Lett. 68, 73–87. http://dx.doi.org/10.1016/0012-821X(84)90141-9.

Halbach, P., Segl, M., Puteanus, D., Mangini, A., 1983. Co-fluxes and growth rates in ferromanganese deposits from central Pacific seamount areas. Nature 304, 716–719. http://dx.doi.org/10.1038/304716a0.

Halbach, P.E., Sattler, C.-D., Teichmann, F., Wahsner, M., 1989. Cobalt rich and platinum bearing manganese crust deposits on seamounts: Nature, formation metal potential. Mar. Miner. 8, 23–39.

Hein, J.R., Koschinsky, A., 2014. Deep-ocean ferromanganese crusts and nodules. Treatise on Geochemistry. Elsevier, pp. 273–291.

Hein, J.R., Yeh, H.-W., Gunn, S.H., Sliter, W.V., Benninger, L.M., Wang, C.-H., 1993. Two major Cenozoic episodes of phosphogenesis recorded in equatorial Pacific seamount deposits. Paleoceanography 8, 293–311. http://dx.doi.org/10.1029/93PA00320.

Hein, J.R., Koschinsky, A., Bau, M., Manheim, F.T., Kang, J.-K., Roberts, L., 2000. Cobalt-rich ferromanganese crusts in the Pacific: chapter 9. Handbook of Marine Mineral Deposits. CRC Press, Boca Raton, Florida, pp. 239–279.

Hein, J.R., Koschinsky, A., McIntyre, B.R., 2005. Mercury- and silver-rich ferromanganese oxides, Southern California Borderland: deposit model and environmental implications. Econ. Geol. 100, 1151–1168. http://dx.doi.org/10.2113/gsecongeo.100.6.1151.

Hein, J.R., Zierenberg, R.A., Maynard, J.B., Hannington, M.D., 2007. Barite-forming environments along a rifted continental margin, Southern California Boderland. Deep Sea Res. Part II Top. Stud. Oceanogr. 54, 1327–1349. http://dx.doi.org/10.1016/j.dsr2.2007.04.011.

Hein, J.R., Conrad, T.A., Dunham, R.E., 2009. Seamount characteristics and mine-site model applied to exploration- and mining-lease-block selection for cobalt-rich ferromanganese crusts. Mar. Georesour. Geotechnol. 27, 160–176. http://dx.doi.org/10.1080/10641190902852485.

Hein, J.R., Conrad, T., Staudigel, H., 2010a. Seamount mineral deposits: a source of rare metals for high-technology industries. Oceanography 23, 184–189. http://dx.doi.org/10.5670/oceanog.2010.70.

Hein, J.R., Reid, J.A., Conrad, T.A., Dunham, R.E., Clague, D.A., Schulz, M.S., Davis, A.S., 2010b. Seamounts and ferromanganese crusts within and near the U.S. EEZ off California – data for RV Farnella cruise F7-87-SC (No. 2010-1069). U.S. Geological Survey.

Hein, J.R., Conrad, T.A., Frank, M., Christl, M., Sager, W.W., 2012. Copper-nickel-rich, amalgamated ferromanganese crust-nodule deposits from Shatsky Rise, NW Pacific: Shatsky Rise Cu-rich Fe-Mn crusts. Geochem. Geophys. Geosyst. 13. http://dx.doi.org/10.1029/2012GC004286 n/a-n/a.

Hein, J.R., Mizell, K., Koschinsky, A., Conrad, T.A., 2013. Deep-ocean mineral deposits as a source of critical metals for high- and green-technology applications: comparison with land-based resources. Ore Geol. Rev. 51, 1–14. http://dx.doi.org/10.1016/j.oregeorev.2012.12.001.

Hein, J.R., Conrad, T., Mizell, K., Banakar, V.K., Frey, F.A., Sager, W.W., 2016. Controls on ferromanganese crust composition and reconnaissance resource potential, Ninetyeast Ridge, Indian Ocean. Deep Sea Res. Part Oceanogr. Res. Pap. 110, 1–19. http://dx.doi.org/10.1016/j.dsr.2015.11.006.

Holt, J.W., Holt, E.W., Stock, J.M., 2000. An age constraint on Gulf of California rifting from the Santa Rosalia basin, Baja California Sur, Mexico. Geol. Soc. Am. Bull. 112, 540–549. http://dx.doi.org/10.1130/0016-7606(2000)112<540:AACOGO>2.0.CO;2.

Horner, T.J., Williams, H.M., Hein, J.R., Saito, M.A., Burton, K.W., Halliday, A.N., Nielsen, S.G., 2015. Persistence of deeply sourced iron in the Pacific Ocean. Proc. Natl. Acad. Sci. 112, 1292–1297. http://dx.doi.org/10.1073/pnas.1420188112.

Hsieh, Y.-T., Henderson, G.M., Thomas, A.L., 2011. Combining seawater ^{232}Th and ^{230}Th concentrations to determine dust fluxes to the surface ocean. Earth Planet. Sci. Lett. 312, 280–290. http://dx.doi.org/10.1016/j.epsl.2011.10.022.

Humayun, M., 2004. Geochemical evidence for excess iron in the mantle beneath Hawaii. Science 306, 91–94. http://dx.doi.org/10.1126/science.1101050.

Hyeong, K., Kim, J., Yoo, C.M., Moon, J.-W., Seo, I., 2013. Cenozoic history of phosphogenesis recorded in the ferromanganese crusts of central and western Pacific seamounts: Implications for deepwater circulation and phosphorus budgets. Palaeogeogr. Palaeoclimatol. Palaeoecol. 392, 293–301. http://dx.doi.org/10.1016/j.palaeo.2013.09.012.

Johnson, K.S., Coale, K.H., Berelson, W.M., Gordon, R.M., 1996. On the formation of the manganese maximum in the oxygen minimum. Geochim. Cosmochim. Acta 60, 1291–1299. http://dx.doi.org/10.1016/0016-7037(96)00005-1.

Johnson, K.S., Gordon, R.M., Coale, K.H., 1997. What controls dissolved iron concentrations in the world ocean? Mar. Chem. 57, 137–161. http://dx.doi.org/10.1016/S0304-4203(97)00043-1.

Johnson, H.P., Hautala, S.L., Bjorklund, T.A., Zarnetske, M.R., 2006. Quantifying the North Pacific silica plume: North Pacific silica plume. Geochem. Geophys. Geosyst. 7. http://dx.doi.org/10.1029/2005GC001065 n/a-n/a.

Klemm, V., Levasseur, S., Frank, M., Hein, J., Halliday, A., 2005. Osmium isotope stratigraphy of a marine ferromanganese crust. Earth Planet. Sci. Lett. 238, 42–48. http://dx.doi.org/10.1016/j.epsl.2005.07.016.

Klovan, J.E., Imbrie, J., 1971. An algorithm and FORTRAN-IV program for large-scale Q-mode factor analysis and calculation of factor scores. J. Int. Assoc. Math. Geol. 3, 61–77. http://dx.doi.org/10.1007/BF02047433.

Koschinsky, A., Halbach, P., 1995. Sequential leaching of marine ferromanganese precipitates: genetic implications. Geochim. Cosmochim. Acta 59, 5113–5132. http://dx.doi.org/10.1016/0016-7037(95)00358-4.

Koschinsky, A., Hein, J.R., 2003. Uptake of elements from seawater by ferromanganese crusts: solid-phase associations and seawater speciation. Mar. Geol. 198, 331–351. http://dx.doi.org/10.1016/S0025-3227(03)00122-1.

Koschinsky, A., Stascheit, A., Bau, M., Halbach, P., 1997. Effects of phosphatization on the geochemical and mineralogical composition of marine ferromanganese crusts. Geochim. Cosmochim. Acta 61, 4079–4094. http://dx.doi.org/10.1016/S0016-7037(97)00231-7.

Laurent, D., de Kaenel, E., Spangenberg, J.E., Föllmi, K.B., 2015. A sedimentological model of organic-matter preservation and phosphogenesis in the Miocene Monterey Formation at Haskells Beach, Goleta (central California). Sediment. Geol. 326, 16–32. http://dx.doi.org/10.1016/j.sedgeo.2015.06.008.

Lundsten, L., McClain, C., Barry, J., Cailliet, G., Clague, D., DeVogelaere, A., 2009. Ichthyofauna on three seamounts off southern and central California, USA. Mar. Ecol. Prog. Ser. 389, 223–232. http://dx.doi.org/10.3354/meps08181.

Mackey, D.J., O'Sullivan, J.E., Watson, R.J., Dal Pont, G., 2002. Trace metals in the Western Pacific: temporal and spatial variability in the concentrations of Cd, Cu, Mn and Ni. Deep Sea Res. Part Oceanogr. Res. Pap. 49, 2241–2259. http://dx.doi.org/10.1016/S0967-0637(02)00124-3.

Mangini, A., Key, R., 1983. A ^{230}Th profile in the Atlantic Ocean. Earth Planet. Sci. Lett. 62, 377–384. http://dx.doi.org/10.1016/0012-821X(83)90008-0.

Manheim, F.T., Lane-Bostwick, C.M., 1988. Cobalt in ferromanganese crusts as a monitor of hydrothermal discharge on the Pacific sea floor. Nature 335, 59–62. http://dx.doi.org/10.1038/335059a0.

Marsaglia, K.M., Davis, A.S., Rimkus, K., Clague, D.A., 2006. Evidence for interaction of a spreading ridge with the outer California borderland. Mar. Geol. 229, 259–272. http://dx.doi.org/10.1016/j.margeo.2006.02.006.

McLennan, S.M., 1989. Rare earth elements in sedimentary rocks; influence of provenance and sedimentary processes. In: Lipin, B.R., McKay, G.A. (Eds.), Geochemistry and Mineralogy of Rare Earth ElementsRev. in Mineralogy. Mineralogical Society of America, Washington, D.C., USA, pp. 169–200.

McManus, J., Berelson, W.M., Severmann, S., Johnson, K.S., Hammond, D.E., Roy, M., Coale, K.H., 2012. Benthic manganese fluxes along the Oregon–California continental shelf and slope. Cont. Shelf Res. 43, 71–85. http://dx.doi.org/10.1016/j.csr.2012.04.016.

Morel, F.M.M., Milligan, A.J., Saito, M.A., 2014. Marine bioinorganic chemistry: the role of trace metals in the oceanic cycles of major nutrients. Treatise on Geochemistry. Elsevier, pp. 123–150.

Muiños, S.B., Hein, J.R., Frank, M., Monteiro, J.H., Gaspar, L., Conrad, T., Pereira, H.G., Abrantes, F., 2013. Deep-sea Fe-Mn crusts from the northeast Atlantic Ocean: composition and resource considerations. Mar. Georesources Geotechnol. 31, 40–70. http://dx.doi.org/10.1080/1064119X.2012.661215.

Nozaki, Y., Yang, H.-S., Yamada, M., 1987. Scavenging of thorium in the ocean. J. Geophys. Res. 92, 772. http://dx.doi.org/10.1029/JC092iC01p00772.

Oskin, M., Stock, J., 2003. Pacific–North America plate motion and opening of the Upper Delfin basin, northern Gulf of California, Mexico. Geol. Soc. Am. Bull. 115, 1173. http://dx.doi.org/10.1130/B25154.1.

Paduan, J.B., Clague, D.A., Davis, A.S., 2009. Evidence that three seamounts off southern California were ancient islands. Mar. Geol. 265, 146–156. http://dx.doi.org/10.1016/j.margeo.2009.07.003.

Paytan, A., Griffith, E.M., 2007. Marine barite: recorder of variations in ocean export productivity. Deep Sea Res. Part II Top. Stud. Oceanogr. 54, 687–705. http://dx.doi.org/10.1016/j.dsr2.2007.01.007.

Paytan, A., Mearon, S., Cobb, K., Kastner, M., 2002. Origin of marine barite deposits: Sr and S isotope characterization. Geology 30, 747. http://dx.doi.org/10.1130/0091-7613(2002)030<0747:OOMBDS>2.0.CO;2.

Pisias, N.G., Murray, R.W., Scudder, R.P., 2013. Multivariate statistical analysis and partitioning of sedimentary geochemical data sets: general principles and specific MATLAB scripts: technical brief. Geochem. Geophys. Geosystems 14, 4015–4020. http://dx.doi.org/10.1002/ggge.20247.

Powell, R.E., Weldon, R.J., 1992. Evolution of the San Andreas Fault. Annu. Rev. Earth Planet. Sci. 20, 431–468. http://dx.doi.org/10.1146/annurev.ea.20.050192.002243.

Puteanus, D., Halbach, P., 1988. Correlation of Co concentration and growth rate — a method for age determination of ferromanganese crusts. Chem. Geol. 69, 73–85. http://dx.doi.org/10.1016/0009-2541(88)90159-3.

Qin, L., Humayun, M., 2008. The Fe/Mn ratio in MORB and OIB determined by ICP-MS. Geochim. Cosmochim. Acta 72, 1660–1677. http://dx.doi.org/10.1016/j.gca.2008.01.012.

Rajani, R.P., Banakar, V.K., Parthiban, G., Mudholkar, A.V., Chodankar, A.R., 2005. Compositional variation and genesis of ferromanganese crusts of the Afanasiy–Nikitin Seamount, Equatorial Indian Ocean. J. Earth Syst. Sci. 114, 51–61. http://dx.doi.org/10.1007/BF02702008.

Rowden, A.A., Dower, J.F., Schlacher, T.A., Consalvey, M., Clark, M.R., 2010. Paradigms in seamount ecology: fact, fiction and future: paradigms in seamount ecology. Mar. Ecol. 31, 226–241. http://dx.doi.org/10.1111/j.1439-0485.2010.00400.x.

Roy-Barman, M., Chen, J.H., Wasserburg, G.J., 1996. ^{230}Th—^{232}Th systematics in the central Pacific Ocean: the sources and the fates of thorium. Earth Planet. Sci. Lett. 139, 351–363. http://dx.doi.org/10.1016/0012-821X(96)00017-9.

Rudnick, R.L., Gao, S., 2014. Composition of the continental crust. Treatise on Geochemistry. Elsevier, pp. 1–51.

Ryan, W.B.F., Carbotte, S.M., Coplan, J.O., O'Hara, S., Melkonian, A., Arko, R., Weissel, R.A., Ferrini, V., Goodwillie, A., Nitsche, F., Bonczkowski, J., Zemsky, R., 2009. Global Multi-Resolution Topography synthesis. Geochem. Geophys. Geosyst. 10, Q03014. http://dx.doi.org/10.1029/2008GC002332.

Talley, L.D., 2008. Freshwater transport estimates and the global overturning circulation: shallow, deep and throughflow components. Prog. Oceanogr. 78, 257–303. http://dx.doi.org/10.1016/j.pocean.2008.05.001.

Talley, L.D., Joyce, T.M., 1992. The double silica maximum in the North Pacific. J. Geophys. Res. 97, 5465. http://dx.doi.org/10.1029/92JC00037.

Taylor, S.R., McLennan, S.M., 1985. The continental crust: its composition and evolution. Geol. Mag. 122, 673. http://dx.doi.org/10.1017/S0016756800032167.

White, W.M., Klein, E.M., 2014. Composition of the oceanic crust. Treatise on Geochemistry. Elsevier, pp. 457–496.

Chapter 2. River sediment sources to the Monterey Canyon Submarine Canyon System- constraints from Fe-Mn crust Os, Nd, and Pb isotopes

Tracey A. Conrad[a,b]*, Sune Nielsen[b], Bernhard Peucker-Ehrenbrink[b], Jurek Blusztajn[b], Dustin Winslow, James R. Hein[c], and Adina Paytan[a]

[a] University California Santa Cruz, 1156 High Street, Santa Cruz, CA 95060, USA

[b] Woods Hole Oceanographic Institute, WHOI, 266 Woods Hole Road, Woods Hole, MA 02543, USA

USA

[c] U.S. Geological Survey, PCMSC, 2885 Mission St., Santa Cruz, CA, 95060, USA

*Corresponding Author: Tracey A. Conrad

Submitted: *Geoscience, Geophysics, Geosystems*

Abstract

The sources of terrestrial material delivered to the California margin over the past 7 Myr were assessed using $^{187}Os/^{188}Os$, ƐNd, and Pb isotopes in hydrogenetic ferromanganese (Fe-Mn) crusts from three seamounts along the central and southern California margin. From 6.8±0.5 to 4.5±0.5 Ma, all three isotope systems had more radiogenic values at Davidson Seamount, located near the base of the Monterey Canyon System, than in Fe-Mn crusts from Taney and Hoss seamounts farther away. Osmium isotopes also deviate from the Cenozoic osmium isotope seawater curve towards more radiogenic values from 6.8±0.5 to 4.5±0.5 Ma at the Taney Seamounts, approximately 150 km farther offshore from Davidson Seamount. However, unlike samples from Davidson Seamount, Pb and Nd isotopes in Taney Seamount Fe-Mn crusts do not deviate from regional seawater values. None of the isotopes deviate from seawater values in Fe-Mn crusts from Hoss Seamount located approximately 450 km to the south. Our data indicate that substantial input of dissolved and particulate terrestrial material are responsible for the local deviations in the seawater Nd, Pb, and Os isotopes from 6.8±0.5 to 4.5±0.5 Ma. The isotope ratios are consistent with a southern Sierra Nevada or western Basin and Range provenance of the terrestrial material delivered via riverine input to the canyon during that time period. The initiation of the modern Monterey Canyon incision has been constrained to between 10 Ma and 6.8±0.5 Ma based on our data, the age of incised strata, and the paleo location of the Monterey Canyon relative to paleo-coastline.

2.1 Introduction

The Monterey Canyon (MC) is the main channel of the Ascension-Monterey Canyon system and the dominant feature of central California's Monterey Bay National Marine Sanctuary [Greene et al., 1989; Greene and Hicks, 1990; Eittreim et al., 2002]. On scale with the Grand Canyon, the MC has a maximum vertical relief of 1700 m, width of ~12 km, and length including the fan-valley of 470 km [Greene et al., 2002]. The age and history of the canyon system are poorly known. Here hydrogenetic ferromanganese crust records of paleo-seawater chemistry are used to shed new light on terrestrial inputs into the California margin proximal to the canyon system.

2.1.1 Canyon Systems

The Ascension-Monterey Canyon system includes six canyons with sixteen canyon heads and extends 153 km off the modern shoreline, reaching a depth of 3600 m below sea level [Greene and Hicks, 1990; Greene et al., 2002]. The Ascension Canyon system located north of the MC includes the three canyons, that do not reach the modern coastline, and the fan-valley combines with that of the Monterey Canyon system (MCS) at ~3,290 m water depth [Greene and Hicks, 1990]. Above ~3,290 m, the Ascension and Monterey Canyon systems are separated by a smooth ridge with chemosynthetic communities and active methane seep-induced carbonate precipitation [Greene and Hicks, 1990; Greene et al., 2002]. The MCS includes the Soquel, and Carmel canyons, which join the MC at 970 m and ~2000 m water depths, respectively [Greene and Hicks, 1990; Greene et al., 2002]. It has been proposed that

the MCS was initially incised in the Oligocene to early Miocene, near the current location of California's Transverse Range, possibly subaerially [Greene, 1977; Greene and Hicks, 1990]. That paleo MC was then filled and re-exhumed possibly more than once to form the modern MC [Greene, 1977; Greene and Hicks, 1990]. Overall, the age and initial formation of the modern MC and MCS are poorly known.

Today, the Monterey and Carmel canyons are the only canyons extending to the shoreline. Several rivers drain into Monterey Bay north and south of the MC, but only the Salinas River and Elkhorn Slough feed into the MC at Moss Landing [Best and Griggs, 1991; Eittreim et al., 2002; Greene et al., 2002]. Active sediment deposition during the modern sea-level highstand in the MC is consistent with submarine canyons studied off southern California [Eittreim et al., 2002; Covault et al., 2007]. In addition to fluvial sediments, the MCS also traps sediment carried by longshore currents and from local erosion of sea cliffs, gullies, and mountain streams [Best and Griggs, 1991; Eittreim et al., 2002; Greene et al., 2002]. Trapped sediment is carried down canyon episodically by turbidity events and causes further canyon incision [Greene and Hicks, 1990; Paull et al., 2003; Covault et al., 2007].

2.1.2 Geology

The MCS lies along an active tectonic margin spanning the boundary of the Pacific and North American plates [Anima et al., 2002; Eittreim et al., 2002; Greene et al., 2002]. The region is dominated by right-lateral strike slip movement from the San Andreas and San Gregorio fault systems [Anima et al., 2002]. The MCS primarily cuts into the allochthonous Salinian block, which is bounded to the east by

the San Andreas fault and is mainly composed of Cretaceous granite, bounded by rocks of the Franciscan complex [Greene, 1977; Anima et al., 2002; Barbeau et al., 2005]. The complex tectonic environment makes reconstructing movement difficult. It is thought that parts of the Ascension Canyon system, the Año Nuevo Canyon, originated as a channel to the Monterey Canyon during the Pliocene lowstand (~3.8 Ma) [Nagel et al., 1986; Greene and Hicks, 1990]. It is presumed that other canyons in the Ascension canyon system originated from the lower MC during sea level lowstands and have undergone displacement to reach their present locations [Greene and Hicks, 1990]. If that is true, right lateral motion or excavation of the canyon systems would have increased as there is an increased distance between canyons of the Ascension Canyon System (1 to 4 km apart) and the Monterey Canyon System around 30 km apart, with time starting from around 10 to 7 Ma [Greene and Hicks, 1990].

Sedimentary particulate and dissolved inputs through the MCS and sediment deposition on the continental shelf and in the Monterey Fan are affected by tectonic, eustatic, climatic, and oceanographic processes [Griggs and Hein, 1980; Edwards, 2002; Lewis et al., 2002]. Rivers are the main source of sedimentary and dissolved material to the California margin [Griggs and Hein, 1980; Best and Griggs, 1991]. Modern river sediment fluxes are affected by anthropogenic activities with many activities causing an increase in sediment flux while reservoir building and conservation activities decrease the sediment flux [Meade, 1969; Griggs and Hein, 1980; Jeandel and Oelkers, 2015]. This is reflected in California's rivers where

mining, agriculture, and timber harvesting have increased the sediment and dissolved load [Griggs and Hein, 1980]. Inputs through the MCS have been affected by anthropogenic activities, making the volume and source of paleo-inputs unclear and identifying the past source of material transported to the MCS challenging.

Reconstructing the stratigraphy of sedimentary sequences in the Monterey Bay region is also complicated by unconformities. Previous work around the Monterey Bay has shown that primarily Neogene strata overlies the Mesozoic basement complex without the presence of Paleogene deposits [Greene, 1977; Greene and Hicks, 1990]. There are also unconformities bounding sedimentary deposits of late Miocene to Pliocene, and late Pliocene to Holocene, ages [Greene, 1977]. Seismic-reflection data show that the MC and some related canyons incised into Mesozoic basement rock and are filled with middle Miocene and younger sediment, implying a pre-middle Miocene origin for the paleo-canyons [Greene, 1977; Greene and Hicks, 1990]. Uninterrupted sedimentation occurred in the Monterey Bay region during the middle to late Miocene, evidenced by conformable strata filling canyons in the upper MCS near the coastline on seismic-reflection profiles. The modern MC cuts through this material indicating incision of the canyon occurred since the middle Miocene [Greene, 1977; Greene and Hicks, 1990]. Formation of the modern MC is thought to have begun in the late Pliocene by erosion of canyon fill from seaward sediment transport [Greene and Hicks, 1990]. It has also been proposed that the MC was re-exhumed during two separate events occurring in the late Miocene and the Pleistocene [Greene, 1977; Greene and Hicks, 1990].

During the early to middle Miocene, the coastline was further east (inland) than today (Fig. 2.1) [Bowersox, 2005; Müller et al., 2008]. The San Joaquin Basin, southeast of the modern Monterey Bay, was connected to the Pacific in the west and extended to the Sierra Nevada Mountains in the east with a depth of ~250 m below sea level (bsl) in the center of the basin [Johnson and Graham, 2007; Pyenson et al., 2009]. By the late Miocene to Pliocene, the major rivers draining the southern Sierra Nevada flowed westward, possibly emptying into the San Joaquin Basin [Graham et al., 1988; Reid, 1995; Wakabayashi and Sawyer, 2001; Bowersox, 2004, 2005]. This resulted in rates of sediment deposition that equaled or exceeded the rate of basin subsidence, causing gradual, progressive shallowing of the basin with a maximum rate of 140 cm/kyrs in the early Pliocene during uplift of the Coast Range [Loomis, 1990; Bowersox, 2004, 2005]. In the late Pliocene, after the uplift of the Temblor and Gabilan Ranges along the western margin of the San Joaquin Basin, the basin was connected to the Pacific only through the Priest Valley Strait, which closed around 2.2 Ma due to tectonic uplift and sedimentation [Loomis, 1990; Bowersox, 2004, 2005].

2.1.3 Hydrogenetic Ferromanganese Crust Paleo-Seawater Records

The inputs into the California margin proximal to the MCS were determined using hydrogenetic ferromanganese (Fe-Mn) crust records of paleo-seawater chemistry. Fe-Mn crusts grow over millions of years on elevated rock surfaces, such as seamounts, when slope or submarine currents are sufficient to prevent sediment accumulation [Bonatti et al., 1972; Hein and Koschinsky, 2014]. Hydrogenous Fe-Mn

crusts grow very slowly (1 to 5 mm/Myr) by precipitation of dissolved elements from seawater and they record changes in seawater chemistry over the time of their growth [Halbach and Puteanus, 1984; Hein and Koschinsky, 2014].

Numerous seamounts exist along the California Margin including several (Guide, Pioneer, Gumdrop, Davidson) proximal to the MCS as well as farther away from the MCS on the Pacific plate. Hydrogenetic Fe-Mn crust samples were selected from Davidson, Taney B and D, and Hoss seamounts (Fig. 2.1). Davidson seamount overlies the Salinian granitic block at the base of the MC fan and would have moved with the MCS since emplacement of the block 14.8 to 9.8 Ma [Davis et al., 2002; Clague et al., 2009]. Taney B and D seamounts lie approximately 150 km offshore from the MC on the Pacific Plate. They are part of a chain of five seamounts and formed approximately 26 Ma [Coumans et al., 2015]. Hoss seamount was selected to provide a regional control away from the MCS as it is also located on the Pacific Plate, but is significantly farther south of the MCS, offshore of San Diego. Hoss Seamount is estimated to be 22 to 17 Ma [Hein et al., 2010; Conrad et al., 2017a].

2.1.4 Osmium Isotopes

Estimates of the residence time of osmium in seawater vary from few thousand to about 50 kyr, pegging this element at the transition between an ocean-wide well mixed reservoir [Levasseur et al., 1999] and tracers that can show regional variations in isotope composition [Paquay and Ravizza, 2012]. Having such an interesting residence time not only makes the marine Os isotope system responsive to climatic (short-term) as well as tectonic (long-term) forcings, it also increases the

likelihood of observing strong regional forcings from inputs with isotope signatures very different from that of contemporaneous seawater. Most of the scarce water column profiles of Os are consistent with conservative behavior in seawater with an $^{187}Os/^{188}Os$ ~1.06, though indications of non-conservative behavior in oxygen minimum zones have been observed [Sharma and Wasserburg, 1997; Levasseur et al., 1999; Woodhouse et al., 1999; Peucker-Ehrenbrink and Ravizza, 2000; Zeng et al., 2014]. Osmium is not subject to significant diffusive re-equilibration in Fe-Mn crusts [Burton et al., 1999b; Klemm et al., 2005]. This allows Os to be used to develop age models for the Fe-Mn crust samples by comparing the $^{187}Os/^{188}Os$ of subsamples collected through a crust with the Cenozoic Os isotope seawater curve [Burton et al., 1999b; Klemm et al., 2005; Peucker-Ehrenbrink and Ravizza, 2012] (A2.1.2 Osmium Isotopes).

2.1.5 Neodymium Isotopes

Neodymium has a residence time in seawater of 400 to 950 years, shorter than the ~1000 year mixing time of the global ocean [David et al., 2001; Lacan et al., 2012]. The Nd isotope composition of seawater is controlled by the isotopic signature of the source inputs, which in turn is controlled by weathering of source rocks, and varies in different water masses in the oceans [Goldstein et al., 1984; Frank, 2002; van de Flierdt et al., 2016]. Fluvial and aeolian inputs are both important sources of Nd to the ocean but cannot account for the mass balance of Nd in seawater [Goldstein et al., 1984; van de Flierdt et al., 2016]. Other sources of Nd that influence seawater near the continental margin include submarine groundwater discharge, reversible

scavenging, fluxes from sediment pore waters, and chemical reactions between terrestrial particles and seawater “boundary exchange” [Lacan and Jeandel, 2005; Jeandel and Oelkers, 2015; Du et al., 2016]. The Nd isotope signature of Fe-Mn crusts is generally thought to reflect changes in water masses, but continental input, benthic flux, and boundary exchange processes with the continental shelf and slope must also be taken into account particularly in coastal areas [Abouchami et al., 1997; Jeandel and Oelkers, 2015; van de Flierdt et al., 2016]**.** In Fe-Mn crusts, Nd does not re-equilibrate with modern seawater or diffuse noticeably within the crust [Abouchami et al., 1997; Frank, 2002; Bau and Koschinsky, 2006].

2.1.6 Lead Isotopes

Lead is considered to be a closed system in Fe-Mn crusts [Abouchami et al., 1997; Ling et al., 2005; Chen et al., 2013]. In seawater, Pb has a scavenged-type element profile with a relatively short residence time of 80-100 years [Flegal and Patterson, 1983]. Aeolian dust, fluvial input, and hydrothermal fluids are all sources of Pb to the oceans [Frank, 2002]. Anthropogenic activity has altered the dissolved seawater lead isotope signature in the modern oceans [Boyle et al., 2014]. Minerals hosing Pb have different time-integrated U-Pb and Th-Pb compositions and different susceptibilities to weathering resulting in variations between the Pb isotope composition of source rocks and the transported weathered material [Erel et al., 1994; Frank, 2002].

2.2 Methods

The geochemical composition of bulk Fe-Mn crust samples has been analyzed previously [Conrad et al., 2017a]. The Fe-Mn crusts used are hydrogenetic with Fe/Mn ratios ranging from 1.00 to 1.53. A hydrogenetic origin was confirmed by plotting the data for selected Fe-Mn crust samples on the ternary discrimination diagram with Fe, Mn, and Co+Ni+Cu end members [Bonatti et al., 1972; Conrad et al., 2017a]. When possible, the thickest crusts from each seamount were chosen as these are typically the oldest crusts and allow for a higher temporal resolution and longer duration records. Consideration was also given to water depth; the two samples from Davidson and the two samples from Taney seamounts differ in water depth by approximately 1000 m (and may represent different water masses). Samples were encased in Tap Plastic Clear-Lite Casting Resin and cut using a sintered diamond blade into billets perpendicular to the growth layers. Samples for Os and Nd isotopes were subsampled using a New Wave Micromill with Brasslinger 1 mm cylindrical (flat head) diamond tipped drill bit. Osmium was sampled at 2 mm intervals through the crust. Neodymium was sampled at 0.3 mm intervals. However, for both isotope systems not every subsample was analyzed, resulting in a sampling resolution lower than the sampling interval.

All three isotope systems, Os, Nd, and Pb were analyzed at the Woods Hole Oceanographic Institute (WHOI) inductively coupled plasma mass spectrometer (ICPMS) facility using a Thermo Finnigan NEPTUNE multi-collector ICPMS (MC-ICPMS). Two Fe-Mn crusts each were selected from the Hoss, Davidson, and Taney

seamounts (B and D) to measure Os isotopes and create age models for paleoceanographic study. USGS nodule standard A-1 was prepared together with the crust samples using an Anton Parr high-pressure asher (HPA-S). Osmium isotopes were measured using an Ar gas sparging method with three ion counters on the NEPTUNE ICPMS [Sen and Peucker-Ehrenbrink, 2014]. Measurements of Re concentrations on an Element 2 ICPMS showed that Re concentration in the in the Fe-Mn crust samples was extremely low and that in-growth corrections of ^{187}Os to account for the decay of ^{187}Re within the crusts was not necessary, even in the bottom (oldest) sections of these samples, a finding consistent with previous studies [Klemm et al., 2008]. Multiple analysis (n=48) of the LoOsStd reference standard over multiple analysis sessions yielded an average $^{187}Os/^{188}Os$ value of 0.1098±0.0041, within error of the reference value (0.1069) and a 2σ standard deviation of 0.0042 [Sen and Peucker-Ehrenbrink, 2014] (Supplemental Table S2.1). Multiple analysis of the USGS A-1 nodule standard, prepared with the Fe-Mn crust samples yielded an average $^{187}Os/^{188}Os$ value of 0.9693±0.0129 (n=15) and a 2σ standard deviation of 0.0252, when three samples with anomalously low $^{187}Os/^{188}Os$ are excluded. Two of the excluded samples A1-9 and A1-10 had unknown contamination on the ^{185}Re, ^{194}Pt, and ^{196}Pt masses (mass/charge) (see A2.1.2 Osmium Isotopes).

Neodymium isotopes were measured in four Fe-Mn crusts that had an Os age model, one each from Hoss and Taney B, and two Fe-Mn crusts from Davidson seamounts. Nodule standards USGS A-1 and P-1 were prepared together with the Fe-Mn crust samples using 50-100 μm particle size Eichrom Ln resin and analyzed on

the MC-ICPMS following the method of Scher and Delaney (2010). Neodymium isotopes are corrected to JNdi-1 = 0.512115 and expressed as ƐNd, which is the $^{143}Nd/^{144}Nd$ ratio normalized to Chondritic Uniform Reservoir (CHUR = 0.512638), [ƐNd(($^{143}Nd/^{144}Nd_{samp}$/CHUR)-1) x 1000] [Jacobsen and Wasserburg, 1980]. Measurements Nd occurred in the fall of 2014 and the spring of 2015, analyses of the JNdi-1 standard yielded 2σ ƐNd 0.29 (n=31), and 2σ ƐNd 0.10 (n=14) respectively. (Supplemental Table S2.2). Analysis of the USGS A-1 nodule standard (n=16) gave an average value of 0.5121770 (ƐNd = -9.13) and a 2σ ƐNd 0.31.

Lead isotopes were measured in three Fe-Mn crusts and in pressed pellets of USGS nodule standards A-1 and P-1 using NewWave/Merchantek NWR-193 homogenized ArF excimer laser ablation (LA) system coupled with the NEPTUNE MC-ICPMS [Foster and Vance, 2006b]. Standard sample bracketing was used to correct for Pb isotope fractionation as the Tl fractionation factor was not resolvable. Repeated analysis of the USGS A-1 nodule standard yielded average values of $^{206}Pb/^{204}Pb$ (19.211, 2σ 0.078), $^{207}Pb/^{204}Pb$ (15.980, 2σ 0.090), and $^{208}Pb/^{204}Pb$ (39.916, 2σ 0.291), (n=85). Repeated analysis of the USGS P-1 nodule standard yielded average values of $^{206}Pb/^{204}Pb$ (18.958, 2σ 0.0836), $^{207}Pb/^{204}Pb$ (15.936, 2σ 0.0478), and $^{208}Pb/^{204}Pb$ (39.668, 2σ 0.304), (n=85). A Python code was written to process the laser ablation Pb isotopic data, including separating background from sample data and applying corrections based on the paired standards bracketing the samples (see A2.1.5 Python Code and supplemental materials S2.1-S2.3).

2.3 Results

2.3.1 Osmium Isotopes

Osmium $^{187}Os/^{188}Os$ were measured in 86 samples from six Fe-Mn crusts and plotted against the Cenozoic seawater Os isotope curve to determine ages (Fig. 2.2, Supplemental Table S2.1). Samples from the control site Hoss Seamount generally can be fitted to the seawater curve and yield maximum ages of 20.5 ±0.5 Myr for D11-4 (2,540-2,560 mbsl) and 5.4±0.5 Myr for D11-11 (2,540-2,560 mbsl) with variable growth rates. Fe-Mn crust samples D173-R2 Taney B (3,178 mbsl), T121-R5 Taney D (3,887 mbsl), and Davidson T145-R9 (3,298 mbsl) and T141-R5 (2,388 mbsl) fit the seawater curve from approximately 4.5±0.5 Ma to present. All four Fe-Mn crust samples older than 4.5±0.5 Ma deviate from the Cenozoic seawater Os isotope curve towards more radiogenic values (Fig. 2.2), making age determinations impossible. Ages for the samples were therefore extrapolated using a constant growth rate as the most conservative estimate, and are also constrained by the age of the substrate on which they grew. Davidson Seamount Fe-Mn crusts T145-R9 and T141-R5 started growing 6.4±0.5 and 6.7±0.5 Ma respectively, with growth rates of 7.6 and 5.6 mm/Myr. Crust T121-R5 had a growth rate of 6.0 mm/Myr and growth was initiated at 5.6±0.5 Ma, while D173-R2 had a growth rate of 7.5 mm/Myr and is 6.8±0.5 Myr old. The deviation to more radiogenic Os isotopes relative to seawater is detected from the beginning of crust growth and therefore predated Fe-Mn crust accretion of the samples studied. The oldest Fe-Mn crust to show this deviation is D173-R2 from Taney B Seamount with an estimated age of 6.8±0.5 Myr. That

provides a minimum age range for the radiogenic Os isotope excursion of 6.9 to 4.5 Ma, spanning at least 2.3 Myr.

2.3.2 Neodymium Isotopes

Neodymium isotopes were measured in 190 samples from four of the six Fe-Mn crusts for which Os isotope age models were created. Fe-Mn crusts D11-4 (Hoss) and D173-R2 (Taney) have ƐNd values consistent with those from central Pacific Fe-Mn crusts [Ling et al., 1997, 2005; Frank, 2002; Chen et al., 2013] (Supplemental Fig. A2.6; Supplemental Table S2.2). Both Davidson Seamount Fe-Mn crusts T145-R9 and T141-R5 show deviations in ƐNd towards more radiogenic values that may have started before the crusts began to grow. The deviation from regional seawater values, represented by Hoss D11-4, is particularly prominent in crust T145-R9 which, increases from -3.3 to -2.0 ƐNd units from ~6.7±0.5 to 4.5±0.5 Ma (Fig. 2.3). There is only a minor radiogenic ƐNd excursion in T141-R5 which is most noticeable from ~4.5±0.5 to 5.3±0.5 Ma and then becomes slightly less radiogenic in the oldest part of the crust returning to ƐNd values consistent with Hoss D11-4 from ~6.4±0.5 to 6.2±0.5 Ma. The Fe-Mn crust D173-R2 from Taney B Seamount does not show the excursion seen in the two Davidson Seamount crusts.

2.3.3 Lead Isotopes

Three Fe-Mn crusts with a total of 400 samples, D11-4 (188), D173-R2 (87), and T145-R9 (125) from Hoss, Taney, and Davidson Seamounts respectively, were analyzed for Pb isotopes at high resolution using LA-MC-ICPMS (Supplemental

Table S2.3; A2.6). The Pb isotope ratios in T145-R9 from Davidson Seamount deviate from 5.3±0.5 to 4.8±0.5 Ma away from regional seawater values, recorded in Hoss Fe-Mn crust D11-4. However, the Pb isotope ratios in Fe-Mn crusts D173-R2 and D11-4 from Taney B and Hoss seamounts do not show any significant changes during that time. The unusually radiogenic $^{206}Pb/^{204}Pb$, $^{207}Pb/^{204}Pb$, and $^{208}Pb/^{204}Pb$ values in T145-R9 lasted for about 500 kyr, and a possible second, minor peak at 5.5±0.5 Ma lasted for about 200 kyr this is also apparent when comparing $^{207}Pb/^{206}Pb$ where lower values represent the excursion (Fig. 2.3; A2.9).

2.4 Discussion

2.4.1 Isotope Excursions in California Margin Fe-Mn Crusts

The deviation of $^{187}Os/^{188}Os$ away from the Cenozoic Os isotope seawater curve towards more radiogenic values from about 6.8±0.5 or prior to 4.5±0.5 Ma is accompanied by Nd isotope deviations recorded in the two Davidson Seamount Fe-Mn crusts over the same time period, which also coincide with an excursion towards radiogenic Pb isotope values in T145-R9 (Fig. 2.3). The changes towards more radiogenic Os isotope values relative to the Os isotope seawater curve in the four Fe-Mn crusts from Davidson and Taney seamounts was surprising given the long residence time and uniform distribution of Os in seawater [Levasseur et al., 1999; Peucker-Ehrenbrink and Ravizza, 2000, 2012]. Approximately 80% of the Os in seawater is from continental crustal material, with hydrothermal, and extraterrestrial

sources providing the remainder [Sharma and Wasserburg, 1997; Williams and Turekian, 2002].

Modern seawater has an $^{187}Os/^{188}Os$ of ~1.06 [Peucker-Ehrenbrink and Ravizza, 2000] whereas fresh Mid-Ocean Ridge Basalt (MORB) is characterized by a value of 0.133 [Gannoun et al., 2006; Zeng et al., 2014], slightly less radiogenic than unaltered abyssal peridotite ($^{187}Os/^{188}Os = 0.121$) [Harvey et al., 2011; Zeng et al., 2014]. Hydrothermal $^{187}Os/^{188}Os$ values at the Juan de Fuca Ridge, approximately 1,200 km north of the MCS, range from 0.11 to 1.04 [Sharma et al., 2000, 2007]. Hydrothermal seafloor massive sulfides have $^{187}Os/^{188}Os$ between 0.968 to 1.209 [Zeng et al., 2014]. Hydrothermal inputs are therefore unlikely to have provided the radiogenic Os observed in Taney and Davidson seamount Fe-Mn crusts.

Extraterrestrial sources have a much less radiogenic $^{187}Os/^{188}Os$ signature than seawater of ~0.12 – 0.13 and have high Os concentrations [Peucker-Ehrenbrink and Ravizza, 2000; Horan et al., 2003; Brandon et al., 2006]. Extraterrestrial material would therefore cause an excursion in the opposite direction to that observed in Davidson and Taney seamount Fe-Mn crusts. Fe-Mn crusts with $^{187}Os/^{188}Os$ that plot below the Os seawater curve have been shown to contain micrometeorite fragments [Peucker-Ehrenbrink and Ravizza, 2000; Klemm et al., 2005]. A few Fe-Mn crust samples analyzed here show less radiogenic values relative to the Os seawater curve. attribute these values to the presence of extraterrestrial material. Specifically, Hoss D11-4 has an Os isotope ratio below the seawater curve ~2.6±0.5 Ma, the timing of

which is within error of the Eltanin asteroid impact (2.51±0.07) in the South Pacific [Goff et al., 2012].

Change in water column processes such as changes in ocean productivity may affect the concentrations of Os, Nd, and Pb available to be incorporated into Fe-Mn crusts, but are unlikely to impact the isotope ratios recorded in the crusts. Unlike Nd concentration data which mimic nutrient-like depth profiles in seawater, ƐNd appears to trace water masses and does not co-vary with chlorophyll-a [Stichel et al., 2012; Jeandel and Oelkers, 2015; Hu et al., 2016]. Lead isotopes are even less likely to be influenced by primary productivity, as Pb is not utilized by primary producers [Chow and Patterson, 1962; Flegal and Patterson, 1983]. Increased burial of Os caused by enhanced primary productivity or decrease in deep-water dissolved oxygen concentrations does not affect the $^{187}Os/^{188}Os$ values as evident from measurements at ODP site 849 that is located in the eastern equatorial Pacific [Dalai et al., 2005]. Hence changes in marine primary productivity cannot explain the isotopic offset observed prior to 4.5±0.5 Ma in Fe-Mn crusts collected close to the MCS.

Aeolian dust transported to seawater has an $^{187}Os/^{188}Os$ of 1.05±0.2 and an Os concentration of ~30 pg/g [Peucker-Ehrenbrink and Jahn, 2001], but little of the Os in dust is expected to dissolve in seawater. The $^{187}Os/^{188}Os$ of average fluvial inputs is likely more radiogenic (~1.4) than average crustal material because easily weatherable, Os-rich lithologies, such as sediments rich in organic matter, have more radiogenic isotope values [Peucker-Ehrenbrink and Ravizza, 2000; Dubin and Peucker-Ehrenbrink, 2015]. Overall, aerosol deposition is likely a small fraction of

the overall continental input [Sharma and Wasserburg, 1997; Williams and Turekian, 2002]. This favors fluvial input of Os into the California margin through the MCS as the most likely source. Inputs from rivers transporting dissolved and particulate terrestrial material has been shown to affect local seawater $^{187}Os/^{188}Os$ [Sharma et al., 1999; Martin et al., 2000].

Model calculations using ƐNd over the past 14 Myr from North Pacific Fe-Mn crusts indicate that dust dissolution provided just a few percent of dissolved Nd in this region for the time of interest, >6.8 to 4.5 Ma [Pettke et al., 2000; van de Flierdt et al., 2004a]. Rivers are the main source of sediment to the central California margin, a region that has storm-dominated shelves where sediment input is often dominated by episodic floods [Best and Griggs, 1991; Edwards, 2002; Lewis et al., 2002]. Fluvial sediment is normally transported past the littoral zone and may be deposited on or off the continental shelf [Edwards, 2002; Lewis et al., 2002]. On-shelf sediments can subsequently be advectied, or resuspended during high-energy events, and transported significant distances along-shore [Best and Griggs, 1991; Ogston and Sternberg, 1999; Edwards, 2002].

Resuspension and transport of sediment may affect the concentrations and isotope signatures of Os and Nd. Marine Os is scavenged in estuary and coastal zone sediments, reducing the flux of dissolved fluvial Os transported to the ocean [Martin et al., 2000, 2001; Williams and Turekian, 2004]. However, it is also possible that changes in salinity may cause the release of previously non-soluble Os sequestered in sediments [Martin et al., 2001]. It has been well documented that the release of Nd

from sediments along continental margins due to the dissolution of terrestrial particulate material can change the ƐNd signature of regional seawater [Lacan and Jeandel, 2005; Arsouze et al., 2007; Stichel et al., 2012; Garcia-Solsona et al., 2014; Jeandel and Oelkers, 2015]. Sediment resuspension and release of Nd and possibly Os are potential sources of these elements to California margin seawater from >6.8 to 4.5±0.5 Ma. Based on these observations and arguments, we attribute the Os, Nd, and Pb isotope excursions from >6.8 to 4.5±0.5 Ma to large volumes of radiogenic terrestrial material entering the California margin at that time. This is consistent with sedimentation rates observed in the San Joaquin Basin when infill of the basin occurred as the rate of sedimentation exceeded subsidence rates; in the latest Miocene the basin was subsiding at rates of approximately 25 cm/kyr, but a maximum rate of 140 cm/kyrs occurred in the early Pliocene during uplift of the Coast Range, and rates slowed to 11 to 86 cm/kyr in the late to latest Pliocene [Bowersox, 2005].

2.4.2 Timing the incision of the modern Monterey Canyon

Isotope records in continent proximal Fe-Mn crusts, reported here, show that from before 6.8±0.5 Ma and up to 4.5±0.5 Ma the base of the MCS at Davidson Seamount was bathed in more radiogenic dissolved Os, Nd, and Pb. For Os, the radiogenic signature was apparent for ~150 km farther offshore and was also recorded in Fe-Mn crusts from the Taney Seamount chain. We propose that the radiogenic Os isotope signal reflects large volumes of terrestrial material transported into the system from prior to 6.8±0.5 and until 4.5±0.5 Myr. Such inputs may reflect increased incision of canyons along the coast. A case for an increase in incision due to greater

river transport is supported by the increase in spacing observed between the canyon heads of the Ascension and Monterey Canyon Systems [Nagel et al., 1986; Greene and Hicks, 1990]. If it is true, that the canyon heads in the Ascension Canyon System were at one time part of the MCS and have since been offset, then sediment transport down the MCS or right lateral motion must have increased from 10 to 7 Ma to account for the increased distances between the upper reaches of the canyons along the coast (Fig. 2.1) [Greene and Hicks, 1990]. This observation is consistent with the timing of the radiogenic isotope excursion recorded in Fe-Mn crusts from prior to 6.8±0.5 until 4.5±0.5 Ma.

Constraining total right-lateral offset within the Monterey Bay and slip rates is challenging. The Salinian block and MCS is bisected by several faults including the Palo Colorado-San Gregorio fault zone which caused northward displacement of canyons in the Ascension Canyon System from the MCS [Greene and Hicks, 1990]. The San Gregorio fault in Monterey Bay has only a moderate dip, a change from the steep near vertical dip observed along the rest of the San Gregorio Fault indicating strike slip movement, this may be due to interaction with the Monterey Bay Fault Zone and other nearby faults or changes in fault geometry within Monterey Bay [Langenheim et al., 2013]. This makes determining the slip rates in for the San Gregorio Fault in Monterey Bay difficult, especially since estimates and reconstructions of slip rates and total strike-slip offsets along the length of the San Gregorio fault vary widely [Dickinson et al., 2005; Langenheim et al., 2013].

The input of radiogenic material into the MCS most likely began before Fe-Mn crusts on Taney and Davidson Seamounts started to grow, ~6.8±0.5 and 6.4±0.5 Ma, respectively for the two oldest crusts. Since the modern MC cuts through middle Miocene strata, the incision of the canyon must have also occurred since the middle Miocene [Greene, 1977; Greene and Hicks, 1990]. This is supported by seismic-reflection profiles showing uninterrupted sedimentation in the canyons during the late to middle Miocene [Greene, 1977; Greene and Hicks, 1990]. Miocene strata form uniformly thick flat beds on either side of the MC but thin towards the canyon center, indicating possible incision of the MC in the late Miocene to Pliocene [Greene, 1977].

Approximately 10 Ma the MC would have been located south and slightly east of the canyon's current location, inland from present day San Diego and seaward from the paleo-coastline [Wilson et al., 2005; Müller et al., 2008; DeMets and Merkouriev, 2016]. By around 5 Ma the MC was on the coastline and would have been near the southern edge of the San Joaquin Basin (Fig 2.1) [Wilson et al., 2005; Müller et al., 2008; DeMets and Merkouriev, 2016]. The approximate reconstructed location of the MC was seaward of the coastline at 10 Ma, which makes incision of the canyon system due to fluvial input unlikely. However, submarine incision of the canyon due to down-canyon transport, hyperpycnal flows, and other turbidity currents is possible [Greene and Hicks, 1990; Mulder and Syvitski, 1995]. Large volumes of terrestrial material were deposited into the San Joaquin Basin as evidenced by late Pliocene sedimentary deposits up to 2,470 m thick, and by deposition exceeding the

subsidence rate of 140 cm/ky in the early Pliocene [Loomis, 1990; Bowersox, 2005]. By 5 Ma the reconstructed location of the MC head was coincident with the coastline, or very slightly landward [Bowersox, 2004, 2005; Wilson et al., 2005; DeMets and Merkouriev, 2016]. Incision of the modern MC occurred since the late Miocene (11.63 Ma) as the canyon cuts through late Miocene sediments. As the MC was seaward from the paleo-coastline at 10 Ma it is likely that incision of the canyon started after that time, closer to 7 Ma, after the canyon was closer to river and sediment sources. Around 7 Ma the head of the MC was near or above sea level and was located at the paleo-coastline. That is consistent with the >6.8±0.5 Ma onset of radiogenic Os and Nd isotope excursions in Davidson Seamount Fe-Mn crusts.

During the late Miocene the San Joaquin Basin southeast of the modern Monterey Bay was a shallow sea open to the Pacific on the western side that captured westward drainage from the southern Sierra Nevada [Loomis, 1988, 1990; Reid, 1995; Stanton and Dodd, 1997; Bowersox, 2005; Müller et al., 2008]. By the late Pliocene the basin was connected to the Pacific only through the Priest Valley Strait that connected to the Pacific near the modern location of the MC [Loomis, 1990; Bowersox, 2004, 2005]. Once cut off from open-ocean circulation, the San Joaquin Basin likely had a very different isotopic signature from that of open-ocean seawater. However, the connection to the Pacific was likely over 300 km north of the MC at 5 Ma. The Priest Valley Strait closed completely ~2.2 Ma while the isotope excursion in Davidson and Taney seamount Fe-Mn crusts had already returned to open-ocean seawater values by 4 Ma [Bowersox, 2005].

The return to open-ocean seawater values in Davidson and Taney seamount Fe-Mn crusts at 4.5±0.5 Ma coincides with the Pliocene orogeny in western California [Page et al., 1998; DeMets and Merkouriev, 2016]. Reconstruction of plate slip and rotation of the Sierra Nevada and Great Valley blocks with reference to the Pacific plate show that from 9 to 5.2 Ma, the plates were parallel to the San Andreas Fault, but that from 5.2 Ma onwards progressive clockwise rotation from the San Andreas Fault has occurred [DeMets and Merkouriev, 2016]. The Sierra Nevada-Great Valley block and the Pacific plate began to converge at an angle orthogonal to the San Andreas Fault from 5.2 to 4.2 Ma [DeMets and Merkouriev, 2016]. That coincides with the onset of the orogeny determined in other studies, with uplift of the Santa Lucia Range starting around 6 Ma and estimated onset of shortening in central California at around 3.9 to 3.4 Ma [Page et al., 1998; Ducea et al., 2003]. Most of Monterey Bay was emergent by the late Pliocene to early Pleistocene in part due to marine regression in addition to regional uplift [Nagel et al., 1986; Greene and Hicks, 1990]. We propose that this uplift of the California Coast Range and emergence of the Monterey Bay region may have terminated the isotopic excursion through a change in the dominant sediment sources. The change in Fe-Mn crust Os, Nd, and Pb isotope values towards compositions consistent with regional seawater at ~4.5±0.5 Ma may reflect a change in sediment type and river transport from fine-grained material and a larger dissolved fraction, to a coarser-grained river sediment load and a reduced dissolved flux. A decrease in catchment basin areas may also have decreased the amount of fluvial material transported into the MCS.

Incision of the modern MC starting in the late Miocene is consistent with the Os isotope excursion recorded in Fe-Mn crusts from Taney and Davidson seamounts. This helps to constrain the start of modern MC incision to the late Miocene between the start of the late Miocene 11.63 Ma to 6.8±0.5 Ma. This timing is earlier than the late Pliocene (~2.6 Myr) incision of the modern MC as proposed by Greene and Hicks [Greene and Hicks, 1990]. There is also no evidence in the Os, Nd, or Pb isotope records from any of the Fe-Mn crusts for a second separate event occurring in the Pleistocene (<2.6 Ma), as proposed by Greene [Greene, 1977]. However, a shorter incision event in the MCS since ~4 Ma that did not change the seawater isotope signature locally over several hundred thousand years, and was therefore not recorded in Fe-Mn crusts is possible as indicated by active transport in the canyon and associated incision continuing today.

2.4.3 Source Areas of Fluvial Input

To examine potential sources of the terrestrial material responsible for the more radiogenic signatures in Davidson Seamount Fe-Mn crust T145-R9, 207Pb/206Pb was plotted against ƐNd (Fig. 2.4). Source regions were selected inland from the MCS to incorporate possible catchment regions, and extended from north of San Francisco Bay to the Mojave Desert in the south, and to the Colorado Plateau in the east[Feuerbach et al., 1993; Cousens, 1996; Reid and Ramos, 1996; Beard and Johnson, 1997; Heumann and Davies, 1997, 1997, 1997; Miller et al., 2000; Wannamaker et al., 2000; Farmer et al., 2002; Schott et al., 2004; Wolff et al., 2005]. Data over the period of interest, (~ 7.5 to 4 Ma) from central Pacific Fe-Mn crusts,

outside the influence of the MCS, are used to represent open-ocean seawater isotopic values, and data from D11-4 at Hoss Seamount are plotted as a regional control [Ling et al., 1997, 2005; Chen et al., 2013]. The Pb and Nd composition from Davidson Seamount rock samples was also used as a comparison [Castillo et al., 2010]. Using Pb isotopic data from terrestrial source rocks to identify the source of the dissolved marine material has inherent uncertainties as the Pb isotope composition of labile Pb can differ from that of the bulk rock [Erel et al., 1994; Frank, 2002]. The Colorado Plateau is not a likely source as it has a higher 207Pb/206Pb and more positive ƐNd than the Fe-Mn crust [Beard and Johnson, 1997; Wannamaker et al., 2000; Wolff et al., 2005]. It is not possible to exclude the granitic Sierra Nevada as a potential source region due to overlap in the data. In addition, the Salinian block, on which Davidson Seamount and the head of the MCS rests, was derived from the southern Sierra Nevada by strike-slip motion [Barbeau et al., 2005; Chapman et al., 2014]. However, the most likely source of the terrestrial material was erosion of the Big Pine Volcanic Field along the border of the southern Sierra Nevada and western Basin and Range (Fig. 2.4).

An additional potential source of radiogenic Os to the MCS, which would account for the radiogenic $^{187}Os/^{188}Os$ deviation from the osmium isotope seawater curve prior to 4.5±0.5 Ma, even beyond average continental river values (~1.4), is organic-rich black shale from the Monterey Formation. Radiogenic Os is efficiently mobilized during weathering of organic-rich shale, that can lose 45 to 90% of its initial Os [Ravizza and Esser, 1993; Peucker-Ehrenbrink and Blum, 1998; Peucker-

Ehrenbrink and Ravizza, 2000]. Rivers draining shale deposits frequently have high $^{187}Os/^{188}Os$, and it has been proposed that black shale can provide a more radiogenic flux of Os than other rock types [Ravizza and Esser, 1993; Singh et al., 1999; Dalai and Ravizza, 2010]. However, Os released from shale can be incorporated into secondary iron oxides and clay minerals during weathering and in rivers, which may restrict the flux of labile, radiogenic Os [Pierson-Wickmann et al., 2002; Dalai and Ravizza, 2010]. A possible scenario is that a river or tributary sourced near the Big Pine Volcanic Field flowed through shale deposits in California's Central Valley, or near the coast, transporting radiogenic Os into the ocean.

2.5 Conclusion

We analyzed Os, Nd, and Pb isotopes in Fe-Mn crusts on three seamounts, Davidson proximal to the MCS, Taney offshore from the MCS, and Hoss, well-removed from the MCS. Four Fe-Mn crust records from Davidson and Taney seamounts deviated from the Cenozoic seawater Os isotope curve towards more radiogenic values from >6.8±0.5 to 4.5±0.5 Ma. We attribute this to input of radiogenic material to the MCS that started in the late Miocene since ~10 Ma to 6.8±0.5 Ma and ended about 4.5±0.5 Ma, causing the $^{187}Os/^{188}Os$ in the Fe-Mn crusts to return to a seawater-dominated isotopic signature. This is supported by more positive εNd and more radiogenic Pb in Fe-Mn crusts from Davidson Seamount when compared to regional seawater isotope values of similar ages from >6.8±0.5 to 4.5±0.5 Ma. This constrains the start of modern MC incision to between 10 Ma and 6.8±0.5 Ma and provides a minimum age of 6.8 ±0.5 Ma for the MC.

The most likely source of radiogenic Os, which would also account for the trends observed in Nd and Pb, is fluvial input of continental material with a radiogenic $^{187}Os/^{188}Os$ signature transported through the MCS. The most likely origin is terrestrial fluvial material that appears to be sourced from near the border of the southern Sierra Nevada and southern edge of the western Basin and Range. Any input of weathered or dissolved material from organic-rich shale along the fluvial transport pathway could contribute to the radiogenic Os isotope signature. The isotope values in Davidson and Taney seamount Fe-Mn crusts returned to regional seawater values after 4.5±0.5 Ma. The timing of the end of the isotope excursion is concurrent, within error, with the orogeny of the California Coast Range. This may have led to a change in the source material, sediment type, or drainage basin, thereby reducing the radiogenic signature of the fluvial material, which, resulted in seawater near the MCS reverting to regional values subsequently recorded in the Fe-Mn crusts.

Acknowledgments

Supporting data including data tables and Python code for Pb processing is available in the supplemental materials of this publication.

Funding gratefully accepted from the United States Geological Survey Pacific Coastal and Marine Science Center Marine Minerals Group, the University of California Santa Cruz, scholarship for re-entry women in science, and the UCSC Earth and Planetary Science Department, Waters Award.

We would like to thank the Monterey Bay Aquarium Research Institute (MBARI) for providing samples and the crew of the R.V. *Western Flyer* and the

operators of the ROV *Doc Ricketts*. We would also like to thank David Clague and Jenny Paduan, for help in sample collection. We thank the Captain and crew of the RV *Farnella* cruise F7-87-SC for sample collection. We are also grateful to the researchers Tristian Horner, Jeremy Owens and Gretchen Swarr at the Woods Hole Oceanographic Institution.

References

Abouchami, W., S. L. Goldstein, S. J. G. Gazer, A. Eisenhauer, and A. Mangini (1997), Secular changes of lead and neodymium in central Pacific seawater recorded by a Fe□ Mn crust, *Geochim. Cosmochim. Acta*, *61*(18), 3957–3974.

Anima, R. J., S. L. Eittreim, B. D. Edwards, and A. J. Stevenson (2002), Nearshore morphology and late Quaternary geologic framework of the northern Monterey Bay Marine Sanctuary, California, *Mar. Geol.*, *181*(1–3), 35–54, doi:10.1016/S0025-3227(01)00260-2.

Arsouze, T., J. C. Dutay, F. Lacan, and C. Jeandel (2007), Modeling the neodymium isotopic composition with a global ocean circulation model, *Chem. Geol.*, *239*(1–2), 165–177, doi:10.1016/j.chemgeo.2006.12.006.

Barbeau, D. L., M. N. Ducea, G. E. Gehrels, S. Kidder, P. H. Wetmore, and J. B. Saleeby (2005), U-Pb detrital-zircon geochronology of northern Salinian basement and cover rocks, *Geol. Soc. Am. Bull.*, *117*(3–4), 466–481, doi:10.1130/B25496.1.

Bau, M., and A. Koschinsky (2006), Hafnium and neodymium isotopes in seawater and in ferromanganese crusts: The "element perspective," *Earth Planet. Sci. Lett.*, *241*(3–4), 952–961, doi:10.1016/j.epsl.2005.09.067.

Beard, B. L., and C. M. Johnson (1997), Hafnium isotope evidence for the origin of Cenozoic basaltic lavas from the southwestern United States, *J. Geophys. Res. Solid Earth*, *102*(B9), 20149–20178, doi:10.1029/97JB01731.

Best, T. C., and G. B. Griggs (1991), A Sediment Budget for the Santacruz Littoral Cell, California, *Soc. Sediment. Geol.*, (Special Publication No. 46), 35–50.

Bird, P. (2003), An updated digital model of plate boundaries: UPDATED MODEL OF PLATE BOUNDARIES, *Geochem. Geophys. Geosystems*, *4*(3), doi:10.1029/2001GC000252.

Bonatti, E., T. Kraemer, and H. A. N. Abdulla (1972), Classification and genesis of submarine iron-manganese deposits, in *Ferromanganese Deposits on the Ocean Floor*, edited by D. R. Horn, pp. 149–166, National Science Foundation, Washington, D.C. USA.

Bowersox, J. R. (2004), Community structure, faunal distribution, and environmental forcing of the extinction of marine molluscs in the Pliocene San Joaquin Basin, Central California,

Bowersox, J. R. (2005), Reassessment of extinction patterns of Pliocene molluscs from California and environmental forcing of extinction in the San Joaquin Basin, *Palaeogeogr. Palaeoclimatol. Palaeoecol.*, *221*(1–2), 55–82, doi:10.1016/j.palaeo.2005.02.004.

Boyle, E. et al. (2014), Anthropogenic Lead Emissions in the Ocean: The Evolving Global Experiment, *Oceanography*, *27*(1), 69–75, doi:10.5670/oceanog.2014.10.

Brandon, A. D., R. J. Walker, and I. S. Puchtel (2006), Platinum–osmium isotope evolution of the Earth's mantle: Constraints from chondrites and Os-rich alloys, *Geochim. Cosmochim. Acta*, *70*(8), 2093–2103, doi:10.1016/j.gca.2006.01.005.

Burton, K. W., B. Bourdon, J. L. Birck, C. J. Allègre, and J. R. Hein (1999), Osmium isotope variations in the oceans recorded by FeMn crusts, *Earth Planet. Sci. Lett.*, *171*(1), 185–197, doi:10.1016/S0012-821X(99)00139-9.

Castillo, P. R., D. A. Clague, A. S. Davis, and P. F. Lonsdale (2010), Petrogenesis of Davidson Seamount lavas and its implications for fossil spreading center and intraplate magmatism in the eastern Pacific: DAVIDSON FOSSIL SPREADING CENTER LAVA PETROGENESIS, *Geochem. Geophys. Geosystems*, *11*(2), n/a-n/a, doi:10.1029/2009GC002992.

Chapman, A. D., M. N. Ducea, S. Kidder, and L. Petrescu (2014), Geochemical constraints on the petrogenesis of the Salinian arc, central California: Implications for the origin of intermediate magmas, *Lithos*, *200–201*, 126–141, doi:10.1016/j.lithos.2014.04.011.

Chen, T.-Y., H. F. Ling, R. Hu, M. Frank, and S. Y. Jiang (2013), Lead isotope provinciality of central North Pacific Deep Water over the Cenozoic, *Geochem. Geophys. Geosystems*, *14*(5), 1523–1537, doi:10.1002/ggge.20114.

Chow, T. J., and C. C. Patterson (1962), The occurrence and significance of lead isotopes in pelagic sediments, *Geochim. Cosmochim. Acta*, *26*(2), 263–308, doi:10.1016/0016-7037(62)90016-9.

Clague, D. A., J. B. Paduan, R. A. Duncan, J. J. Huard, A. S. Davis, P. R. Castillo, P. Lonsdale, and A. DeVogelaere (2009), Five million years of compositionally diverse, episodic volcanism: Construction of Davidson Seamount atop an abandoned spreading center: Davidson Seamount ages and glass chemistry, *Geochem. Geophys. Geosystems*, *10*(12), n/a-n/a, doi:10.1029/2009GC002665.

Conrad, T., J. R. Hein, A. Paytan, and D. A. Clague (2017a), Formation of Fe-Mn crusts within a continental margin environment, *Ore Geol. Rev.*, *87*, 25-40, doi:10.1016/j.oregeorev.2016.09.010.

Coumans, J. P., J. Stix, D. A. Clague, and W. G. Minarik (2015), The Magmatic Architecture of Taney Seamount-A, NE Pacific Ocean, *J. Petrol.*, *56*(6), 1037–1067, doi:10.1093/petrology/egv027.

Cousens, B. L. (1996), Magmatic evolution of Quaternary mafic magmas at Long Valley Caldera and the Devils Postpile, California: Effects of crustal contamination on lithospheric mantle-derived magmas, *J. Geophys. Res. Solid Earth*, *101*(B12), 27673–27689, doi:10.1029/96JB02093.

Covault, J. A., W. R. Normark, B. W. Romans, and S. A. Graham (2007), Highstand fans in the California borderland: The overlooked deep-water depositional systems, *Geology*, *35*(9), 783–786, doi:10.1130/G23800A.1.

Dalai, T. K., and G. Ravizza (2010), Investigation of an early Pleistocene marine osmium isotope record from the eastern equatorial Pacific, *Geochim. Cosmochim. Acta*, *74*(15), 4332–4345, doi:10.1016/j.gca.2010.04.062.

Dalai, T. K., K. Suzuki, M. Minagawa, and Y. Nozaki (2005), Variations in seawater osmium isotope composition since the last glacial maximum: A case study from the Japan Sea, *Chem. Geol.*, *220*(3–4), 303–314, doi:10.1016/j.chemgeo.2005.04.012.

David, K., M. Frank, R. K. O'Nions, N. S. Belshaw, and J. W. Arden (2001), The Hf isotope composition of global seawater and the evolution of Hf isotopes in the deep Pacific Ocean from Fe–Mn crusts, *Chem. Geol.*, *178*(1–4), 23–42, doi:10.1016/S0009-2541(00)00427-7.

Davis, A. S., L. B. Gray, D. A. Clague, and J. R. Hein (2002), The Line Islands revisited: New 40Ar/39Ar geochronologic evidence for episodes of volcanism due to lithospheric extension: Line Islands revisited, *Geochem. Geophys. Geosystems*, *3*(3), 1–28, doi:10.1029/2001GC000190.

DeMets, C., and S. Merkouriev (2016), High-resolution reconstructions of Pacific–North America plate motion: 20 Ma to present, *Geophys. J. Int.*, *207*(2), 741–773, doi:10.1093/gji/ggw305.

Dickinson, W. R., M. Ducea, L. I. Rosenberg, H. G. Greene, S. A. Graham, J. C. Clark, G. E. Weber, S. Kidder, W. G. Ernst, and E. E. Brabb (2005), Net dextral slip, Neogene San Gregorio–Hosgri fault zone, coastal California: Geologic evidence and tectonic implications, *Geol. Soc. Am. Spec. Pap.*, *391*, 1–43, doi:10.1130/0-8137-2391-4.1.

Du, J., B. A. Haley, and A. C. Mix (2016), Neodymium isotopes in authigenic phases, bottom waters and detrital sediments in the Gulf of Alaska and their implications for paleo-circulation reconstruction, *Geochim. Cosmochim. Acta*, *193*, 14–35, doi:10.1016/j.gca.2016.08.005.

Dubin, A., and B. Peucker-Ehrenbrink (2015), The importance of organic-rich shales to the geochemical cycles of rhenium and osmium, *Chem. Geol.*, *403*, 111–120, doi:10.1016/j.chemgeo.2015.03.010.

Ducea, M., M. A. House, and S. Kidder (2003), Late Cenozoic denudation and uplift rates in the Santa Lucia Mountains, California, *Geology*, *31*(2), 139–142, doi:10.1130/0091-7613(2003)031<0139:LCDAUR>2.0.CO;2.

Edwards, B. D. (2002), Variations in sediment texture on the northern Monterey Bay National Marine Sanctuary continental shelf, *Mar. Geol.*, *181*(1–3), 83–100, doi:10.1016/S0025-3227(01)00262-6.

Eittreim, S. L., R. J. Anima, and A. J. Stevenson (2002), Seafloor geology of the Monterey Bay area continental shelf, *Mar. Geol.*, *181*(1), 3–34.

Erel, Y., Y. Harlavan, and J. D. Blum (1994), Lead isotope systematics of granitoid weathering, *Geochim. Cosmochim. Acta*, *58*(23), 5299–5306, doi:10.1016/0016-7037(94)90313-1.

Farmer, G. L., A. F. Glazner, and C. R. Manley (2002), Did lithospheric delamination trigger late Cenozoic potassic volcanism in the southern Sierra Nevada, California?, *Geol. Soc. Am. Bull.*, *114*(6), 754–768, doi:10.1130/0016-7606(2002)114<0754:DLDTLC>2.0.CO;2.

Feuerbach, D. L., E. I. Smith, J. D. Walker, and J. A. Tangeman (1993), The role of the mantle during crustal extension: Constraints from geochemistry of volcanic rocks in the Lake Mead area, Nevada and Arizona, *Geol. Soc. Am. Bull.*, *105*(12), 1561–1575.

Fildani, A., and W. R. Normark (2004), Late Quaternary evolution of channel and lobe complexes of Monterey Fan, *Mar. Geol.*, *206*(1–4), 199–223, doi:10.1016/j.margeo.2004.03.001.

Flegal, A. R., and C. C. Patterson (1983), Vertical concentration profiles of lead in the Central Pacific at 15°N and 20°S, *Earth Planet. Sci. Lett.*, *64*(1), 19–32, doi:10.1016/0012-821X(83)90049-3.

van de Flierdt, T., M. Frank, D.-C. Lee, A. N. Halliday, B. C. Reynolds, and J. R. Hein (2004), New constraints on the sources and behavior of neodymium and hafnium in seawater from Pacific Ocean ferromanganese crusts, *Geochim. Cosmochim. Acta*, *68*(19), 3827–3843, doi:10.1016/j.gca.2004.03.009.

van de Flierdt, T., A. M. Griffiths, M. Lambelet, S. H. Little, T. Stichel, and D. J. Wilson (2016), Neodymium in the oceans: a global database, a regional comparison and implications for palaeoceanographic research, *Phil Trans R Soc A*, *374*(2081), 20150293, doi:10.1098/rsta.2015.0293.

Foster, G. L., and D. Vance (2006), Negligible glacial–interglacial variation in continental chemical weathering rates, *Nature*, *444*(7121), 918–921, doi:10.1038/nature05365.

Frank, M. (2002), Radiogenic Isotopes: Tracers of Past Ocean Circulation and Erosional Input, *Rev. Geophys.*, *40*(1), 1–1, doi:10.1029/2000RG000094.

Gannoun, A., K. W. Burton, N. Vigier, S. R. Gíslason, N. Rogers, F. Mokadem, and B. Sigfússon (2006), The influence of weathering process on riverine osmium isotopes in a basaltic terrain, *Earth Planet. Sci. Lett.*, *243*(3–4), 732–748, doi:10.1016/j.epsl.2006.01.024.

Garcia-Solsona, E., C. Jeandel, M. Labatut, F. Lacan, D. Vance, V. Chavagnac, and C. Pradoux (2014), Rare earth elements and Nd isotopes tracing water mass mixing and particle-seawater interactions in the SE Atlantic, *Geochim. Cosmochim. Acta*, *125*, 351–372, doi:10.1016/j.gca.2013.10.009.

Goff, J., C. Chagué-Goff, M. Archer, D. Dominey-Howes, and C. Turney (2012), The Eltanin asteroid impact: possible South Pacific palaeomegatsunami footprint and potential implications for the Pliocene–Pleistocene transition, *J. Quat. Sci.*, *27*(7), 660–670, doi:10.1002/jqs.2571.

Goldstein, S. L., R. K. O'Nions, and P. J. Hamilton (1984), A Sm-Nd isotopic study of atmospheric dusts and particulates from major river systems, *Earth Planet. Sci. Lett.*, *70*(2), 221–236, doi:10.1016/0012-821X(84)90007-4.

Graham, S. A., A. R. Carroll, and G. E. Miller (1988), Kern River Formation as a Recorder of Uplift and Glaciation of the Southern Sierra Nevada, , 319–331.

Greene, H. G. (1977), *Geology of the Monterey Bay region, California*, Open-File Report, USGS Numbered Series, U.S. Geological Survey,.

Greene, H. G., and K. R. Hicks (1990), Ascension-Monterey Canyon system: history and development, , *67*, 229–250.

Greene, H. G., W. L. Stubblefield, and A. E. Theberge (1989), *Geology of the Monterey submarine canyon system and adjacent areas, offshore central California*, Open-File Report, USGS Numbered Series, U.S. Geological Survey,.

Greene, H. G., N. M. Maher, and C. K. Paull (2002), Physiography of the Monterey Bay National Marine Sanctuary and implications about continental margin development, *Mar. Geol.*, *181*(1), 55–82.

Griggs, G. B., and J. R. Hein (1980), Sources, Dispersal, and Clay Mineral Composition of Fine-Grained Sediment off Central and Northern California, *J. Geol.*, *88*(5), 541–566.

Halbach, P., and D. Puteanus (1984), The influence of the carbonate dissolution rate on the growth and composition of Co-rich ferromanganese crusts from Central Pacific seamount areas, *Earth Planet. Sci. Lett.*, *68*(1), 73–87, doi:10.1016/0012-821X(84)90141-9.

Harvey, J., C. W. Dale, A. Gannoun, and K. W. Burton (2011), Osmium mass balance in peridotite and the effects of mantle-derived sulphides on basalt petrogenesis, *Geochim. Cosmochim. Acta*, *75*(19), 5574–5596, doi:10.1016/j.gca.2011.07.001.

Hein, J. R., and A. Koschinsky (2014), Deep-Ocean Ferromanganese Crusts and Nodules, in *Treatise on Geochemistry*, pp. 273–291, Elsevier.

Hein, J. R., J. A. Reid, T. A. Conrad, R. E. Dunham, D. A. Clague, M. S. Schulz, and A. S. Davis (2010), *Seamounts and ferromanganese crusts within and near the U.S. EEZ off California - Data for RV Farnella cruise F7-87-SC*, U.S. Geological Survey.

Heumann, A., and G. R. Davies (1997), Isotopic and chemical evolution of the post-caldera rhyolitic system at Long Valley, California, *J. Petrol.*, *38*(12), 1661–1678.

Horan, M. F., R. J. Walker, J. W. Morgan, J. N. Grossman, and A. E. Rubin (2003), Highly siderophile elements in chondrites, *Chem. Geol.*, *196*(1–4), 27–42, doi:10.1016/S0009-2541(02)00405-9.

Hu, R., A. M. Piotrowski, H. C. Bostock, S. Crowhurst, and V. Rennie (2016), Variability of neodymium isotopes associated with planktonic foraminifera in the Pacific Ocean during the Holocene and Last Glacial Maximum, *Earth Planet. Sci. Lett.*, *447*, 130–138, doi:10.1016/j.epsl.2016.05.011.

Jacobsen, S. B., and G. J. Wasserburg (1980), Sm-Nd isotopic evolution of chondrites, *Earth Planet. Sci. Lett.*, *50*(1), 139–155, doi:10.1016/0012-821X(80)90125-9.

Jeandel, C., and E. H. Oelkers (2015), The influence of terrigenous particulate material dissolution on ocean chemistry and global element cycles, *Chem. Geol.*, *395*, 50–66, doi:10.1016/j.chemgeo.2014.12.001.

Johnson, C. L., and S. A. Graham (2007), Middle Tertiary Stratigraphic Sequences of the San Joaquin Basin, California, *Pet. Syst. Geol. Assess. Oil Gas San Joaquin Basin Prov. Calif. US Geol. Surv. Prof. Pap.*, *1713*, 1–18.

King, C. SanctuarySIMoN.org, accessed Nov. 2016

Klemm, V., S. Levasseur, M. Frank, J. Hein, and A. Halliday (2005), Osmium isotope stratigraphy of a marine ferromanganese crust, *Earth Planet. Sci. Lett.*, *238*(1–2), 42–48, doi:10.1016/j.epsl.2005.07.016.

Klemm, V., M. Frank, S. Levasseur, A. N. Halliday, and J. R. Hein (2008), Seawater osmium isotope evidence for a middle Miocene flood basalt event in ferromanganese crust records, *Earth Planet. Sci. Lett.*, *273*(1–2), 175–183, doi:10.1016/j.epsl.2008.06.028.

Lacan, F., and C. Jeandel (2005), Neodymium isotopes as a new tool for quantifying exchange fluxes at the continent–ocean interface, *Earth Planet. Sci. Lett.*, *232*(3–4), 245–257, doi:10.1016/j.epsl.2005.01.004.

Lacan, F., K. Tachikawa, and C. Jeandel (2012), Neodymium isotopic composition of the oceans: A compilation of seawater data, *Chem. Geol.*, *300–301*, 177–184, doi:10.1016/j.chemgeo.2012.01.019.

Langenheim, V. E., R. C. Jachens, R. W. Graymer, J. P. Colgan, C. M. Wentworth, and R. G. Stanley (2013), Fault geometry and cumulative offsets in the central Coast Ranges, California: Evidence for northward increasing slip along the San Gregorio–San Simeon–Hosgri fault, *Lithosphere*, *5*(1), 29–48, doi:10.1130/L233.1.

Levasseur, S., J.-L. Birck, and C. J. Allègre (1999), The osmium riverine flux and the oceanic mass balance of osmium, *Earth Planet. Sci. Lett.*, *174*(1–2), 7–23, doi:10.1016/S0012-821X(99)00259-9.

Lewis, R. C., K. H. Coale, B. D. Edwards, M. Marot, J. N. Douglas, and E. J. Burton (2002), Accumulation rate and mixing of shelf sediments in the Monterey Bay National Marine Sanctuary, *Mar. Geol.*, *181*(1–3), 157–169, doi:10.1016/S0025-3227(01)00265-1.

Ling, H. F., K. W. Burton, R. K. O'Nions, B. S. Kamber, F. von Blanckenburg, A. J. Gibb, and J. R. Hein (1997), Evolution of Nd and Pb isotopes in Central Pacific seawater from ferromanganese crusts, *Earth Planet. Sci. Lett.*, *146*(1–2), 1–12, doi:10.1016/S0012-821X(96)00224-5.

Ling, H.-F., S. Y. Jiang, M. Frank, H.-Y. Zhou, F. Zhou, Z. L. Lu, X. M. Chen, Y. H. Jiang, and C.-D. Ge (2005), Differing controls over the Cenozoic Pb and Nd isotope evolution of deepwater in the central North Pacific Ocean, *Earth Planet. Sci. Lett.*, *232*(3–4), 345–361, doi:10.1016/j.epsl.2004.12.009.

Loomis, K. B. (1988), Paleoenvironmental and Paleoclimatic Interpretation of Upper Miocene - Pliocene Lithofacies and Macrobiota of the Etchegoin Group, Jacalitos Canyon, San Joaquin Valley, California, , 303–318.

Loomis, K. B. (1990), Depositional Environments and Sedimentary History of the Etchegoin Group, West-Central San Joaquin Valley, California, , 231–246.

Martin, C. E., B. Peucker-Ehrenbrink, G. J. Brunskill, and R. Szymczak (2000), Sources and sinks of unradiogenic osmium runoff from Papua New Guinea, *Earth Planet. Sci. Lett.*, *183*(1–2), 261–274, doi:10.1016/S0012-821X(00)00281-8.

Martin, C. E., B. Peucker-Ehrenbrink, G. Brunskill, and R. Szymczak (2001), Osmium isotope geochemistry of a tropical estuary, *Geochim. Cosmochim. Acta*, *65*(19), 3193–3200, doi:10.1016/S0016-7037(01)00654-8.

Meade, R. H. (1969), Errors in Using Modern Stream-Load Data To Estimate Natural Rates of Denudation, *Geol. Soc. Am. Bull.*, *80*(7), 1265–1274, doi:10.1130/0016-7606(1969)80[1265:EIUMSD]2.0.CO;2.

Miller, J. S., A. F. Glazner, G. L. Farmer, I. B. Suayah, and L. A. Keith (2000), A Sr, Nd, and Pb isotopic study of mantle domains and crustal structure from Miocene volcanic rocks in the Mojave Desert, California, *Geol. Soc. Am. Bull.*, *112*(8), 1264–1279.

Mulder, T., and J. P. M. Syvitski (1995), Turbidity Currents Generated at River Mouths during Exceptional Discharges to the World Oceans, *J. Geol.*, *103*, 285–299, doi:10.1086/629747.

Müller, R. D., M. Sdrolias, C. Gaina, and W. R. Roest (2008), Age, spreading rates, and spreading asymmetry of the world's ocean crust: DIGITAL MODELS OF THE WORLD'S OCEAN CRUST, *Geochem. Geophys. Geosystems*, *9*(4), n/a-n/a, doi:10.1029/2007GC001743.

Nagel, D. K., H. T. Mullins, and H. G. Greene (1986), Ascension Submarine Canyon, California — Evolution of a multi-head canyon system along a strike-slip continental margin, *Mar. Geol.*, *73*(3), 285–310, doi:10.1016/0025-3227(86)90019-8.

Ogston, A. S., and R. W. Sternberg (1999), Sediment-transport events on the northern California continental shelf, *Mar. Geol.*, *154*(1–4), 69–82, doi:10.1016/S0025-3227(98)00104-2.

Page, B. M., R. G. Coleman, and G. A. Thompson (1998), OVERVIEW: Late Cenozoic tectonics of the central and southern Coast Ranges of California, *Geol. Soc. Am. Bull.*, *110*(7), 846–876, doi:10.1130/0016-7606(1998)110<0846:OLCTOT>2.3.CO;2.

Paquay, F. S., and G. Ravizza (2012), Heterogeneous seawater $^{187}Os/^{188}Os$ during the Late Pleistocene glaciations, *Earth Planet. Sci. Lett.*, *349–350*, 126–138, doi:10.1016/j.epsl.2012.06.051.

Paull, C. K., W. Ussler, H. G. Greene, R. Keaten, P. Mitts, and J. Barry (2003), Caught in the act: the 20 December 2001 gravity flow event in Monterey Canyon, *Geo-Mar. Lett.*, *22*(4), 227–232, doi:10.1007/s00367-003-0117-2.

Pettke, T., A. N. Halliday, C. M. Hall, and D. K. Rea (2000), Dust production and deposition in Asia and the north Pacific Ocean over the past 12 Myr, *Earth Planet. Sci. Lett.*, *178*(3–4), 397–413, doi:10.1016/S0012-821X(00)00083-2.

Peucker-Ehrenbrink, B., and J. D. Blum (1998), Re-Os isotope systematics and weathering of Precambrian crustal rocks: implications for the marine osmium isotope record, *Geochim. Cosmochim. Acta*, *62*(19–20), 3193–3203, doi:10.1016/S0016-7037(98)00227-0.

Peucker-Ehrenbrink, B., and B. Jahn (2001), Rhenium-osmium isotope systematics and platinum group element concentrations: Loess and the upper continental crust, *Geochem. Geophys. Geosystems*, *2*(10), 1061, doi:10.1029/2001GC000172.

Peucker-Ehrenbrink, B., and G. Ravizza (2000), The marine osmium isotope record, *Terra Nova*, *12*(5), 205–219, doi:10.1046/j.1365-3121.2000.00295.x.

Peucker-Ehrenbrink, B., and G. Ravizza (2012), Chapter 8 - Osmium Isotope Stratigraphy, in *The Geologic Time Scale*, pp. 145–166, Elsevier, Boston.

Pierson-Wickmann, A.-C., L. Reisberg, and C. France-Lanord (2002), Behavior of Re and Os during low-temperature alteration: Results from Himalayan soils and altered black shales, *Geochim. Cosmochim. Acta*, *66*(9), 1539–1548, doi:10.1016/S0016-7037(01)00865-1.

Pyenson, N. D., R. B. Irmis, J. H. Lipps, L. G. Barnes, E. D. Mitchell, and S. A. McLeod (2009), Origin of a widespread marine bonebed deposited during the middle Miocene Climatic Optimum, *Geology*, *37*(6), 519–522, doi:10.1130/G25509A.1.

Ravizza, G., and B. K. Esser (1993), A possible link between the seawater osmium isotope record and weathering of ancient sedimentary organic matter, *Chem. Geol.*, *107*(3), 255–258, doi:10.1016/0009-2541(93)90186-M.

Reid, M. R., and F. C. Ramos (1996), Chemical dynamics of enriched mantle in the southwestern United States: Thorium isotope evidence, *Earth Planet. Sci. Lett.*, *138*(1–4), 67–81.

Reid, S. A. (1995), Miocene and Pliocene Depositional Systems of the Southern San Joaquin Basin and Formation of Sandstone Reservoirs in the Elk Hills Area, California, , 131–150.

Schott, R. C., C. M. Johnson, and J. R. O'Neil (2004), Late Cretaceous tectonic history of the Sierra-Salinia-Mojave arc as recorded in conglomerates of the Upper Cretaceous and Paleocene Gualala Formation, northern California: CRETACEOUS HISTORY OF THE GUALALA BASIN, *J. Geophys. Res. Solid Earth*, *109*(B2), doi:10.1029/2003JB002845.

Sen, I. S., and B. Peucker-Ehrenbrink (2014), Determination of Osmium Concentrations and ^{187}Os/^{188}Os of Crude Oils and Source Rocks by Coupling High-Pressure, High-Temperature Digestion with Sparging OsO_4 into a Multicollector Inductively Coupled Plasma Mass Spectrometer, *Anal. Chem.*, *86*(6), 2982–2988, doi:10.1021/ac403413y.

Sharma, M., and G. J. Wasserburg (1997), Osmium in the rivers, *Geochim. Cosmochim. Acta*, *61*(24), 5411–5416, doi:10.1016/S0016-7037(97)00329-3.

Sharma, M., G. J. Wasserburg, A. W. Hofmann, and G. J. Chakrapani (1999), Himalayan uplift and osmium isotopes in oceans and rivers, *Geochim.*

Cosmochim. Acta, *63*(23–24), 4005–4012, doi:10.1016/S0016-7037(99)00305-1.

Sharma, M., G. J. Wasserburg, A. W. Hofmann, and D. A. Butterfield (2000), Osmium isotopes in hydrothermal fluids from the Juan de Fuca Ridge, *Earth Planet. Sci. Lett.*, *179*(1), 139–152, doi:10.1016/S0012-821X(00)00099-6.

Sharma, M., E. J. Rosenberg, and D. A. Butterfield (2007), Search for the proverbial mantle osmium sources to the oceans: Hydrothermal alteration of mid-ocean ridge basalt, *Geochim. Cosmochim. Acta*, *71*(19), 4655–4667, doi:10.1016/j.gca.2007.06.062.

Singh, S. K., J. R. Trivedi, and S. Krishnaswami (1999), Re-Os isotope systematics in black shales from the Lesser Himalaya: their chronology and role in the $^{187}Os/^{188}Os$ evolution of seawater, *Geochim. Cosmochim. Acta*, *63*(16), 2381–2392, doi:10.1016/S0016-7037(99)00201-X.

Stanton, R. J., and J. R. Dodd (1997), Lack of stasis in late Cenozoic marine faunas and communities, central California, *Lethaia*, *30*(3), 239–256, doi:10.1111/j.1502-3931.1997.tb00466.x.

Stichel, T., M. Frank, J. Rickli, and B. A. Haley (2012), The hafnium and neodymium isotope composition of seawater in the Atlantic sector of the Southern Ocean, *Earth Planet. Sci. Lett.*, *317–318*, 282–294, doi:10.1016/j.epsl.2011.11.025.

Wakabayashi, J., and T. L. Sawyer (2001), Stream incision, tectonics, uplift, and evolution of topography of the Sierra Nevada, California, *J. Geol.*, *109*(5), 539–562.

Wannamaker, P. E., J. B. Hulen, and M. T. Heizler (2000), Early Miocene lamproite from the Colorado Plateau tectonic province, Southeastern Utah, USA, *J. Volcanol. Geotherm. Res.*, *96*(3–4), 175–190, doi:10.1016/S0377-0273(99)00146-8.

Williams, G. A., and K. K. Turekian (2002), Atmospheric supply of osmium to the oceans, *Geochim. Cosmochim. Acta*, *66*(21), 3789–3791, doi:10.1016/S0016-7037(02)00922-5.

Williams, G. A., and K. K. Turekian (2004), The glacial–interglacial variation of seawater osmium isotopes as recorded in Santa Barbara Basin, *Earth Planet. Sci. Lett.*, *228*(3–4), 379–389, doi:10.1016/j.epsl.2004.10.004.

Wilson, D. S., P. A. McCrory, and R. G. Stanley (2005), Implications of volcanism in coastal California for the Neogene deformation history of western North America, *Tectonics*, *24*(3), doi:10.1029/2003TC001621.

Wolff, J. A., M. C. Rowe, R. Teasdale, J. N. Gardner, F. C. Ramos, and C. E. Heikoop (2005), Petrogenesis of Pre-caldera Mafic Lavas, Jemez Mountains Volcanic Field (New Mexico, USA), *J. Petrol.*, *46*(2), 407–439, doi:10.1093/petrology/egh082.

Woodhouse, O. B., G. Ravizza, K. Kenison Falkner, P. J. Statham, and B. Peucker-Ehrenbrink (1999), Osmium in seawater: vertical profiles of concentration and isotopic composition in the eastern Pacific Ocean, *Earth Planet. Sci. Lett.*, *173*(3), 223–233, doi:10.1016/S0012-821X(99)00233-2.

Zeng, Z., S. Chen, D. Selby, X. Yin, and X. Wang (2014), Rhenium–osmium abundance and isotopic compositions of massive sulfides from modern deep-sea hydrothermal systems: Implications for vent associated ore forming processes, *Earth Planet. Sci. Lett.*, *396*, 223–234, doi:10.1016/j.epsl.2014.04.017.

Figures

Figure 2.1 Location map of the central and southern California coast with the Davidson, Taney, and Hoss Seamounts, the Monterey Submarine Canyon System and Fan, the San Andreas Fault, Paleo San Joaquin Basin with Priest Strait, paleo coast line and MC locations at 5 Ma and 10 Ma indicated (GeomapApp.org). References, subscripts in key: 1. [Müller et al., 2008]; 2. [Bowersox, 2005]; 3. [Bird, 2003]; 4. [Fildani and Normark, 2004]; 5. [Wilson et al., 2005]; 6. [DeMets and Merkouriev, 2016]; 7. [King, SIMoN.org]; 8. [Greene and Hicks, 1990].

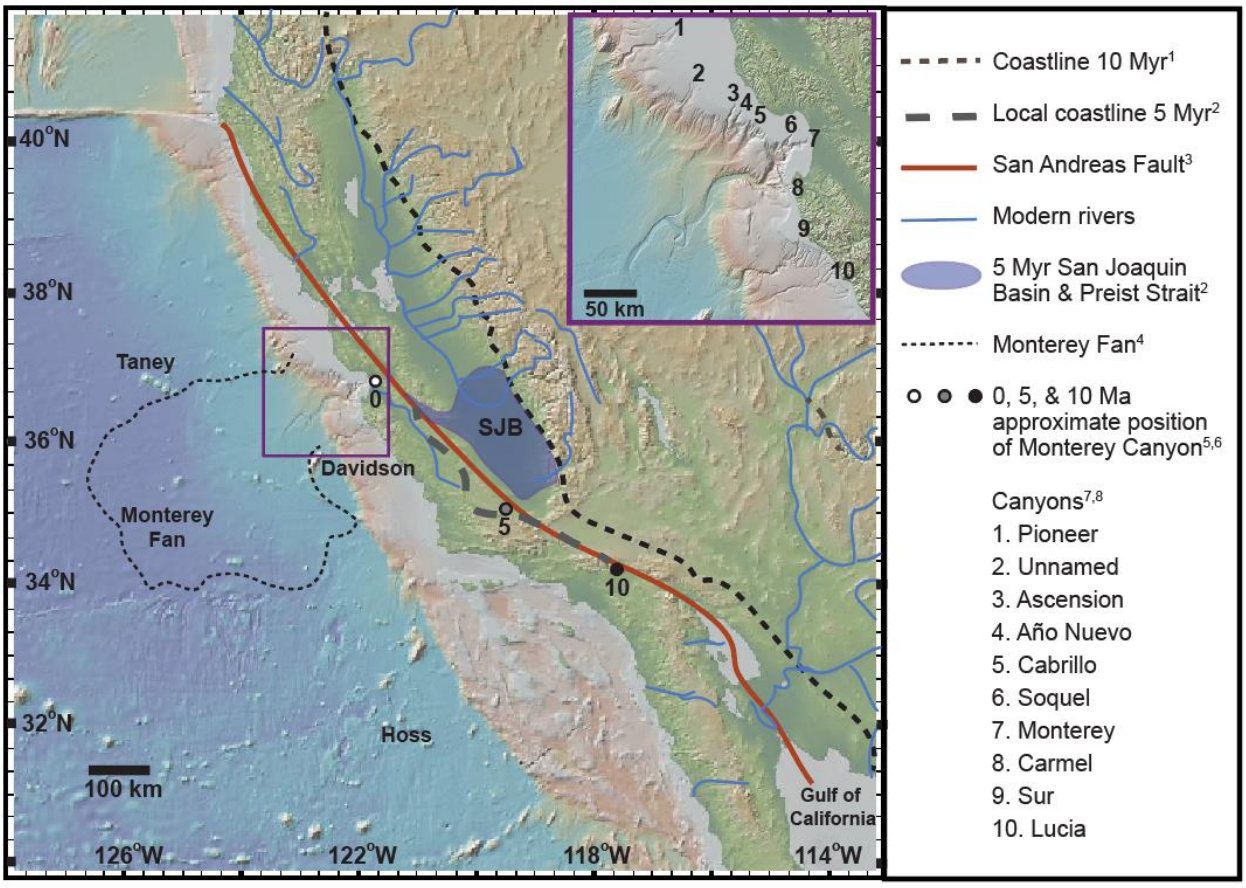

Figure 2.2 Plot of $^{187}Os/^{188}Os$ in six CCM Fe-Mn crust samples over the past 9 Myr. The gray shaded region is the Cenozoic Osmium isotope seawater curve [Peucker-Ehrenbrink and Ravizza, 2012]. Solid samples were analyzed for Pb.

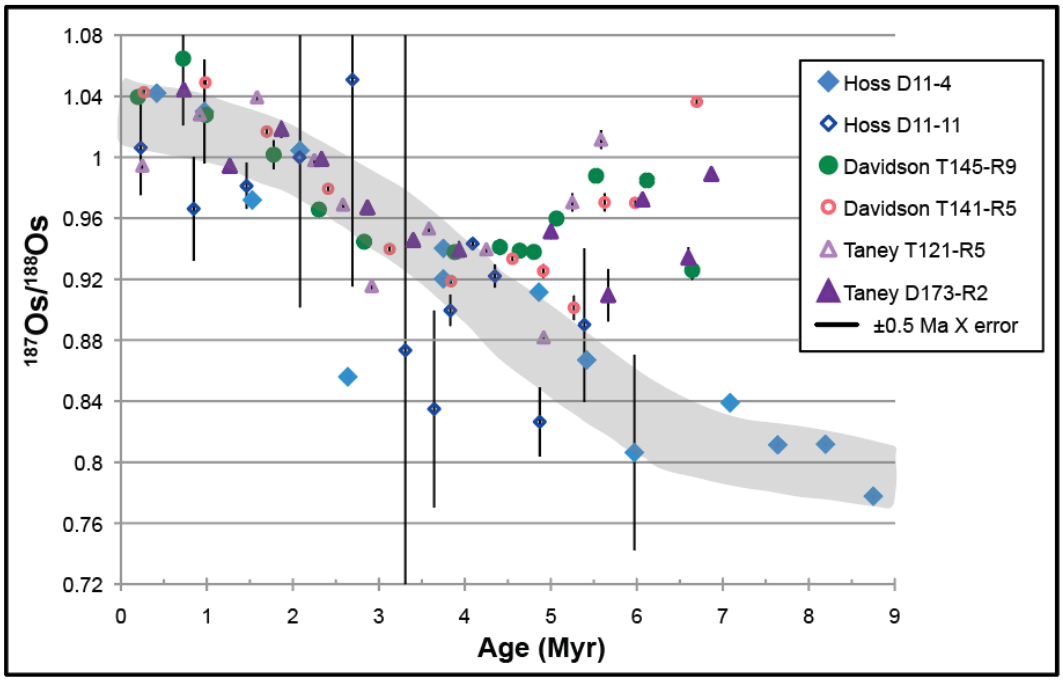

Figure 2.3 Isotope values for $^{187}Os/^{188}Os$, ƐNd, and $^{206}Pb/^{204}Pb$ for Fe-Mn crust T145-R9, Davidson Seamount are shown relative to Hoss D11-4, representing regional seawater. For ƐNd, and $^{206}Pb/^{204}Pb$ Central Pacific seawater, in gray, is represented by Fe-Mn crusts CD29-2 and D11-1 [Ling et al., 1997]. The Cenozoic Os isotope seawater curve is used for $^{187}Os/^{188}Os$ [Peucker-Ehrenbrink and Ravizza, 2012]. The region highlighted in yellow, from ~ 7 to 4.5 Myr shows deviation away from regional seawater at Davidson Seamount. Error for ƐNd and $^{206}Pb/^{204}Pb$ are 2σ for all runs of the USGS A-1 nodule standard, n=16 and 85, respectively. Error for $^{187}Os/^{188}Os$ is 2σ of A-1 excluding the lowest 3 values, 2 of which had contamination on ^{185}Re, n=13. Instrumental error over this amount is shown for individual points.

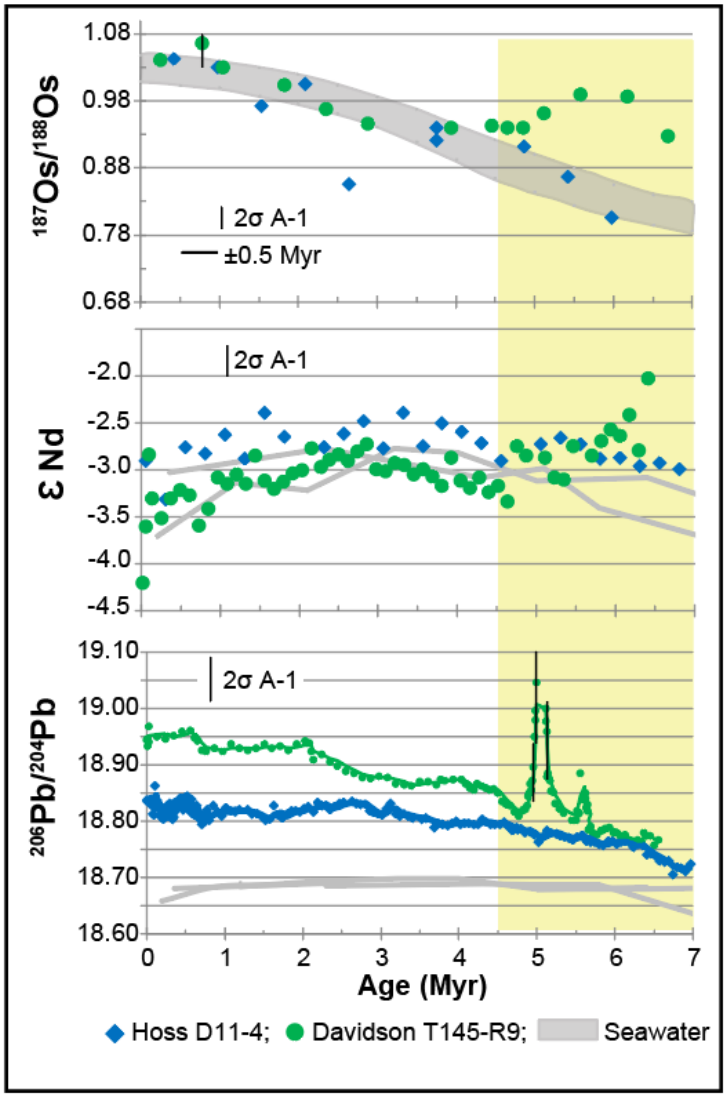

Figure 2.4 A. Location map of the south-western United States showing sample locations. B. Plot of average $^{207}Pb/^{206}Pb$ and ƐNd isotope values by region. C. Inset box with individual $^{207}Pb/^{206}Pb$ and ƐNd data points. Samples from Davidson and Hoss Fe-Mn crusts have 2-4 average Pb measurements for Nd each sample. Only data from 7 to 4.5 Myr is shown for California Margin and Central Pacific Fe-Mn crusts. All Nd data is normalized to JNdi-1= 0.512115 for comparison. Southern Sierras includes data from Kern, San Joaquin, and Kings volcanic fields.
References: 1. Ling et al., 1997; 2. Chen et al., 2013; 3. Castillo et al., 2010; 4. Beard & Johnson 1997; 5. Wannamaker et al., 2000; 6. Wolff et al., 2005; 7. Heumann & Davies 1997; 8. Cousens 1991; 9. Farmer et al., 2002; 10. Schott et al., 2004; 11. Feuerbach et al., 1993; 12. Reid and Ramos 1996; 13. Miller et al., 2002

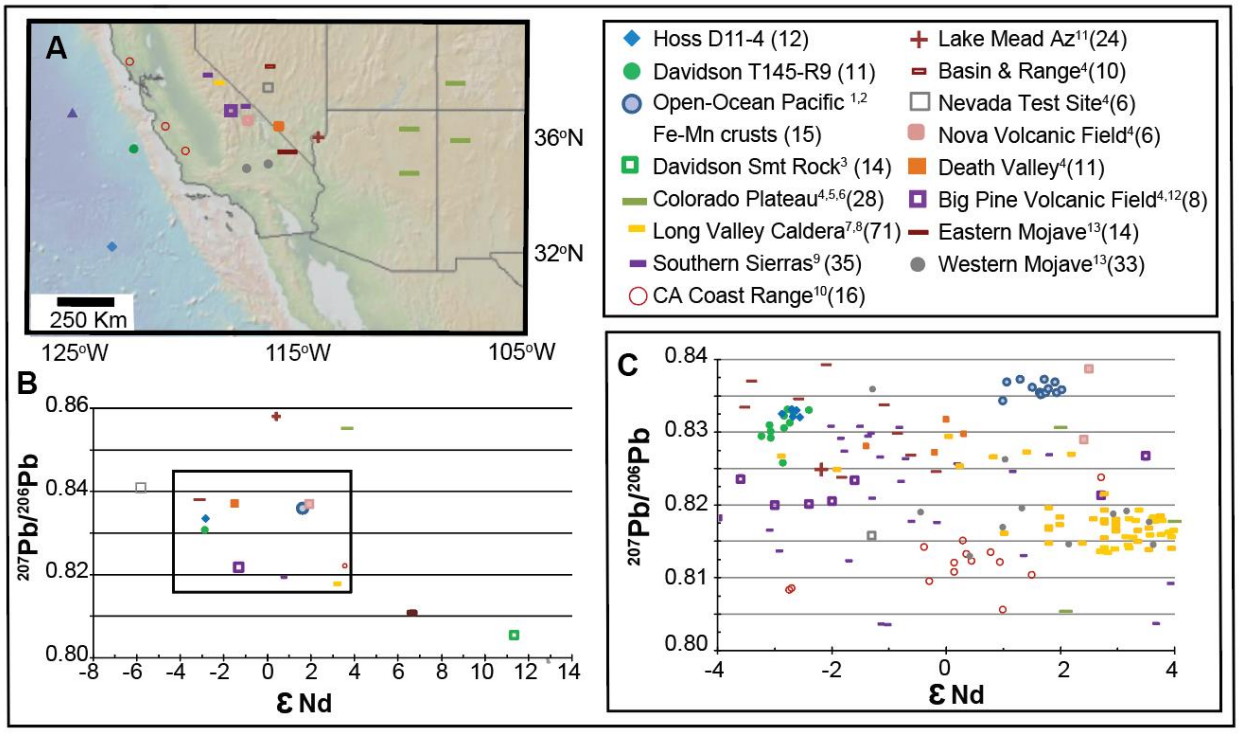

Chapter 3. High resolution time-series of Pb and Nd isotopes recorded in ferromanganese crusts from the northeast Pacific

Tracey A. Conrad[a]*, Sune G. Nielsen[b], Jurek Blusztajn[b], James R. Hein[c], Adina Paytan[a]

[a] University California Santa Cruz, 1156 High Street, Santa Cruz, CA 95060, USA
[b] Woods Hole Oceanographic Institution, 360 Woods Hole Road, Woods Hole, MA 02543, USA
[c] U.S. Geological Survey, PCMSC, 2885 Mission St., Santa Cruz, CA, 95060, USA

*Corresponding Author: Tracey A. Conrad

Abbreviations: Fe-Mn = ferromanganese; CCM = California Continental Margin; Myr = million years; Ma = Million years ago; ROV = remotely operated vehicle; bsl = below sea level; MC-ICPMS = multicollector-inductively coupled plasma mass spectrometer; NPIW = North Pacific Intermediate Water; PDW = Pacific Deep Water; GOA= Gulf of Alaska

Keywords: Ferromanganese Crusts; Neodymium isotopes, Lead isotopes, northeast Pacific deep water

Abstract

High-resolution time series data for Pb and Nd isotopes from hydrogenetic ferromanganese crusts along the California continental margin (CCM) in the eastern North Pacific are evaluated and compared to data from central Pacific, North Pacific, and Arctic Ocean crusts. These Fe-Mn crusts provide isotope records for approximately the past 7 to 9 Myr and were collected from three separate seamounts, covering a considerable region of the CCM. Surface ƐNd from CCM Fe-Mn crusts collected above 3000 m plots off of a North Pacific Intermediate Water and Pacific Deep Water mixing line towards more radiogenic ƐNd values from sediment pore-water. This is evidence for sediment pore-water benthic fluxes affecting the ƐNd signal in the continental margin Fe-Mn crusts. Similar ƐNd trends are recorded in Fe-Mn crusts from the central Pacific. Crusts from both regions show an increase in ƐNd from ~7 to ~3 Ma, likely due to an increase in Nd from young radiogenic Pacific arcs, and after ~3 Ma ƐNd decreases towards the present. Based on the ƐNd ratios and input timing of circum-Pacific sources, this decrease in ƐNd is most plausibly attributed to cyclic failure of glacial lakes that transported material from older-inland North American rocks into the Pacific, which initiated ~2.5 Ma. Lead isotopic ratios in near-shore California margin Fe-Mn crusts resemble those found in crusts from the North Pacific and Arctic Ocean and show increasing $^{206}Pb/^{204}Pb$ from the late Miocene to present. The isotope ratios of Pb suggest that this increase in radiogenic Pb reflects terrestrial material sourced from the North American continent and delivered to the ocean via riverine transport, rather than from Asian dust.

3.1 Introduction

Radiogenic isotopes with residence times shorter than that of global ocean mixing (Hf, Be, Nd, Pb, among others) can be used to study paleoceanographic conditions including ocean circulation, changes in climate, and inputs due to changes in continental weathering or uplift [Frank, 2002; van de Flierdt et al., 2003, 2004a]. Here, high resolution Pb and Nd isotopic profiles for three hydrogenetic ferromanganese (Fe-Mn) crusts from the northeast Pacific along the California Continental Margin are discussed (CCM) (Fig. 3.1).

Hydrogenetic Fe-Mn crusts are rock deposits that form as chemo-stratigraphic precipitates on elevated rock surfaces when submarine currents or the degree of slope prevents sediment from accumulating and burying the slowly growing (1-10 mm/Myr) Fe-Mn crusts [Bonatti et al., 1972; Hein et al., 2000; Conrad et al., 2017a]. Ferromanganese crusts record the chemical and isotopic signature of seawater as they grow, providing low-resolution, long-term archives of paleo-seawater [Frank, 2002; Hein and Koschinsky, 2014]. Elements with low diffusive re-equilibration within the Fe-Mn crusts, including Os, Hf, Be, Pb, and Nd, among others, can be used as paleo-seawater archives [Abouchami et al., 1997; O'Nions et al., 1998; Abouchami et al., 1999; Frank, 2002; van de Flierdt et al., 2004a; Klemm et al., 2005; Nielsen et al., 2009; Horner et al., 2010; Nielsen et al., 2011; Chen et al., 2013]. Other elements including Sr and Li, and to a lesser degree U, re-equilibrate with seawater or have diffusion coefficients in Fe-Mn crusts too high for use as paleoceanographic archives [Ingram et al., 1990; Frank, 2002; Chan and Hein, 2007]. Due to slow growth rates,

variations in paleo-seawater recorded in Fe-Mn crusts are averaged over tens to hundreds of thousand years; shorter-term perturbations in seawater chemistry cannot be identified.

Most studies have utilized Fe-Mn crusts from the open ocean [Abouchami et al., 1997, 1999; Christensen, 1997; Ling et al., 1997; Klemm et al., 2005, 2007; Horner et al., 2010; Nielsen et al., 2011; Chen et al., 2013]. Comparatively less work has been conducted on Fe-Mn crusts from the northeast Pacific and continental margin regions [Conrad et al., 2017a]. Time-series studies of two Fe-Mn crusts from the North Pacific measured Pb, Nd, and Hf isotopes [van de Flierdt et al., 2003, 2004a]. One CCM crust, D9-29 was analyzed for pre-anthropogenic Pb isotopes averaged over the past 48 ka by scraping the most recent growth surface and yielded isotopic values more radiogenic than Fe-Mn crusts located in the central and southern Pacific [von Blanckenburg et al., 1996].

3.2 Sample locations

The CCM is a complex, tectonically active environment that undergoes strong, seasonal upwelling of nutrient-rich deep and intermediate water and receives relatively large terrestrial inputs from western North America via aeolian and fluvial sources, resulting in high primary productivity in the surface waters [Barron and Bukry, 2007; Biller and Bruland, 2014; DeMets and Merkouriev, 2016]. Resuspension of continental shelf and slope sediments can also effect the element concentration of seawater within the CCM [Berelson et al., 2013]. Ferromanganese crusts collected from the CCM are enriched in Fe, Si, and Th and have lower

concentrations of P and elements of economic interest (Co, Ni, Cu, and Te, among others) than Fe-Mn crusts from the open-ocean Pacific [Conrad et al., 2017a].

Samples for this study were collected from Hoss, Davidson, and Taney B seamounts (Fig. 3.1). Ferromanganese crust D11-4 was collected on USGS cruise F7-87-SC from Hoss seamount by chain-bag dredge from 2,560-2,540 m below sea level (bsl). Samples T141-R5 and T145-R9 were collected via remotely operated vehicle (ROV) from Davidson Seamount on a Monterey Bay Aquarium Research Institute (MBARI) 2004 cruise, from 2,388 m and 3,298 m bsl, respectively. Ferromanganese crust D173-R2 was collected by ROV on a MBARI 2010 cruise, from the Taney Seamount from 3,178 m water depth.

3.3 Isotopes

3.3.1 Neodymium Isotopes

The isotopic distribution and behavior of Nd in seawater has been the subject of many global studies and Nd has been designated as a key parameter of the GEOTRACES program [Piepgras and Wasserburg, 1980, 1987; Bau and Koschinsky, 2006; Lacan et al., 2012; Lambelet et al., 2016; van de Flierdt et al., 2016]. To date, more data are available for the Atlantic than Pacific Ocean. North Atlantic Deep water has a less radiogenic ƐNd of ~ -13.5, while North Pacific Deep Water has a more radiogenic ƐNd of ~ -4, and the deep water from the Southern and Indian Oceans have values that fall between these two end-members, with ƐNd ~ -7 to -9 [van de Flierdt et al., 2016]. Seawater $^{143}Nd/^{144}Nd$ is expressed as ƐNd, which is the

measured $^{143}Nd/^{144}Nd$ normalized to the chondritic uniform reservoir (CHUR = 0.512638) in parts per 10,000 [Jacobsen and Wasserburg, 1980]. Neodymium has a residence time between 400 to 950 years, shorter than the ~1000 yr circulation time of seawater from the North Atlantic to North Pacific, making ƐNd a useful tracer for water mass mixing [Abouchami et al., 1997; von Blanckenburg and O'Nions, 1999; David et al., 2001; Bau and Koschinsky, 2006; Lacan et al., 2012].

Hydrogenetic Fe-Mn crusts in addition to other stratigraphic records support using ƐNd as a tracer for paleo circulation when sediment benthic fluxes are negligible or are taken into account [Abbott et al., 2016; Du et al., 2016; van de Flierdt et al., 2016]. Ocean basins have distinct ƐNd signatures, due to the differences in ƐNd from continental source rocks surrounding the basins [Jeandel et al., 2007; van de Flierdt et al., 2016]. However, dissolved aeolian and fluvial inputs alone cannot account for the mass balance of Nd in the oceans [Goldstein et al., 1984; Goldstein and Jacobsen, 1988; Tachikawa et al., 1999; Jeandel et al., 2007; van de Flierdt et al., 2016]. Along continental margins "boundary exchange" which describes all chemical transfer reactions between terrestrial particles and seawater (adsorption/desorption, dissolution/precipitation, redox, and ion exchange) is thought to be one of the drivers of ƐNd in the oceans [Lacan and Jeandel, 2005; Jeandel et al., 2007; Jeandel and Oelkers, 2015]. Possible additional inputs of Nd to the oceans from submarine ground water discharge, pore water fluxes, and reversible scavenging have also been considered [Abbott et al., 2015a; Du et al., 2016; van de Flierdt et al., 2016]. There is

a decoupling between Nd concentration and isotopic ratios, the “Nd Paradox” further complicating use of ƐNd in seawater as a tracer or paleo proxy [Stichel et al., 2015].

3.3.2 Lead Isotopes

Dissolved lead in modern seawater has been greatly impacted by anthropogenic sources, however, Fe-Mn crusts make excellent archives of pre-anthropogenic seawater Pb isotopic compositions (e.g. Chen et al., 2013; Christensen, 1997; Foster and Vance, 2006; Klemm et al., 2007). Since the removal of Pb from gasoline and paint, anthropogenic inputs of Pb have decreased leading to higher concentrations of Pb in deep “older” water than in surface waters across most of the ocean [Boyle et al., 2005; Dekov et al., 2006]. Seawater profiles of Pb without anthropogenic influences would show a decrease with water depth, as Pb is rapidly scavenged from seawater and has a residence time of 80-100 years [Abouchami et al., 1997; Frank, 2002]. Hydrothermal sources of Pb are minor, <2% of the total flux [Frank, 2002; van de Flierdt et al., 2004b]. Aeolian dust contributes approximately 10-12% of the natural flux of dissolved Pb to the oceans [Chow and Patterson, 1962; Frank, 2002]. Rivers are considered to be a much greater source of Pb [Frank, 2002]. However, dissolved Pb is rapidly scavenged in estuaries and given the short residence time, dust may be an important source in the open ocean [Jones et al., 2000]. Unlike Nd, Pb undergoes fractionation during weathering. The radiogenic isotopes, ^{206}Pb, ^{207}Pb, ^{208}Pb are loosely bonded and are more easily mobilized than nonradiogenic ^{204}Pb [Erel et al., 1994; Jones et al., 2000; Frank, 2002]. This makes determining the terrestrial source of Pb isotopes in seawater difficult as dissolved Pb in seawater does

not always reflect the source rock isotopic signature [von Blanckenburg and Nägler, 2001; Frank, 2002].

3.4 Methods

Ferromanganese crusts D11-4, T145-R9, T141-R5, and D173-R2 from Hoss, Davidson and Taney Seamounts within the CCM were selected for paleoceanographic study. These crusts were selected based on chemical composition, thickness, and internal growth structures. The selected samples all have Fe/Mn ratios between 1.00 to 1.53 and plot within the hydrogenetic region on genesis discrimination diagrams [Bonatti et al., 1972; Bau et al., 2014; Conrad et al., 2017a]. The internal structures of the samples are laminated or massive, which are preferred for paleoceanographic work as it is easier to sample across a single layer of the crust with a consistent age. Samples were encased in TAP Plastic Clear-Lite casting resin and cut into billets perpendicular to the growth surface. The billets were mounted on glass slides in preparation for subsampling. To determine growth rates and ages of the Fe-Mn crusts, $^{187}Os/^{188}Os$ ratios were compared to the Cenozoic Os isotope seawater curve [Klemm et al., 2005; Sen and Peucker-Ehrenbrink, 2014; Conrad et al., 2017b].

Neodymium samples were collected using a New Wave Micromill with diamond tipped flat head bit. Subsamples for Nd were collected continuously down the stratigraphic layers at 0.3 mm resolution. Every second or third Nd subsample was prepared for analysis resulting in a 0.3 mm sample every 0.6 to 1.2 mm. Samples were prepared for Nd analysis by column chemistry using Eichrom Ln resin 50-100 μm particle size after the method of [Scher and Delaney, 2010] and analyzed on a

Neptune multicollector-inductively coupled plasma mass spectrometer (MC-ICPMS) at the Woods Hole Oceanographic Institute (WHOI) Non-traditional Isotope Research on Various Advanced Novel Applications (NIRVANA) facility [Conrad et al., 2017b]. Standard JNdi-1 with a reference value of $^{143}Nd/^{144}Nd$ 0.512115± 7 was used for data correction and to determine accuracy. A value of 0.512115 ± 7 for standard JNdi-1 corresponds to a value 0.511858 ± 7 for the La Jolla Nd standard [Tanaka et al., 2000]. Over the course of the study JNdi-1 had a 2 σ standard deviation of $^{143}Nd/^{144}Nd$ = 3.82E-5, n=48. United States Geological Survey nodule standards A-1 and P-1 were prepared along with the samples and compared to previously published values [Foster and Vance, 2006a].

Lead isotopes were analyzed on three Fe-Mn crusts using an NWR193 laser ablation connected to a Neptune MC-ICPMS after the method of [Foster and Vance, 2006b]. Billets of these crusts were placed into an aluminum foil lined ablation cell sample holder and packed with Crayola air-dry clay along with three pressed powder pellets of both the USGS A-1 and P-1 nodule standards. Pellets were prepared using a hand press at the WHOI experimental petrology lab. Setting the samples and pellets in clay created a very level surface on which to focus the laser and allowed sequential sampling of USGS A-1 and P-1 nodule standards and Fe-Mn crust samples. Standard sample bracketing was used to correct the Pb data for internal fractionations; the Tl fractionation factor could not be resolved [Conrad et al., 2017b]. In total, 40 pairs of USGS A-1 and P-1 nodule standards were run with a 2 σ standard deviation for A-1 – P-1 of ±0.03 $^{206}Pb/^{204}Pb$, ±0.02 $^{207}Pb/^{204}Pb$, and ±0.05 $^{208}Pb/^{204}Pb$.

3.5 Results

3.5.1 Neodymium Isotopes Time Series

Neodymium isotopes were measured in four Fe-Mn crusts: Hoss D11-4 (n=44), Taney D173-R2 (n=56), and Davidson T145-R9 (n=42) and T141-R5 (n=31). Sample ages and water depths are presented in Table 1. Neodymium isotope data for samples older than ~ 4.5 Ma from Davidson Fe-Mn crusts were excluded as those data show a trend away from regional values due to large local inputs, and have been previously discussed [Conrad et al., 2017b]. The ƐNd values in CCM samples range from a high of -1.86 in the upper crust layer, most recent growth layer, of D173-2 (0.03±0.5 Ma) to a low of -4.21 in the upper layer of T145-R9 (0.03±0.5 Ma). The surface layers of T141-R5 and D11-4 are -2.60 and -2.90 ƐNd, respectively (Table 3.1, Figure 3.2). When averaged over approximately 1 Myr, D11-4, D173-R2, T141-R5, and T145-R9 have ƐNd values of -2.95, -2.70, -2.80, and -4.21, respectively (Table 3.1). Davidson Seamount Fe-Mn crust T145-R9 from 3298 m bsl is offset from the other three CCM crusts by approximately 0.5 ƐNd units. This offset is particularly noticeable when comparing T145-R9 against the other Davidson crust T141-R5 from 2388m water depth. Overall, the four CCM Fe-Mn crusts show similar trends with ƐNd increasing from around 7 Ma until around 3 Ma by approximately 0.7 ƐNd units before declining towards modern values (Fig. 3.3). Although, ƐNd in crust D173-R2 increases in the surface as does crust T141-R5. The peak at ~3 Ma is consistent with ƐNd data recorded in central Pacific Fe-Mn crusts (see discussion).

3.5.2 Pb Isotopes Time Series

Lead isotopes were measured in three Fe-Mn crusts, Hoss D11-4 (n=188), Davidson T145-R9 (n=125), and Taney D173-R2 (n=87). Sample T141-R5 from Davidson seamount was not analyzed for Pb isotopes. Ferromanganese crust D11-4 from Hoss Seamount was analyzed for Pb isotopes from 8.7±0.5 Ma to present but not through the older section of the crust. These exclusions allowed for development of higher resolution records over the period of greatest interest. Data from Davidson Fe-Mn crust T145-R9, from 6.1 to 4.8 Myr show a large radiogenic signature due to local inputs which was discussed previously and will not be further discussed here as it does not represent basin wide trends [Conrad et al., 2017b].

In general, all three CCM Fe-Mn crusts measured for Pb isotopes trend towards more radiogenic values with time, consistent with other North Pacific Fe-Mn crusts (see discussion). That trend is most noticeable for $^{206}Pb/^{204}Pb$, which shows a large increase from 18.72 at 8.5±0.5 Ma to 18.86 at 0.10 ±0.5 Ma for Hoss D11-4 (Fig. 3.4). Davidson and Taney crusts show even more radiogenic $^{206}Pb/^{204}Pb$ signatures. Davidson Fe-Mn crust T145-R9 goes from 18.88 at 6.6±0.5 Ma to a high of 18.96 at 0.6±0.5 Ma before decreasing slightly to a modern $^{206}Pb/^{204}Pb$ of 18.95. Taney, D173-R2, shows a very similar trend in $^{206}Pb/^{204}Pb$ with 18.72 at 6.1±0.5 Ma and a high modern seawater ratio of 18.95. Unlike $^{206}Pb/^{204}Pb$ ratios in CCM Fe-Mn crusts, $^{207}Pb/^{204}Pb$ does not change towards radiogenic values relative to central Pacific data until a slight increase in the uppermost layers of Taney D173-R2 and Hoss Dll-4. The average $^{207}Pb/^{204}Pb$ for D11-4, T145-R9, and D173-R2 is 15.64 for

all three crusts with n values of 199, 80 and 87, respectively. Although there are changes in the $^{207}Pb/^{204}Pb$ ratio over time, the scale is much smaller than that of $^{206}Pb/^{204}Pb$. The $^{207}Pb/^{204}Pb$ was nearly consistent through the entire region, whereas $^{206}Pb/^{204}Pb$ showed much greater increase towards radiogenic values at Davidson and Taney seamounts than at Hoss. When comparing the last 1 Myr mean of $^{206}Pb/^{204}Pb$ values, Hoss Seamount (D11-4) is 18.82 (n=63), Davidson (T145-R9) is $^{206}Pb/^{204}Pb$= 18.94 (n=16), and Taney D173-R2 is $^{206}Pb/^{204}Pb$= 18.93 (n=19). All three CCM Fe-Mn crusts show a very similar trend for $^{208}Pb/^{204}Pb$, which starts within the range of central Pacific data with a low of 38.63 at 8.4±0.5 Ma in D11-4 and gradually increases starting at ~6 Ma to a high of 39.02 at 0.1±0.5 Ma in D11-4.

3.6 Results

3.6.1 Sources of Nd to the northeast Pacific deep water

Neodymium isotopes in Fe-Mn crusts can be used as tracers of water masses and water mixing, presuming that ƐNd reflects conservative water-mass mixing [Abouchami et al., 1997; Frank, 2002; Abbott et al., 2015a]. However, that is unlikely to be the case along continental margins where ƐNd may be altered by boundary exchange processes [Abbott et al., 2015a; Stichel et al., 2015]. Further contributing to the non-conservative nature of ƐNd are benthic pore water fluxes from sediment [Abbott et al., 2015b; Du et al., 2016]. Input of Nd from benthic flux and possibly reversible scavenging into bottom waters means that ƐNd in the Pacific is not conservative within water masses [Du et al., 2016]. Northeast Pacific, Gulf of Alaska

(GOA) pore waters have a more radiogenic ƐNd than bottom water and GOA bulk sediment [Du et al., 2016]. Sediment, seawater, and pore fluid samples from the Oregon margin show that seawater ƐNd remains constant with depth, -2.5 at 1200 m and -2.3 at 3000 m bsl, which is within error [Abbott et al., 2015a]. If the ƐNd were recording water mass mixing between North Pacific Intermediate Water (NPIW) and Pacific Deep Water (PDW), then ƐNd would be expected to become less radiogenic with depth towards a PDW ƐNd signature, -3 to -3.5 [Haley et al., 2014; Abbott et al., 2015a]. Instead ƐNd deviates towards pore fluid values from sediments (-0.2 to -1.8) showing the importance of benthic fluxes from sediment pore fluids to bottom water [Abbott et al., 2015a]. This is consistent with ƐNd measurements on core-top sediments from the GOA that show ƐNd of core top leachates, representing sediment pore fluid, are more radiogenic than bottom water and that measured seawater profiles deviate towards the sediment and therefore the pore fluid values [Du et al., 2016]. It should be noted that Fe-Mn oxyhydroxides (diagenetic micronodules and grain coatings) in the core-tops were the main Nd bearing phases and acquired their ƐNd signature from the pore water then, once formed, acted to buffer the benthic flux [Du et al., 2016].

To evaluate ƐNd in the northeast Pacific ƐNd from the uppermost layers of CCM, central Pacific, and northeast Pacific Fe-Mn crusts were compared to ƐNd of core top leachates, seawater profiles from the GOA, sediment and sediment pore water from the Oregon coast, and the predicted ƐNd for 1200 year old conservative mixed water (NPIW and PDW) from along the northeastern Pacific coast (Fig. 3.2)

[Haley et al., 2014; Abbott et al., 2015a; Du et al., 2016]. Surface data from Davidson T141-R5 (2,398m) and Hoss D11-4 (~2550 m) plot along the GOA seawater profiles and show slightly more radiogenic ƐNd values than the modeled conservative mixing line, trending towards sediment benthic flux values. Central Pacific CD29-2 (ƐNd -3.71) plots essentially on the modeled conservative mix line for NPIW and PDW. Northeast Pacific D4-13A from the GOA (ƐNd -1.87) is within error of the seawater profiles but trends slightly towards pore water values. Taney D173-R2 (3178 m) shows slightly higher ƐNd and plots off the GOA seawater profiles towards GOA sediment pore fluids, almost congruent with Oregon sediment pore fluid values. These data indicate that benthic fluxes from sediment pore waters influence ƐNd in PDW along the CCM to a depth of ~3000 m, in good agreement with published data [Haley et al., 2014; Abbott et al., 2015b, 2015a, 2016; Du et al., 2016].

3.6.2 Evidence for the presence of Pacific bottom water

A less radiogenic ƐNd was measured from the surface of Davidson crust T145-R9 (3298 m, ƐNd -4.21) than in surface samples from the other CCM Fe-Mn crusts. The second youngest layer in T145-R9 (ƐNd -3.61) falls between the modeled NPIW-PDW mixing line and the GOA seawater profiles (Fig. 3.2). The -4.21 ƐNd value from T145-R9 is consistent with a lower ƐNd signature in T145-R9 overall. When comparing ƐNd in CCM Fe-Mn crusts over the past 9 Myr, Hoss D11-4, Taney D173-R2, and Davidson T141-R5 show a very similar range of ƐNd values despite the different water depths, distances between the samples, and proximity to the continental shelf (Fig. 3.3). Davidson T141-R5 generally falls between D173-R2 and

D11-4, with D173-R2 having the most radiogenic ƐNd values. The two Davidson Fe-Mn crusts T145-R9 (3298m) and T141-R5 (2388) have similar trends but the deeper water T145-R9 is 0.42 ƐNd units less radiogenic on average and appears to plot closer to some of the central Pacific Fe-Mn crust data. Central Pacific Fe-Mn crusts VA13/2 and MDD53 have less radiogenic ƐNd than T145-R9, for some data points. For both crusts this was attributed to the Pacific bottom water signature [Ling et al., 1997; Chen et al., 2013].

Davidson crust T145-R9 is the deepest water CCM sample and Davidson Seamount is closest to the continental shelf where it is more likely to be influenced by upwelling and shelf boundary exchange processes. Pacific bottom water has a less radiogenic ƐNd (-4.5 to -6) signal than PDW (-3.5) and NPIW (-3.0), and northeast Pacific surface water with ƐNd ~ -2.2 to 0.2 [Piepgras and Jacobsen, 1988; Shimizu et al., 1994; Amakawa et al., 2004a, 2004b; Haley et al., 2014; Abbott et al., 2015b]. Pacific bottom water is the most likely source of the Nd providing the less radiogenic ƐNd observed in crust T145-R9, even with a diluted, more radiogenic ƐNd value due to the influence of benthic flux from sediment pore water. Other potential sources of Nd including boundary exchange from the shelf and terrestrial input from the continent would be apparent in crust T141-R5 and would have a more radiogenic ƐNd as would submarine ground water discharge [Haley et al., 2014,2004; Johannesson and Burdige, 2007]. Hydrothermal systems are not a significant source of Nd as it is scavenged before the Nd isotope signature of the surrounding water can be affected [van de Flierdt et al., 2004b].

3.6.3 ƐNd evolution in the northeast Pacific

The most noticeable trend in CCM Fe-Mn crust ƐNd data over the past 9 Myr is a peak in ƐNd around 3 Ma. That peak is also observed in some of the central Pacific crust data, specifically crusts D11-1, CD29-2, MKD13, and CSD55, although given the sampling resolution the exact timing is questionable in some samples (Fig. 3.3) [Ling et al., 1997; Chen et al., 2013]. Other central Pacific Fe-Mn crusts do not show this peak, and the North Pacific crusts D4-13A and 13D-27A show a much broader and slightly older peak that tapers off and decreases slightly starting around 5 Ma [van de Flierdt et al., 2004a]. The timing of the ƐNd decrease in North Pacific Fe-Mn crusts coincides with a decrease in ƐNd in Arctic Ocean Fe-Mn crusts attributed to intensification of Northern Hemisphere Glaciation and an increased input of less radiogenic ƐNd material eroded and transported to the Arctic Ocean [van de Flierdt et al., 2004a; Dausmann et al., 2015].

Previous studies attributed the peak in ƐNd values at ~3 Ma in central Pacific Fe-Mn crusts to the closure of the Panama Gateway [Ling et al., 1997]. The hypothesis is that closing of the Panama gateway would have decreased the contribution from North Atlantic Bottom Water (NABW) (ƐNd ~ -13), causing the trend towards more radiogenic ƐNd values observed in Pacific Fe-Mn crusts starting ~ 14 Ma, when the depth of the Isthmus of Panama shoaled enough to restrict mixing of deep waters [Ling et al., 1997; Frank, 2002; Schmittner et al., 2004; Brierley and Fedorov, 2016]. The trend towards less radiogenic ƐNd since ~ 3 Ma was then attributed to an increase in North Atlantic Deep Water (NADW) to the Pacific via

circumpolar circulation [Ling et al., 1997]. This is consistent with ƐNd data from Atlantic Ocean Fe-Mn crusts that trend towards less radiogenic ƐNd values starting at ~ 4 Ma but is not reflected in Fe-Mn crusts from the Southern Ocean [O'Nions et al., 1998; Abouchami et al., 1999; Burton et al., 1999a; Frank, 2002]. It is possible that local inputs from the Southern Ocean control the ƐNd values in Southern Ocean Fe-Mn crusts [Frank, 2002]. Regardless, since the trend towards less radiogenic ƐNd is not present in Southern Ocean crusts circumpolar circulation is unlikely to be the cause of the less radiogenic ƐNd values observed in North Pacific crusts since ~ 4 Ma. New age models for the closing of the Panama gateway also do not fit with this idea [Coates and Stallard, 2013].

An alternative hypothesis attributed the rise in ƐNd to an increase in terrestrial input from young ƐNd radiogenic Pacific volcanic arcs [Ling et al., 2005]. Input from Pacific volcanic arcs and marine basalts could account for the more radiogenic ƐNd signature observed in CCM Fe-Mn crusts until ~3 Ma [van de Flierdt et al., 2004a; Castillo et al., 2010; Haley et al., 2014]. The intensification of Northern Hemisphere Glaciation, which roughly fits the inflection point of the ƐNd peak in CCM Fe-Mn crusts, may have resulted in a change in weathering regimes leading to an influx of eroded continental material [Raymo, 1994; von Blanckenburg and Nägler, 2001; Zachos et al., 2001; Foster and Vance, 2006b]. After ~ 3 Ma, the ƐNd recorded in Pacific Fe-Mn crusts gradually decreased by about 1 ƐNd unit. The cause of this decrease is most likely input of older continental material from North America with less radiogenic ƐNd values than previous Pacific seawater and Pacific volcanic arcs.

Much of the coastal terrain in California is too young and has ƐNd values that are too radiogenic to provide the unradiogenic endmember needed [Heumann and Davies, 1997; Borg et al., 2000; Schmitt et al., 2006]. However, older regions further inland and north of California could have provided the necessary Nd with unradiogenic ƐNd. Continental input delivered into the Pacific along the coast from the Columbia River drainage has modern ƐNd of -3 to -4.5 with most older samples collected from the offshore fan showing ƐNd values of -7.1 to -15.2 [Goldstein and Jacobsen, 1988; Prytulak et al., 2006]. These sediment samples show isotope compositions with a mix of Columbia River Basalts (ƐNd 0) and Proterozoic Belt Supergroup meta-sediments (ƐNd -8 to -30) or northeastern Idaho Batholith (-18 to -21), and were deposited by flood events from cyclical filling and failure of glacial lakes starting at ~ 2.5 Ma with the most recent event at 14 to 13 ka [Prytulak et al., 2006]. That fits very well with the timing of the change towards less radiogenic ƐNd observed in Fe-Mn crusts; suggesting that this caused the trend towards less radiogenic ƐNd observed in some central Pacific Fe-Mn crusts over the same period.

Past formation of PDW in the North Pacific would not result in less radiogenic ƐNd as source rocks for PDW would not provide an unradiogenic Nd endmember, as evidenced by GOA and northeast Pacific sediments [Haley et al., 2014; Abbott et al., 2015b, 2015a; Du et al., 2016]. Future sampling of Nd isotopes in the Pacific on upcoming GEOTRACERS cruises should help to identify the ƐNd of Pacific water masses and to constrain currently poorly understood ƐNd sources from continental margin boundary exchange and benthic fluxes.

3.6.4 Pb evolution and provenance in the northeast Pacific

Lead isotope data from three northeast Pacific CCM Fe-Mn crusts, Hoss D11-4, Davidson T145-R9, and Taney D173-R2, for the past 9 Myr are compared to high-resolution Pb isotope data from North and central Pacific Fe-Mn crusts (Fig. 3.4). Lead isotopes in CCM Fe-Mn crusts have $^{206}Pb/^{204}Pb$ trends similar to North Pacific crusts with ratios moving towards radiogenic values, relative to central Pacific crusts, starting around 7 to 6 Ma [Ling et al., 1997, 2005; van de Flierdt et al., 2003; Chen et al., 2013]. Rates of sedimentation in the GOA, along the Surveyor and Baranoff Fans, show increased sedimentation between 5.91 and 5.50 Ma [Lagoe et al., 1993; van de Flierdt et al., 2003], which matches the inflection towards more radiogenic $^{208}Pb/^{204}Pb$ and $^{206}Pb/^{204}Pb$ in CCM Fe-Mn crusts. All of the Pb isotope ratios have more radiogenic values in Davidson crust T145-R9 and Taney crust D173-R2 than those in North and central Pacific Fe-Mn crusts, while Hoss crust D11-4 has a $^{206}Pb/^{204}Pb$ ratio slightly less radiogenic than the other CCM Fe-Mn crusts and values at Hoss level out ~ 2 Ma, to a trend that resembles central Pacific crusts. This likely reflects a greater influence from NPIW and Asian aerosol sources at Hoss Seamount. That theory is supported by a $^{206}Pb/^{204}Pb$ vs $^{208}Pb/^{204}Pb$ plot of potential sources where Hoss D11-4 trends towards more radiogenic values but deviates from the other CCM crusts in the direction of Asian loess (Fig. 3.5). The bias toward a central Pacific end member is consistent with the location of Hoss Seamount and the greater distance to continental sources than at Davidson Seamount.

The Pb isotope records from Taney crust D173-R2 and Davidson crust T145-R9 are similar. For $^{206}Pb/^{204}Pb$, Taney crust D173-R2 shows step increases at ~ 5.6 Ma, ~ 4.2 Ma, ~ 2.7 Ma, and ~0.3 Ma towards more radiogenic values. Davidson crust T145-R9 shows similar steps at ~ 4.7 Ma, ~ 2.7 Ma, and ~ 0.7 Ma. The same step increases from ~ 4.2 Ma on were found in Arctic Ocean Fe-Mn crusts with the first two steps matching very well and the third occurring within error ~ 0.5 Ma [Dausmann et al., 2015]. The consistency in timing and trends between the CCM and the Arctic indicates that this is likely due to a change in glacial weathering rather than solely an increase or change in local source. The step trends are not apparent in the North Pacific Fe-Mn crusts. Lead undergoes incongruent physical weathering that is likely enhanced during interglacial times, which resulted in the radiogenic Pb signatures recorded in CCM Fe-Mn crusts. The differences among $^{206}Pb/^{204}Pb$, $^{208}Pb/^{204}Pb$, and $^{207}Pb/^{204}Pb$ are likely due to the source rock and not weathering processes or loss of $^{207}Pb/^{204}Pb$ signature along the path to the ocean.

To determine the source of more radiogenic Pb in North Pacific Fe-Mn crusts, [van de Flierdt et al., 2003] used a four-member mixing model that considered the Meiji drift (material from the Bering Sea), GOA sediments from North America, Asian loess, and Aleutian Arc material. Weathering of continental material from North America delivered by rivers (GOA sediments) mixed with material from the Bearing Sea (Meji Drift) as an unradiogenic endmember was considered the most likely source reflected in the radiogenic Pb trends observed in North Pacific Fe-Mn crusts. This led to the conclusion that Pb in the marginal far northeast Pacific reflects

continental river inputs from North America [van de Flierdt et al., 2003]. That is consistent with the findings in Arctic Fe-Mn crusts that show very similar trends among all Pb isotope ratios, shifting towards a terrestrial source supplied by the Mackenzie River at ~4.5 Ma [Dausmann et al., 2015]. Given these previous findings, river sources to the CCM and nearby coast are considered, including lead isotope data from the Columbia, Fraser, Skeena, and Nass river sediments (Fig. 3.1) [Millot et al., 2004; Prytulak et al., 2006]. Hoss crust D11-4 and Davidson crust T145-R9 plot between central Pacific Pb isotope ratios, represented by an average Pacific volcanic arc and crust CD29-2 ratios, towards Columbia and Fraser River ratios (Fig 3.5). While the Fraser River is a much more radiogenic end member, the Columbia River transports more material. Measurements of dissolved seawater Pb isotopes along transect Line P (Fig. 3.1) show Asian dust sources at the western most point of the transect and North American fluvial sources along the line eastward towards the coast [McAlister, 2015]. A terrestrial source of radiogenic Pb delivered to the ocean via fluvial input is consistent with CCM Fe-Mn crust records; the sample closest to shore, Davidson crust T145-R9 shows the most radiogenic ratios, followed by D173-R2. While D11-4, the CCM sample furthest from a Columbia or Fraser River source and the continental shelf, has a less radiogenic signature indicating mixing with central equatorial Pacific lead sources, Asian dust, and Pacific deep water.

3.7 Conclusions

Time-series data for ƐNd and Pb isotopes from regionally distributed CCM Fe-Mn crusts spanning the past 9-7 Ma along the northeastern Pacific are discussed in

the context of similar records from the central Pacific, North Pacific, and Arctic. Variations in radiogenic terrestrial sources delivered to the near-shore northeast Pacific via fluvial input are recorded in these Fe-Mn crusts in both ƐNd and Pb isotope systems.

The ƐNd ratios recorded in Fe-Mn crusts do not fall on the conservative mixing line between NPIW and PDW, but rather deviates towards sediment pore-water fluids supporting benthic flux as one of the sources of Nd in the Pacific Ocean with a radiogenic ƐNd. This conclusion is based on comparisons among ƐNd in CCM Fe-Mn crust surfaces, ƐNd water-depth profiles, and sediment pore-water measurements from the GOA and Oregon coast. The deepest water CCM Fe-Mn crust does not indicate a benthic flux source and instead shows evidence of a less radiogenic ƐNd Pacific Bottom Water mass below 3200 m. All of the CCM Fe-Mn crusts show a general trend towards more radiogenic ƐNd values until ~3 Ma when the trend changes to less radiogenic values towards the present. This is consistent with ƐNd trends observed in some central Pacific crusts. Intensification of Northern Hemisphere Glaciation and repeated failures of glacial lakes beginning at ~2.5 Ma resulted in large amounts of material that were delivered though the Columbia River onto the Astoria Fan providing a source of Nd with unradiogenic ƐNd that changed the ƐNd seawater values recorded in CCM and central Pacific Fe-Mn crusts.

Lead isotopes in CCM Fe-Mn crusts trend away from those of central Pacific Fe-Mn crusts and towards radiogenic terrestrial material from ~7 Ma to present, particularly in the $^{206}Pb/^{204}Pb$ record. This trend is similar to those from far North

Pacific and Arctic Ocean crusts. Fluvial input from North American rivers is the most likely source of the radiogenic Pb. Two of the CCM crusts, from Taney and Davidson Seamounts, fall on a mixing line between central Pacific Fe-Mn crusts and the Columbia River or Fraser River sediments. A third CCM crust, from Hoss Seamount, has slightly less radiogenic $^{206}Pb/^{204}Pb$ ratios than the other CCM crusts and deviates from the central Pacific ratios to a North American river mixing line and then towards Asian dust. This indicates that North American river input has a geographically limited scope as a Pb isotope source, a finding consistent with Pb isotope analysis along transect Line P off the coast of Vancouver Island.

Acknowledgements

We would like to thank the Monterey Bay Aquarium Research Institute (MBARI) for providing samples. We thank the crew of the R.V. *Western Flyer* and the operators of the ROV *Doc Ricketts*. We would also like to thank David Clague and Jenny Paduan, for help in sampling and data retrieval. We thank the Captain and crew of the RV *Farnella* cruise F7-87-CP for sample collection. We are also grateful to the researchers and support staff at the Woods Hole Oceanographic Institution particularly Tristan Horner and Jeremy Owens.

References

Abbott, A. N., B. A. Haley, and J. McManus (2015a), Bottoms up: Sedimentary control of the deep North Pacific Ocean's εNd signature, *Geology*, *43*(11), 1035–1035, doi:10.1130/G37114.1.

Abbott, A. N., B. A. Haley, J. McManus, and C. E. Reimers (2015b), The sedimentary flux of dissolved rare earth elements to the ocean, *Geochim. Cosmochim. Acta*, *154*, 186–200, doi:10.1016/j.gca.2015.01.010.

Abbott, A. N., B. A. Haley, and J. McManus (2016), The impact of sedimentary coatings on the diagenetic Nd flux, *Earth Planet. Sci. Lett.*, *449*, 217–227, doi:10.1016/j.epsl.2016.06.001.

Abouchami, W., S. L. Goldstein, S. J. G. Gazer, A. Eisenhauer, and A. Mangini (1997), Secular changes of lead and neodymium in central Pacific seawater recorded by a Fe-Mn crust, *Geochim. Cosmochim. Acta*, *61*(18), 3957–3974.

Abouchami, W., S. J. G. Galer, and A. Koschinsky (1999), Pb and Nd isotopes in NE Atlantic Fe–Mn crusts: proxies for trace metal paleosources and paleocean circulation, *Geochim. Cosmochim. Acta*, *63*(10), 1489–1505.

Amakawa, H., D. S. Alibo, and Y. Nozaki (2004a), Nd concentration and isotopic composition distributions in surface waters of Northwest Pacific Ocean and its adjacent seas, *Geochem. J.*, *38*(6), 493–504, doi:10.2343/geochemj.38.493.

Amakawa, H., Y. Nozaki, D. S. Alibo, J. Zhang, K. Fukugawa, and H. Nagai (2004b), Neodymium isotopic variations in Northwest Pacific waters1, *Geochim. Cosmochim. Acta*, *68*(4), 715–727, doi:10.1016/S0016-7037(03)00501-5.

Barron, J. A., and D. Bukry (2007), Development of the California Current during the past 12,000 yr based on diatoms and silicoflagellates, *Palaeogeogr. Palaeoclimatol. Palaeoecol.*, *248*(3–4), 313–338, doi:10.1016/j.palaeo.2006.12.009.

Bau, M., and A. Koschinsky (2006), Hafnium and neodymium isotopes in seawater and in ferromanganese crusts: The "element perspective," *Earth Planet. Sci. Lett.*, *241*(3–4), 952–961, doi:10.1016/j.epsl.2005.09.067.

Bau, M., K. Schmidt, A. Koschinsky, J. Hein, T. Kuhn, and A. Usui (2014), Discriminating between different genetic types of marine ferro-manganese crusts and nodules based on rare earth elements and yttrium, *Chem. Geol.*, *381*, 1–9, doi:10.1016/j.chemgeo.2014.05.004.

Berelson, W. M., J. McManus, S. Severmann, and C. E. Reimers (2013), Benthic flux of oxygen and nutrients across Oregon/California shelf sediments, *Cont. Shelf Res.*, *55*, 66–75, doi:10.1016/j.csr.2013.01.009.

Biller, D. V., and K. W. Bruland (2014), The central California Current transition zone: A broad region exhibiting evidence for iron limitation, *Prog. Oceanogr.*, *120*, 370–382, doi:10.1016/j.pocean.2013.11.002.

von Blanckenburg, F., and T. F. Nägler (2001), Weathering versus circulation-controlled changes in radiogenic isotope tracer composition of the Labrador Sea and North Atlantic Deep Water, *Paleoceanography*, *16*(4), 424–434, doi:10.1029/2000PA000550.

von Blanckenburg, F., and R. . O'Nions (1999), Response of beryllium and radiogenic isotope ratios in Northern Atlantic Deep Water to the onset of northern hemisphere glaciation, *Earth Planet. Sci. Lett.*, *167*(3–4), 175–182, doi:10.1016/S0012-821X(99)00028-X.

von Blanckenburg, F., R. K. O'Nions, and J. R. Hein (1996), Distribution and sources of pre-anthropogenic lead isotopes in deep ocean water from FeMn crusts, *Geochim. Cosmochim. Acta*, *60*(24), 4957–4963, doi:10.1016/S0016-7037(96)00310-9.

Bonatti, E., T. Kraemer, and H. A. N. Abdulla (1972), Classification and genesis of submarine iron-manganese deposits, in *Ferromanganese Deposits on the Ocean Floor*, edited by D. R. Horn, pp. 149–166, National Science Foundation, Washington, D.C. USA.

Borg, L. E., A. D. Brandon, M. A. Clynne, and R. J. Walker (2000), Re–Os isotopic systematics of primitive lavas from the Lassen region of the Cascade arc, California, *Earth Planet. Sci. Lett.*, *177*(3), 301–317.

Boyle, E. A., B. A. Bergquist, R. A. Kayser, and N. Mahowald (2005), Iron, manganese, and lead at Hawaii Ocean Time-series station ALOHA: Temporal variability and an intermediate water hydrothermal plume, *Geochim. Cosmochim. Acta*, *69*(4), 933–952, doi:10.1016/j.gca.2004.07.034.

Brierley, C. M., and A. V. Fedorov (2016), Comparing the impacts of Miocene–Pliocene changes in inter-ocean gateways on climate: Central American Seaway, Bering Strait, and Indonesia, *Earth Planet. Sci. Lett.*, *444*, 116–130, doi:10.1016/j.epsl.2016.03.010.

Burton, K. W., D.-C. Lee, J. N. Christensen, A. N. Halliday, and J. R. Hein (1999), Actual timing of neodymium isotopic variations recorded by FeMn crusts in the western North Atlantic, *Earth Planet. Sci. Lett.*, *171*(1), 149–156, doi:10.1016/S0012-821X(99)00138-7.

Castillo, P. R., D. A. Clague, A. S. Davis, and P. F. Lonsdale (2010), Petrogenesis of Davidson Seamount lavas and its implications for fossil spreading center and intraplate magmatism in the eastern Pacific: DAVIDSON FOSSIL SPREADING CENTER LAVA PETROGENESIS, *Geochem. Geophys. Geosystems*, *11*(2), n/a-n/a, doi:10.1029/2009GC002992.

Chan, L. H., and J. R. Hein (2007), Lithium contents and isotopic compositions of ferromanganese deposits from the global ocean, *Deep Sea Res. Part II Top. Stud. Oceanogr.*, *54*(11–13), 1147–1162, doi:10.1016/j.dsr2.2007.04.003.

Chen, T. Y., H. F. Ling, R. Hu, M. Frank, and S. Y. Jiang (2013), Lead isotope provinciality of central North Pacific Deep Water over the Cenozoic, *Geochem. Geophys. Geosystems*, *14*(5), 1523–1537, doi:10.1002/ggge.20114.

Chow, T. J., and C. C. Patterson (1962), The occurrence and significance of lead isotopes in pelagic sediments, *Geochim. Cosmochim. Acta*, *26*(2), 263–308, doi:10.1016/0016-7037(62)90016-9.

Christensen, J. N. (1997), Climate and Ocean Dynamics and the Lead Isotopic Records in Pacific Ferromanganese Crusts, *Science*, *277*(5328), 913–918, doi:10.1126/science.277.5328.913.

Coates, A. G., and R. F. Stallard (2013), How old is the Isthmus of Panama?, *Bull. Mar. Sci.*, *89*(4), 801–813, doi:10.5343/bms.2012.1076.

Conrad, T., J. R. Hein, A. Paytan, and D. A. Clague (2017a), Formation of Fe-Mn crusts within a continental margin environment, *Ore Geol. Rev.*, *87*, 25-40, doi:10.1016/j.oregeorev.2016.09.010.

Conrad, T., S. G. Nielsen, B. Peucker-Ehrenbrink, J. Blusztajn, D. Winslow, J. R. Hein and A. Paytan (2017b), River sediment sources to the Monterey Submarine Canyon System– constraints from Fe-Mn crust Os, Nd, and Pb isotopes, Submitted *Geochim. Geophys. Geosys.*

Dausmann, V., M. Frank, C. Siebert, M. Christl, and J. R. Hein (2015), The evolution of climatically driven weathering inputs into the western Arctic Ocean since the late Miocene: Radiogenic isotope evidence, *Earth Planet. Sci. Lett.*, *419*, 111–124, doi:10.1016/j.epsl.2015.03.007.

David, K., M. Frank, R. K. O'Nions, N. S. Belshaw, and J. W. Arden (2001), The Hf isotope composition of global seawater and the evolution of Hf isotopes in the deep Pacific Ocean from Fe–Mn crusts, *Chem. Geol.*, *178*(1–4), 23–42, doi:10.1016/S0009-2541(00)00427-7.

Dekov, V. M., G. D. Kamenov, C. Savelli, and J. Stummeyer (2006), Anthropogenic Pb component in hydrothermal ochres from Marsili Seamount (Tyrrhenian Sea), *Mar. Geol.*, *229*(3–4), 199–208, doi:10.1016/j.margeo.2006.03.003.

DeMets, C., and S. Merkouriev (2016), High-resolution reconstructions of Pacific–North America plate motion: 20 Ma to present, *Geophys. J. Int.*, *207*(2), 741–773, doi:10.1093/gji/ggw305.

Du, J., B. A. Haley, and A. C. Mix (2016), Neodymium isotopes in authigenic phases, bottom waters and detrital sediments in the Gulf of Alaska and their implications for paleo-circulation reconstruction, *Geochim. Cosmochim. Acta*, *193*, 14–35, doi:10.1016/j.gca.2016.08.005.

Erel, Y., Y. Harlavan, and J. D. Blum (1994), Lead isotope systematics of granitoid weathering, *Geochim. Cosmochim. Acta*, *58*(23), 5299–5306, doi:10.1016/0016-7037(94)90313-1.

van de Flierdt, T., M. Frank, A. N. Halliday, J. R. Hein, B. Hattendorf, D. Günther, and P. W. Kubik (2003), Lead isotopes in North Pacific deep water – implications for past changes in input sources and circulation patterns, *Earth Planet. Sci. Lett.*, *209*(1–2), 149–164, doi:10.1016/S0012-821X(03)00069-4.

van de Flierdt, T., M. Frank, D. C. Lee, A. N. Halliday, B. C. Reynolds, and J. R. Hein (2004a), New constraints on the sources and behavior of neodymium and hafnium in seawater from Pacific Ocean ferromanganese crusts, *Geochim. Cosmochim. Acta*, *68*(19), 3827–3843, doi:10.1016/j.gca.2004.03.009.

van de Flierdt, T., M. Frank, A. N. Halliday, J. R. Hein, B. Hattendorf, D. Günther, and P. W. Kubik (2004b), Tracing the history of submarine hydrothermal inputs and the significance of hydrothermal hafnium for the seawater budget—a combined Pb–Hf–Nd isotope approach, *Earth Planet. Sci. Lett.*, *222*(1), 259–273, doi:10.1016/j.epsl.2004.02.025.

van de Flierdt, T., A. M. Griffiths, M. Lambelet, S. H. Little, T. Stichel, and D. J. Wilson (2016), Neodymium in the oceans: a global database, a regional comparison and implications for palaeoceanographic research, *Phil Trans R Soc A*, *374*(2081), 20150293, doi:10.1098/rsta.2015.0293.

Foster, G. L., and D. Vance (2006a), In situ Nd isotopic analysis of geological materials by laser ablation MC-ICP-MS, *J. Anal. At. Spectrom.*, *21*(3), 288–296, doi:10.1039/B513945G.

Foster, G. L., and D. Vance (2006b), Negligible glacial–interglacial variation in continental chemical weathering rates, *Nature*, *444*(7121), 918–921, doi:10.1038/nature05365.

Frank, M. (2002), Radiogenic Isotopes: Tracers of Past Ocean Circulation and Erosional Input, *Rev. Geophys.*, *40*(1), 1–1, doi:10.1029/2000RG000094.

Goldstein, S. J., and S. B. Jacobsen (1988), Nd and Sr isotopic systematics of river water suspended material: implications for crustal evolution, *Earth Planet. Sci. Lett.*, *87*(3), 249–265, doi:10.1016/0012-821X(88)90013-1.

Goldstein, S. L., R. K. O'Nions, and P. J. Hamilton (1984), A Sm-Nd isotopic study of atmospheric dusts and particulates from major river systems, *Earth Planet. Sci. Lett.*, *70*(2), 221–236, doi:10.1016/0012-821X(84)90007-4.

Haley, B. A., M. Frank, E. Hathorne, and N. Pisias (2014), Biogeochemical implications from dissolved rare earth element and Nd isotope distributions in the Gulf of Alaska, *Geochim. Cosmochim. Acta*, *126*, 455–474, doi:10.1016/j.gca.2013.11.012.

Hein, J. R., and A. Koschinsky (2014), Deep-Ocean Ferromanganese Crusts and Nodules, in *Treatise on Geochemistry*, pp. 273–291, Elsevier.

Hein, J. R., A. Koschinsky, M. Bau, F. T. Manheim, J. K. Kang, and L. Roberts (2000), Cobalt-rich ferromanganese crusts in the Pacific: Chapter 9, in *Handbook of marine mineral deposits*, pp. 239–279, CRC Press, Boca Raton, Florida.

Heumann, A., and G. R. Davies (1997), Isotopic and chemical evolution of the post-caldera rhyolitic system at Long Valley, California, *J. Petrol.*, *38*(12), 1661–1678..

Horner, T. J., M. Schönbächler, M. Rehkämper, S. G. Nielsen, H. Williams, A. N. Halliday, Z. Xue, and J. R. Hein (2010), Ferromanganese crusts as archives of deep water Cd isotope compositions: DATA BRIEF, *Geochem. Geophys. Geosystems*, *11*(4), n/a-n/a, doi:10.1029/2009GC002987.

Ingram, B. L., J. R. Hein, and G. L. Farmer (1990), Age determinations and growth rates of Pacific ferromanganese deposits using strontium isotopes, *Geochim. Cosmochim. Acta*, *54*(6), 1709–1721, doi:10.1016/0016-7037(90)90402-7.

Jacobsen, S. B., and G. J. Wasserburg (1980), Sm-Nd isotopic evolution of chondrites, *Earth Planet. Sci. Lett.*, *50*(1), 139–155, doi:10.1016/0012-821X(80)90125-9.

Jeandel, C., and E. H. Oelkers (2015), The influence of terrigenous particulate material dissolution on ocean chemistry and global element cycles, *Chem. Geol.*, *395*, 50–66, doi:10.1016/j.chemgeo.2014.12.001.

Jeandel, C., T. Arsouze, F. Lacan, P. Téchiné, and J. C. Dutay (2007), Isotopic Nd compositions and concentrations of the lithogenic inputs into the ocean: A compilation, with an emphasis on the margins, *Chem. Geol.*, *239*(1–2), 156–164, doi:10.1016/j.chemgeo.2006.11.013.

Jones, C. E., A. N. Halliday, D. K. Rea, and R. M. Owen (2000), Eolian inputs of lead to the North Pacific, *Geochim. Cosmochim. Acta*, *64*(8), 1405–1416, doi:10.1016/S0016-7037(99)00439-1.

Klemm, V., S. Levasseur, M. Frank, J. Hein, and A. Halliday (2005), Osmium isotope stratigraphy of a marine ferromanganese crust, *Earth Planet. Sci. Lett.*, *238*(1–2), 42–48, doi:10.1016/j.epsl.2005.07.016.

Klemm, V., B. Reynolds, M. Frank, T. Pettke, and A. N. Halliday (2007), Cenozoic changes in atmospheric lead recorded in central Pacific ferromanganese crusts, *Earth Planet. Sci. Lett.*, *253*(1–2), 57–66, doi:10.1016/j.epsl.2006.10.018.

Lacan, F., and C. Jeandel (2005), Neodymium isotopes as a new tool for quantifying exchange fluxes at the continent–ocean interface, *Earth Planet. Sci. Lett.*, *232*(3–4), 245–257, doi:10.1016/j.epsl.2005.01.004.

Lacan, F., K. Tachikawa, and C. Jeandel (2012), Neodymium isotopic composition of the oceans: A compilation of seawater data, *Chem. Geol.*, *300–301*, 177–184, doi:10.1016/j.chemgeo.2012.01.019.

Lagoe, M. B., C. H. Eyles, N. Eyles, and C. Hale (1993), Timing of late Cenozoic tidewater glaciation in the far North Pacific, *Geol. Soc. Am. Bull.*, *105*(12), 1542–1560, doi:10.1130/0016-7606(1993)105<1542:TOLCTG>2.3.CO;2.

Lambelet, M., T. van de Flierdt, K. Crocket, M. Rehkämper, K. Kreissig, B. Coles, M. J. A. Rijkenberg, L. J. A. Gerringa, H. J. W. de Baar, and R. Steinfeldt (2016), Neodymium isotopic composition and concentration in the western North Atlantic Ocean: Results from the GEOTRACES GA02 section, *Geochim. Cosmochim. Acta*, *177*, 1–29, doi:10.1016/j.gca.2015.12.019.

Ling, H. F., K. W. Burton, R. K. O'Nions, B. S. Kamber, F. von Blanckenburg, A. J. Gibb, and J. R. Hein (1997), Evolution of Nd and Pb isotopes in Central Pacific seawater from ferromanganese crusts, *Earth Planet. Sci. Lett.*, *146*(1–2), 1–12, doi:10.1016/S0012-821X(96)00224-5.

Ling, H. F., S. Y. Jiang, M. Frank, H.-Y. Zhou, F. Zhou, Z. L. Lu, X. M. Chen, Y. H. Jiang, and C. D. Ge (2005), Differing controls over the Cenozoic Pb and Nd isotope evolution of deepwater in the central North Pacific Ocean, *Earth Planet. Sci. Lett.*, *232*(3–4), 345–361, doi:10.1016/j.epsl.2004.12.009.

McAlister, J. (2015), Biogeochemistry of dissolved gallium and lead isotopes in the northeast Pacific and western Arctic Oceans, University of British Columbia, 26 May.

Millot, R., C. J. Allègre, J. Gaillardet, and S. Roy (2004), Lead isotopic systematics of major river sediments: a new estimate of the Pb isotopic composition of the Upper Continental Crust, *Chem. Geol.*, *203*(1–2), 75–90, doi:10.1016/j.chemgeo.2003.09.002.

Nielsen, S. G., S. Mar-Gerrison, A. Gannoun, D. LaRowe, V. Klemm, A. N. Halliday, K. W. Burton, and J. R. Hein (2009), Thallium isotope evidence for a permanent increase in marine organic carbon export in the early Eocene, *Earth Planet. Sci. Lett.*, *278*(3–4), 297–307, doi:10.1016/j.epsl.2008.12.010.

Nielsen, S. G., A. Gannoun, C. Marnham, K. W. Burton, A. N. Halliday, and J. R. Hein (2011), New age for ferromanganese crust 109D-C and implications for isotopic records of lead, neodymium, hafnium, and thallium in the Pliocene Indian Ocean: NEW AGE FOR FERROMANGANESE CRUST 109D-C, *Paleoceanography*, *26*(2), n/a-n/a, doi:10.1029/2010PA002003.

O'Nions, R. K., M. Frank, F. Von Blanckenburg, and H. F. Ling (1998), Secular variation of Nd and Pb isotopes in ferromanganese crusts from the Atlantic, Indian and Pacific Oceans, *Earth Planet. Sci. Lett.*, *155*(1), 15–28.

Piepgras, D. J., and S. B. Jacobsen (1988), The isotopic composition of neodymium in the North Pacific, *Geochim. Cosmochim. Acta*, *52*(6), 1373–1381, doi:10.1016/0016-7037(88)90208-6.

Piepgras, D. J., and G. J. Wasserburg (1980), Neodymium isotopic variations in seawater, *Earth Planet. Sci. Lett.*, *50*(1), 128–138, doi:10.1016/0012-821X(80)90124-7.

Piepgras, D. J., and G. J. Wasserburg (1987), Rare earth element transport in the western North Atlantic inferred from Nd isotopic observations, *Geochim. Cosmochim. Acta*, *51*(5), 1257–1271, doi:10.1016/0016-7037(87)90217-1.

Prytulak, J., J. D. Vervoort, T. Plank, and C. Yu (2006), Astoria Fan sediments, DSDP site 174, Cascadia Basin: Hf–Nd–Pb constraints on provenance and outburst flooding, *Chem. Geol.*, *233*(3–4), 276–292, doi:10.1016/j.chemgeo.2006.03.009.

Raymo, M. E. (1994), The Initiation of Northern Hemisphere Glaciation, *Annu. Rev. Earth Planet. Sci.*, *22*(1), 353–383, doi:10.1146/annurev.ea.22.050194.002033.

Scher, H. D., and M. L. Delaney (2010), Breaking the glass ceiling for high resolution Nd isotope records in early Cenozoic paleoceanography, *Chem. Geol.*, *269*(3–4), 329–338, doi:10.1016/j.chemgeo.2009.10.007.

Schmitt, A. K., R. L. Romer, and J. A. Stimac (2006), Geochemistry of volcanic rocks from the Geysers geothermal area, California Coast Ranges, *Lithos*, *87*(1–2), 80–103, doi:10.1016/j.lithos.2005.05.005.

Schmittner, A. et al. (2004), Global impact of the Panamanian Seaway, *Eos Trans. Am. Geophys. Union*, *85*(49), 526–527.

Sen, I. S., and B. Peucker-Ehrenbrink (2014), Determination of Osmium Concentrations and ^{187}Os/^{188}Os of Crude Oils and Source Rocks by Coupling High-Pressure, High-Temperature Digestion with Sparging OsO_4 into a Multicollector Inductively Coupled Plasma Mass Spectrometer, *Anal. Chem.*, *86*(6), 2982–2988, doi:10.1021/ac403413y.

Shimizu, H., K. Tachikawa, A. Masuda, and Y. Nozaki (1994), Cerium and neodymium isotope ratios and REE patterns in seawater from the North Pacific Ocean, *Geochim. Cosmochim. Acta*, *58*(1), 323–333, doi:10.1016/0016-7037(94)90467-7.

Stichel, T., A. E. Hartman, B. Duggan, S. L. Goldstein, H. Scher, and K. Pahnke (2015), Separating biogeochemical cycling of neodymium from water mass mixing in the Eastern North Atlantic, *Earth Planet. Sci. Lett.*, *412*, 245–260, doi:10.1016/j.epsl.2014.12.008.

Tachikawa, K., C. Jeandel, and M. Roy-Barman (1999), A new approach to the Nd residence time in the ocean: the role of atmospheric inputs, *Earth Planet. Sci. Lett.*, *170*(4), 433–446, doi:10.1016/S0012-821X(99)00127-2.

Tanaka, T. et al. (2000), JNdi-1: a neodymium isotopic reference in consistency with LaJolla neodymium, *Chem. Geol.*, *168*(3–4), 279–281, doi:10.1016/S0009-2541(00)00198-4.

Zachos, J., M. Pagani, L. Sloan, E. Thomas, and K. Billups (2001), Trends, Rhythms, and Aberrations in Global Climate 65 Ma to Present, *Science*, *292*(5517), 686–693, doi:10.1126/science.1059412.

Figures

Figure 3.1. Location map showing seamount and sample locations for crusts from three California Margin seamounts used in this study, Central Pacific Fe-Mn crusts used for reference from [Christensen, 1997; Ling et al., 1997, 2005; Chen et al., 2013], and North Pacific samples [van de Flierdt et al., 2003]. Line P shows location for Pb isotope data from [McAlister, 2015] and the ellipse labeled Oregon shows locations for pore water samples [Abbott et al., 2015a].

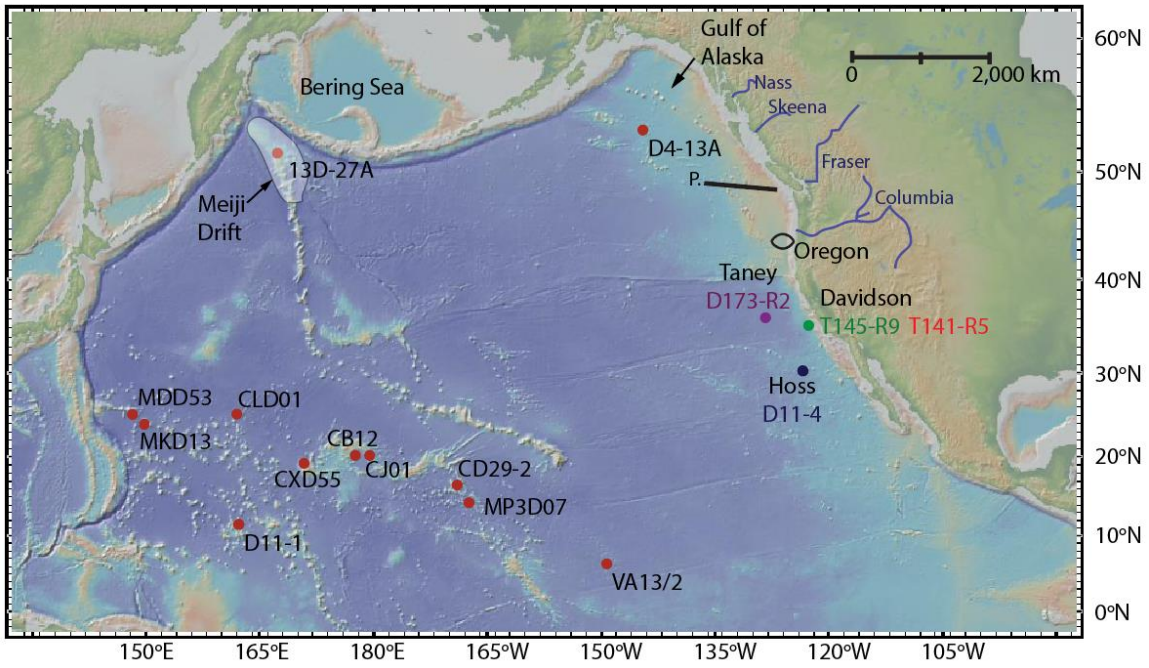

Figure 3.2. Plots showing ƐNd versus water depth for Gulf of Alaska (GOA) core top leachates[1], Oregon sediment and pore fluid samples (HH3000) [1], surface data from four California margin Fe-Mn crusts and comparison with northeast Pacific D4-13A[3] and central Pacific CD29-2[4]. Depth profiles from the Gulf of Alaska (GOA)[5], with a mixing line for North Pacific Intermediate water (NPIW) and North Pacific Deep Water (NPDW)[1] shown for comparison. Surface-water range is also for GOA[1&5]. 1. [Du et al., 2016]; 2. [Abbott et al., 2015a]; 3. [van de Flierdt et al., 2004a] ; 4. [Ling et al., 1997]; 5. [Haley et al., 2014].

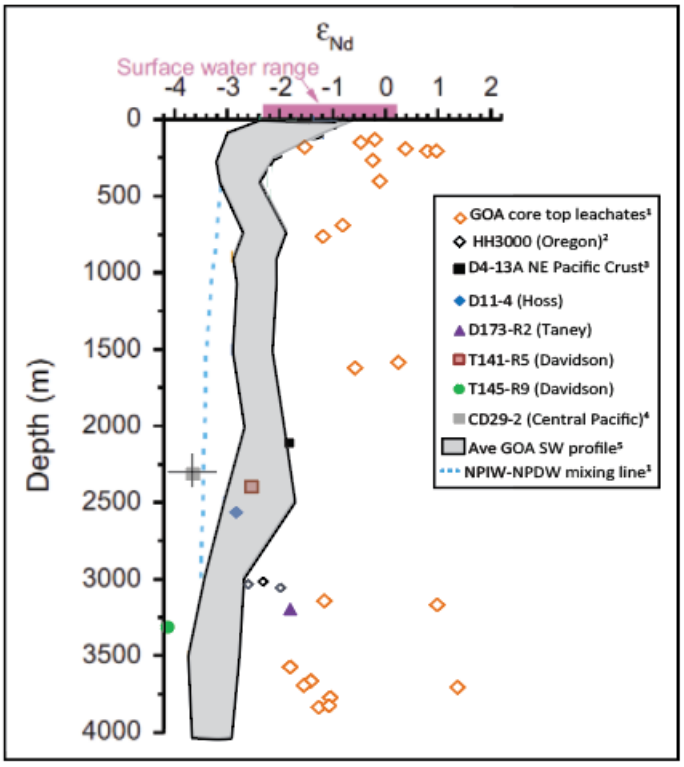

Figure 3.3. Plot showing ƐNd data for four California margin samples compared to Fe-Mn crust samples from the North and central Pacific over the past 9 Myr [Ling et al., 1997, 2005; van de Flierdt et al., 2004a; Chen et al., 2013]. All lines for colored data (California Margin Fe-Mn crusts) are three point moving average trend lines.

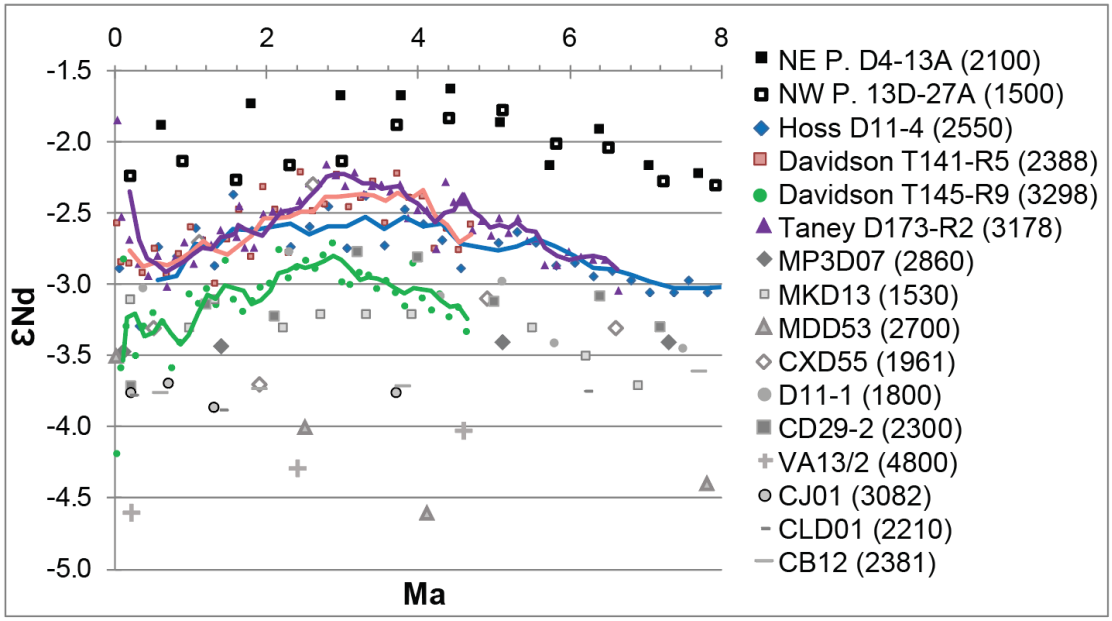

Figure 3.4. Plots of $^{206}Pb/^{204}Pb$, $^{207}Pb/^{204}$, $^{208}Pb/^{204}$, and $^{207}Pb/^{206}Pb$ for California margin samples compared to Fe-Mn crust samples from the northwest Pacific13D-27A (1,500-1,800 m) and northeast Pacific D4-13A (2,100 m) and CD29-2 (2300 m) from the central Pacific along with nine other central Pacific Fe-Mn crusts with lower resolution records for which data were combined to show central Pacific values; MDD53 (2700 m), MKD13 (1530 m), MP3D07(2860 m), CXD55(1961 m) [Chen et al., 2013], D11-1 (1800 m), VA13/2 (4800 m) [Ling et al., 1997] CJ01 (3082 m), CLD01 (2210 m), CB12 (2381 m) [Ling et al., 2005].

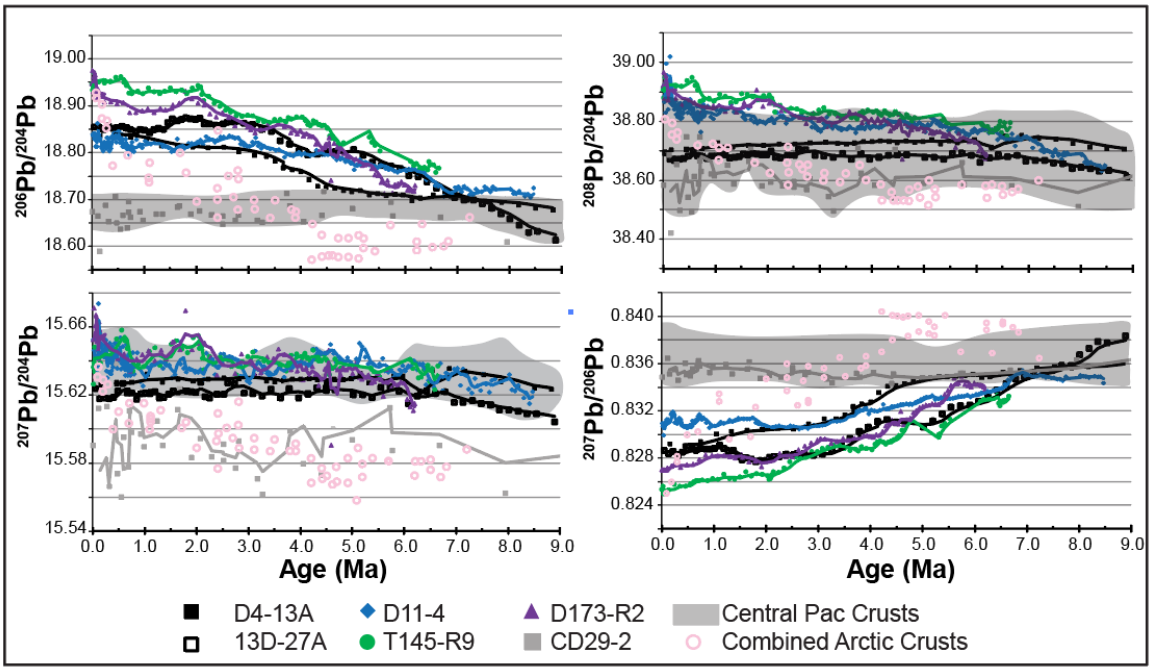

Figure 3.5. Plot of $^{206}Pb/^{204}Pb$ vs. $^{208}Pb/^{204}$ comparison of Fe-Mn crusts to potential sources to the eastern Pacific based on van de Flierdt et al. (2003), showing CCM Fe-Mn crusts, North Pacific Fe-Mn crusts, CD29-2[1,2], Nass, Fraser, and Skeena River sediments[3], Columbia River sediment over the past 8 Myr from the Astoria Fan[4], Average Pacific volcanic arc[5], Average Asian aeolian (loess)[6], Pacific sediments and turbidites[7], Meiji drift[7,1], eastern & central Aleutian Arc[7,1]. Black square in upper panel shown in lower panel.

1. [van de Flierdt et al. 2003]; 2. [Christensen 1997]; 3. Nielsen et al. 2009]; 4. [Millot et al. 2004]; 5. [Prutulak et al. 2006]; 6. [Chen et al. 2013]; 7. [GeoRock]

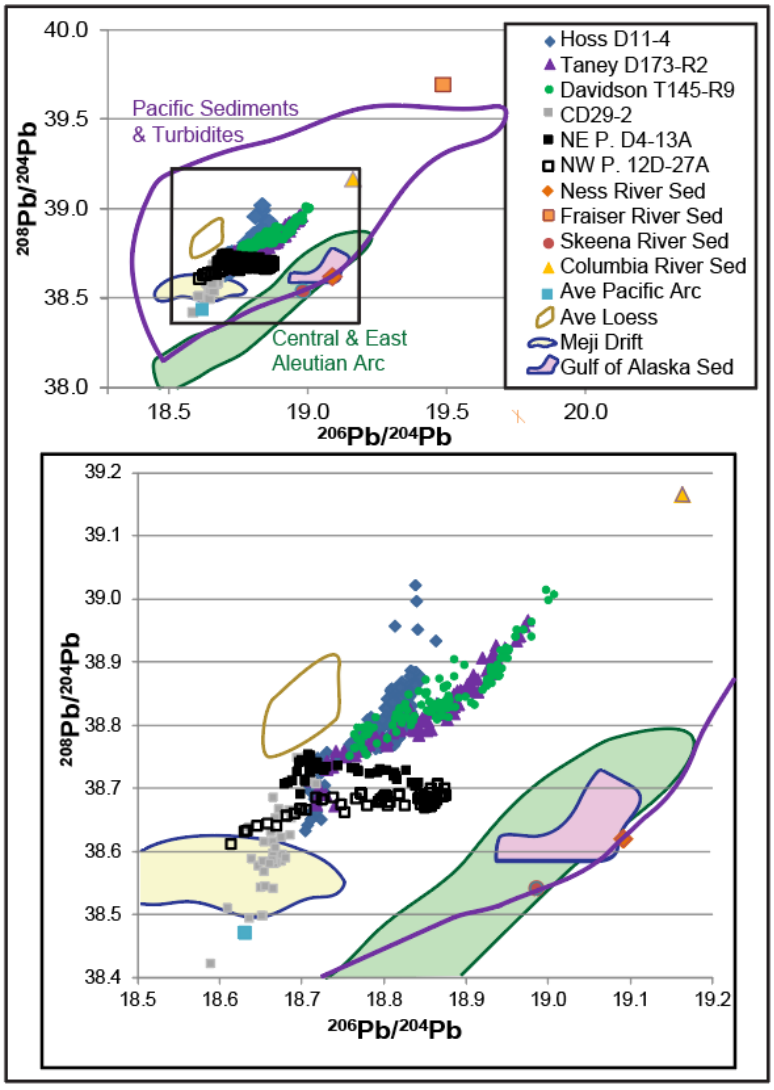

Table 3.1 Surface and upper 1 Ma average ƐNd and Pb isotope ratios

Seamount	Hoss	Taney B	Davidson	Davidson
Crust	D11-4	D173-R2	T141-R5	T145-R9
Water Depth (m)[1]	2,560-2,540	3,178	2,388	3,298
Crust Thickness (mm)	0-45	0-52	0-38	0-51
Age (Ma) ±0.5[2]	20.5	6.9	6.7	6.8
Ave ƐNd ~1 Ma	-2.95	-2.70	-2.80	-3.40
Surface ƐNd	-2.90	-1.86	-2.60	-4.21
Ave $^{206}Pb/^{204}Pb$ ~1 Ma	0.43	18.93	--	18.94
Ave $^{207}Pb/^{204}Pb$ ~1 Ma	18.82	15.65	--	15.64
Ave $^{208}Pb/^{204}Pb$ ~1 Ma	15.64	38.89	--	38.91
Ave $^{207}Pb/^{206}Pb$ ~1 Ma	38.85	0.83	--	0.83
Surface $^{206}Pb/^{204}Pb$	18.84	18.95	--	18.95
Surface $^{207}Pb/^{204}Pb$	15.65	15.65	--	15.64
Surface $^{208}Pb/^{204}Pb$	38.88	38.92	--	38.91
Surface $^{207}Pb/^{206}Pb$	0.83	0.83	--	0.83

1.[Conrad et al., 2017a] 2. [Conrad et al. 2017b]

CONCLUSIONS

The northeast Pacific continental margin is a dynamic, complex environment and studies in this region can be applied to other near-shore areas in the global ocean to answer long-standing questions regarding element sources, fluxes, and sinks. Furthermore, understanding the processes occurring in this continental-margin environment can provide a better understanding of marine geochemical cycling. The research presented in this dissertation used hydrogenetic Fe-Mn crusts to determine geochemical, geological, and oceanographic processes that characterize the northeast Pacific continental margin.

In Chapter 1, the chemistry and mineralogy of hydrogenetic Fe-Mn crusts from the United States Exclusive Economic Zone along the California continental margin (CCM) were evaluated. This chapter provides detailed chemistry and mineralogy for Fe-Mn crusts from an important region for which little existing data are available and evaluates the biogeochemical processes effecting the formation of Fe-Mn crusts in a continent-proximal environment. This chapter provides an extensive dataset of major, minor, and rare earth element chemistry and mineralogy for a large collection of Fe-Mn crust samples from sixteen different seamounts located across the central and southern CCM. Regional inputs and continental-margin influences were recorded in the Fe-Mn crusts throughout the study area, resulting in higher concentrations of Fe and Si in CCM Fe-Mn crusts compared to those from the central Pacific. The Fe enrichment is due to remobilization of metals from

continental-margin sediments and shows the importance of sediment pore fluid fluxes in near-shore environments. The Si enrichment is due to the presence of the North Pacific silica plume and is evidence of regional inputs and element enrichment along the path of circumpolar circulation. The CCM crusts formed from lower oxidation potential seawater than open-ocean crusts and consequently have a different mineralogy, showing birnessite, todorokite, and vernadite rather than solely vernadite as found for open-ocean crusts; vernadite is the most oxidized of the Mn minerals. Prior to this study, Pacific Fe-Mn crusts were thought to have an Fe/Mn ratio of less than 1 and vernadite mineralogy. My research shows for the first time that this is not true for Pacific continental-margin Fe-Mn crusts

The CCM Fe-Mn crusts have lower concentrations of elements considered of economic interest relative to open-ocean Pacific crusts, which has substantial economic implications for Fe-Mn crust resource studies in other continental-margin areas. This study provides information for future policy makers to use in resource assessments and environmental conservation efforts. It also expands our fundamental knowledge of the processes influencing the seawater chemistry of near-shore continental margin environments

For Chapters 2 and 3, the information collected in Chapter 1 was used to select a subset of Fe-Mn crusts to use for paleoceanographic study and osmium, neodymium, and lead isotopes in the crusts were measured to further our understanding of the local and regional processes and sources influencing seawater near the continental margin. Chapter 2 presents evidence of large-scale, local

terrestrial input into the seafloor environment near the base of the Monterey Canyon Submarine Fan and helps to constrain the start of canyon incision. Osmium isotopes were analyzed and compared the data to the Cenozoic Os isotope seawater curve to create an age model, successfully using a recently developed, more efficient analytical method that had not been previously applied to Fe-Mn crusts [Peucker-Ehrenbrink and Ravizza, 2012; Sen and Peucker-Ehrenbrink, 2014]. High-resolution osmium isotope records showed that age of initiation for Fe-Mn crust growth in CCM Fe-Mn crust samples ranged from 6 to 20 Myr. Osmium isotope records also showed evidence of large local inputs of radiogenic terrestrial material from around 7 to 4.5 Myr ago in Fe-Mn crusts near the Monterey Canyon Submarine Fan, a finding confirmed by analysis of neodymium and lead isotopes. These findings greatly enhance our understanding of the timing and processes influencing the formation of the Monterey Submarine Canyon. The long-term variations in local seawater osmium isotopes, where osmium deviates away from the Cenozoic osmium isotope seawater curve towards local source values, has been observed in short-term seawater measurements, but has not been previously observed in long time-scale Fe-Mn crust records [Paquay and Ravizza, 2012].

Chapter 3 evaluates high-resolution time-series neodymium and lead isotope data from CCM Fe-Mn crusts in a regional and global context and provides new insight into the sources and process affecting lead and neodymium along the northeast Pacific continental margin. This third study in the dissertation builds upon the work conducted in the second study and shows that the neodymium isotopic composition of

seawater in the near-shore northeast Pacific has been influenced by sediment pore-water fluxes over long-term (hundred thousand year) time-scales. Additionally, our data show that a trend towards unradiogenic neodymium since 3 Myr ago, also observed in northeast Pacific and central Pacific Fe-Mn crusts, is likely due to a previously unidentified source of inputs from continental North America, rather than seawater circulating from the Atlantic Ocean or Southern Ocean. High-resolution time-series analyses of lead isotope data confirm the importance of terrestrial sourced fluvial material to the region, and show that for the near-shore northeast Pacific, Asian dust is not the most important source of lead to the region at intermediate- and deep-water sites.

Together these studies provide a significant expansion of the global Fe-Mn crust database. They also provide the first time-series studies of osmium, neodymium, and lead isotopic data for this region of the northeast Pacific. The research presented in this dissertation contributes considerably to our understanding of the processes influencing geochemical cycling in the near-shore northeast Pacific and provides insights that can be applied to other continental-margin regions in the global ocean. In continental-margin environments, sediment pore-water fluxes and local to regional scale fluvial inputs of continental material can alter the concentrations and isotopic compositions of elements in seawater over long-term geologic time scales.

References (Conclusions)

Paquay, F. S., and G. Ravizza (2012), Heterogeneous seawater $^{187}Os/^{188}Os$ during the Late Pleistocene glaciations, *Earth Planet. Sci. Lett.*, *349–350*, 126–138, doi:10.1016/j.epsl.2012.06.051.

Peucker-Ehrenbrink, B., and G. Ravizza (2012), Chapter 8 - Osmium Isotope Stratigraphy, in *The Geologic Time Scale*, pp. 145–166, Elsevier, Boston.

Sen, I. S., and B. Peucker-Ehrenbrink (2014), Determination of Osmium Concentrations and ^{187}Os/^{188}Os of Crude Oils and Source Rocks by Coupling High-Pressure, High-Temperature Digestion with Sparging OsO_4 into a Multicollector Inductively Coupled Plasma Mass Spectrometer, *Anal. Chem.*, *86*(6), 2982–2988, doi:10.1021/ac403413y.

APPENDICES

Chapter 1 Formation of Fe-Mn crusts within a continental margin environment

Figure A 1.1 Post-Archean Australian shale (PAAS) normalized rare earth element plot, example from San Juan Seamount [Taylor and Mclennan, 1985], (Supplemental Fig. S1 in text). Sample T665-R17A, in red, shows offset due to diagenetic input.

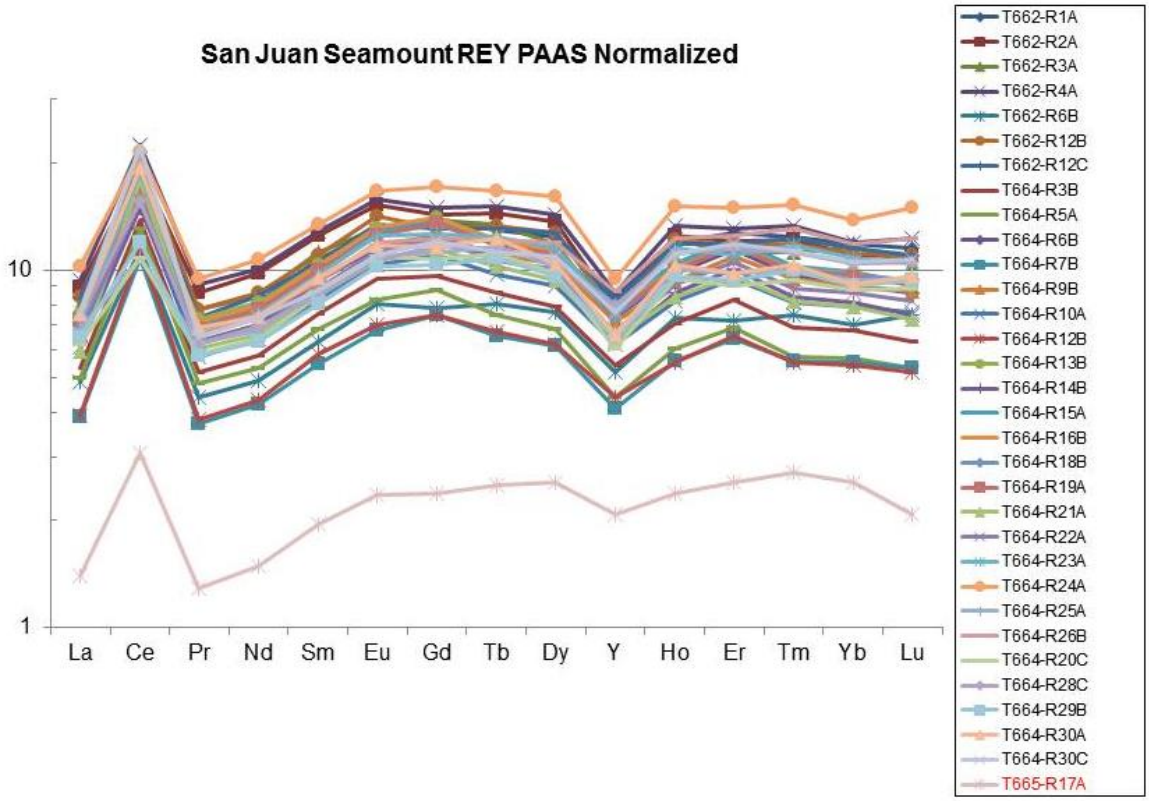

Table A1.1 Seamount information (in text Supplemental Table S1)

Seamount	Lattitude (N)	Longitude (W)	Seamount Age (Ma)	Dating Method	Summit Water Depth (m)	Base Water Depth (m)
Taney Chain[3] (A-E)	36° 45' 00"	125° 20' 00"	26 ± 0.5	$^{40}Ar/^{39}Ar$	2,157 - 3,761	4,150-4,250
Pioneer[4]	37° 21' 10"	123° 26' 10"	13.01 ± 0.16 to 10.94 ± 0.13[8]	$^{40}Ar/^{36}Ar$ & total fusion	820	2,750
Gumdrop[4,5]	37° 27' 00"	123° 28' 00"	16.43 ±0.32 to 14.97 ± 0.32[8]	$^{40}Ar/^{36}Ar$ & total fusion	1,207	1,933
Guide[4]	37° 00' 60"	123° 21' 00"	16.58 ± 0.50	$^{40}Ar/^{39}Ar$	1,682	3,122
Davidson[1,2,4]	35° 43' 00"	121° 04' 80"	14.8-9.8	$^{40}Ar/^{36}Ar$ & total fusion	1,250	3,530
Rodriguez[4,5,6,7]	34° 01' 20"	122° 43' 00"	17.87 ± 0.36 to 9.71 ± 0.34[7]	$^{40}Ar/^{36}Ar$ & total fusion	650	2,325
San Juan[5,6,7]	33° 02' 00"	121° 00' 00"	18.72 ± 0.42 to 2.69 ± 0.05	$^{40}Ar/^{36}Ar$ & total fusion	560	3,400
North East Bank[6,7]	32° 34' 00"	119° 60' 00"	8.76 ± 0.33 to 7.03 ± 0.11	$^{40}Ar/^{36}Ar$ & total fusion	516	1,150
San Marcos[6]	32° 37' 00"	121° 34' 00"	10.12 ± 0.30 to 6.71 ± 0.33	$^{40}Ar/^{39}Ar$ & total fusion	1,900	4,000
Little Joe[5,6]	31° 54' 00"	120° 02' 00"	11.06 ± 0.07	$^{40}Ar/^{39}Ar$ & total fusion	2,210	3,600
Ben[6]	31° 44' 00"	120° 44' 00"	20	Est. & nanofossil	2,600	3,800
Adam[6]	32° 04' 00"	121° 15' 00"	17-22	Est. & nanofossil	2,200	4,000

Hoss[6]	32° 00' 00"	121° 30' 00"	17-22	Est. & nanofossil	2,500	4,000

[1]Clague et al., 2000; [2]Clague et al., 2009; [3]Coumans et al., 2015; [4]Davis et al., 2002; [5]Davis et al., 2010; [6]Hein et al., 2010b; [7]Paduan et al., 2009

Chapter 2 River sediment sources to the Monterey Canyon Submarine Canyon System- constraints from Fe-Mn crust Os, Nd, and Pb isotopes

A2.1 Supplemental Methods

A2.1.1 Sample Preparation:

The Fe-Mn crusts were encased in Tap Plastic Clear Lite Casting Resin and cut into billets perpendicular to the growth surface prior to mounting on large glass slides using Crystalbond 590 adhesive. The samples were then hand sanded to create a smooth and level surface. Subsamples for Os and Nd isotopes were collected using a New Wave Micromill and Brasseler 1 mm cylindrical (flat head) diamond tipped drill bit. For Fe-Mn crust samples the optimal drill rotation was found to be 40-50% depending on crust hardness, with harder crusts requiring faster rotation. The optimal lateral drill speed depended on hardness and ranged from 15-45 µm/s, with slower speeds for harder samples. The plunge speed of the drill, into the sample, ranged from 25 to 50 µm/s. Faster drill speeds increased fracturing along the drill line and faster rotational speeds increased sample loss to air. The sample height, measured by the micromill poking the sample with the drill bit, was only measured on resin encasing the crust, as measurements attempted on samples penetrated the Fe-Mn crust and did not register a sample height. Drilled subsamples were collected with a paintbrush onto weighing paper. The crust surface, drill bit, and paint brush were cleaned between samples using hand-held compressed gas (Dust-Off) and Kimwipes.

Os samples were collected over 2 mm stratigraphic depth, 2 mm deep into the layer, and 10 mm along the layer running parallel to the top of the crust. This yielded a minimum of 15 to 40 mg of material for each subsample. Sampling error, the crust chipping and uncertainty in the sample lines is added to the error in the age model. The amount of sample used in the digestions ranged from 13.75 mg to 38.90 mg. Subsamples for Os were stored in cleaned 1 dram glass vials. Subsamples for Nd isotopes were collected using a New Wave Micromill using a 1 mm cylindrical drill bit penetrating 0.5 mm deeper into the same section of the Fe-Mn crust sampled for Os, at 0.3 mm resolution. Neodymium subsamples were stored in acid washed plastic vials. In both cases, fractures along the drill lines were estimated and included in the

depth of crust error calculations. Samples for Pb isotopes were collected via laser ablation during analysis.

A2.1.2 Osmium Isotopes:

Ferromanganese crust samples were prepared for Os analysis using an Anton Paar High Pressure Asher (HPA-S). Samples were prepared using 30-40 ml reagent grade 15.8 N nitric acid. Reagent grade acid was used since Os is a volatile element that may become more concentrated in distilled acid depending on the distillation process (Mukul Sharma personal communication 9/2013). Samples were spiked with an in-house ^{190}Os standard (BPE95) (Sen and Peucker-Ehrenbrink, 2014) with a concentration of 0.6061 ppb. Polytetrafluoroethylene (PTFE) tape was used to cover the lip of the vessel and a quartz lid was placed over the tape and wrapped with more PTFE tape to create a seal. Digestion used an Anton Paar High Pressure Asher (HPA-S) using 20 ml quartz vessels for the Hoss Seamount samples and 15 ml quartz vessels for the samples from Davidson and Taney B and D Seamounts. USGS A-1 nodule standard was prepared along with all samples, as were blanks, for each HPA run. Samples were digested at 280˚ C and 130 bars (1900 psi) for 1 hour with additional time (~1 hr each) for warm up and cool down. This resulted in digestion of the Fe-Mn material although a residue most likely consisting of aluminosilicates was observed in some of the vials. The quartz vessels were placed in an ice bath to cool and once cool the sample was transferred to 22 ml PFA Teflon beakers and capped tightly. During this process, 1 ml milliQ (MQ) water was used to rinse the vials and added to the sample. Care was taken to exclude detrital silica remnants, which were visually inspected and discarded. PFA Teflon beakers and lids were cleaned by wiping with methanol, rinsed three times with water and then soaked in an acid bath of 50% HNO_3 at 115˚ C for a minimum of ten hours and rinsed three times with MQ water prior to use. Samples were stored in the PFA Teflon beakers in a refrigerator kept at 4˚C until analysis. The storage time ranged from less than half an hour to 10 days. Samples were kept in a cooler on ice until approximately 5 minutes prior to sparging when 100 ml MQ water was added and the PFA Teflon beaker cap was replaced with a sparging cap.

Quartz vials used as digestion vessels in the HPA-S were cleaned by rinsing with deionized (DI) water, dissolving any Fe-Mn crust residue remaining on the sides of the vials with concentrated reagent grade hydrochloric acid, rinsed well with DI water and then cleaned with a cleaning solution of 10 parts MQ water, 5 parts concentrated nitric acid and 1 part concentrated hydrofluoric acid in a sonicator for 1 minute, rinsed well with DI water and run in the HPA-S with 100 ml reagent grade nitric acid. The vials were then rinsed well with MQ water prior to each use.

Samples were analyzed for Os isotopes on a ThermoElectron NEPTUNE MC-ICPMS with three continuous-dynode ion counters at the Woods Hole Oceanographic Institute in the Non-traditional Isotope Research on Various Advanced Novel Applications (NIRVANA) facility after the methods of Sen and Peucker-Ehrenbrink (2014) using the Ar gas sparging technique. A subset of ~10% of the digested Fe-Mn

crust samples and nodule standards contained no Os. It is thought that the Os escaped as a volatile OsO_4 during the digestion and decanting process. Another 21% of the subsamples had an unknown contaminant on the ^{185}Re, ^{194}Pt, and ^{196}Pt lines. The presence of another element on the ^{185}Re line resulted in $^{187}Os/^{188}Os$ ratios below the seawater curve and in the case of one sample, D173-R2 41-42, the processed data yielded a negative $^{187}Os/^{188}Os$ ratio, which is not possible. These samples were not used to fit the data to the seawater curve. However, replacing the contaminated ^{185}Re line for these samples with the blank ^{185}Re value brought those data points in line with uncontaminated data and this data is shown on the plots. This was consistent with the nodule standards and Fe-Mn crust samples. Similar contamination was seen previously using this method [Sen and Peucker-Ehrenbrink, 2014] (A2.2, A2.3). Data were processed using mass/charge ratios of ^{194}Pt and ^{196}Pt to correct for interference on ^{190}Os and ^{192}Os and the mass/charge ratio of ^{185}Re to correct for Re interference on the ^{187}Os line [Sen and Peucker-Ehrenbrink, 2014]. This yielded the $^{187}Os/^{188}Os$ ratios that were compared with the Cenozoic Os isotope seawater curve, to determine approximate ages and growth rates for each crust sample. Samples that deviated from the Os seawater curve were not used to determine age; instead, the growth rate was extrapolated as the most conservative estimate.

A subset of 11 subsamples was also spiked with an in-house Re standard prior to digestion in the HPA-S and subsequent Os analysis. The samples were then prepared after the methods of Sen and Peucker-Ehrenbring (2014) and run for Re on the Element Rx ICPMS. Re values of unspiked samples were below the detection limit and Re concentrations were extremely low. This was done to confirm that Os isotopes, in Fe-Mn crusts of this age, do not need to be corrected for Re decay and is consistent with results from other Fe-Mn crust studies [e.g., Klemm et al., 2008, 2005].

A2.1.3 Neodymium Isotopes:

For Nd isotopes, an average of 1.9 mg Fe-Mn crust subsample was rinsed into a 7 ml Teflon beaker with MQ water and the water was evaporated using a hot plate set to 120˚ C for 1.5 hours. To digest the dry sample, 3 ml 6N distilled hydrochloric acid was added and the sample fluxed on a hot plate at 120˚C for a minimum of 8 hours before being re-dried and dissolved in 400 µl 0.25N HCl. Dissolved samples were cooled to room temperature, centrifuged for 3 minutes at 15,000 rpm, and decanted to acid washed 7 ml Teflon beakers to remove undissolved detrital silicate material. Nd was extracted using a single column with a 125 µl stem volume and LN Resi (lanthanide-specific cation exchange resin) [Scher and Delaney, 2010]. Blanks and USGS Fe-Mn nodule standards A-1 and P-1 were prepared with each batch of Fe-Mn crust subsamples. Nd subsamples were run at WHOI on the MC-ICPMS using a 52 sample auto changer using the method of Scher and Delaney (2010). Standard JNdi-1 with a reference value of 0.512116 was used. The mean offset of measured JNdi-1 standard values from the reference value was calculated for each auto-changer

batch and used to correct the $^{143}Nd/^{144}Nd$ ratio. The corrected ratio was then used to calculated ƐNd using the equation; [$ƐNd = ((Cor^{143}Nd/^{144}Nd_{samp}/0.512638)-1) \times 1000$] after the method of [Scher and Delaney, 2010].

A2.1.4 Lead Isotopes:

Lead isotopes on 3 Fe-Mn crusts, from Hoss, Davidson, and Taney B Seamounts were analyzed using a NewWave/Merchantek NWR-193 homogenized ArF excimer laser ablation system coupled with the MC-ICPMS at the WHOI NIRVANA facility [Foster and Vance, 2006]. Pellet standards of USGS A-1 and P-1 nodule standards were prepared at the WHOI experimental petrology lab using a hand press and 5 mm die. Nodule standard powder was pressed at 0.3 tons for 5 minutes to create pressed powder pellets. Three Fe-Mn crust samples analyzed for Pb isotopes and 3 pressed pellets of both the A-1 and P-1 USGS nodule standards were packed into the laser ablation cell. The cell was lined with aluminum foil and filled with Crayola Air-Dry Clay into which the Fe-Mn crust billets, still encased in TAAP Plastic resin and mounted on glass slides, and the standard pellets were placed to create a level surface (Fig. A2.5). For use with laser ablation, it is critical to have as little height variation as possible between the surface of the samples and standards. Future work using this method should encase the bottom of the standard pellets in resin to keep the pellets from adsorbing water from the clay and crumbling.

The laser ablation cell was placed into the chamber, which was purged with He gas. Up to eight sample lines were run between USGS nodule A-1 and P-1 standard pairs. The laser was set to a 50 µm diameter spot size and a 0.5 mm line was used to account for the heterogeneous nature of Fe-Mn crusts. The laser parameters were slightly modified from published work to 70% power with a 5 µm/s scan speed and 20 Hz repetition rate for all samples and standards [Foster and Vance, 2006]. Resolution through the crusts varied. The highest resolution was measured in the upper 2.9 mm of D11-4 from the Hoss Seamount at 50 µm. The lowest resolution was measured in Fe-Mn crust D173-R2 with 50 µm wide lines placed .95 mm apart. The laser ablation cell was not removed from the ablation chamber during continuous run time. The aluminum foil and clay into which the samples and standards were packed was removed from the ablation cell and stored when necessary between runs. This allowed the same lines and reference points to be used for multiple runs. A python code was written and used to process the Pb data during breaks in the run time.

A2.1.5 Python Code for processing Lead Isotope Data:

A Python code was written and used to process Pb isotope data from exp files, allowing for efficient processing of the data during the analysis. The code was run on Python 3.4.3 installed using the anaconda installation package and requires the python launcher. The code has three modules. The first module is *read_exp.py* this reads in the exp files, the raw files containing the data from the LA-MC-ICPMS, and

will output a file list to be modified in excel. A sample list created by the user must be imported and all samples must be bracketed by paired standards. The user must identify each file as std, samp, or bg for standard, sample, or background, respectively. All sample files of raw data must exist in the location the user has indicated or an error message will appear. The sample list must start and end with standards. The second module identifies the raw data to keep and which can be discarded. The raw data used for correction and calculation of Pb ratios include values of non-ratio raw data for ^{204}Pb, ^{206}Pb, ^{207}Pb. ^{208}Pb, ^{203}Tl, ^{204}Tl, ^{205}Tl, and ^{202}Hg. The second module *Parse_exp.py* allows the user to manually separate the files into background and data. This is done using slide bars to set the minimum and maximum for the background and the sample as shown on data graphs. A standard deviation is provided to help select the sample and exclude the background data. This process must be done as one step, the program will not save progress if closed in the middle and must be restarted from the beginning. However, as long as the window remains open the data can be reinterpreted. This uses *Process_exp.py* and calculates the standard sample bracketing correction to process the raw Pb data using the background and sample selected by the user and yields corrected Pb ratios. Further instructions for each module are included in the text files with the code.

Utilizing a Python code to process LA-MC-ICPMS Pb isotope data greatly reduced the time required to process data and allowed for real-time data analysis. Mounting all samples and standards into a stable setting within the laser ablation cell permitted very accurate sample locations and enabled rapid continuation of work if the laser ablation cell needed to be removed or emptied between runs.

Standard values used for processing (Foster and Vance, 2006; Ling et al., 2005) are in (Methods Table A2.21). Additional values used in the processing code: NIST SRM 997 ^{205}Tl/^{203}Tl = 2.388.

Figure A 2.1. Plot of Os isotope standard LoOsStd by date analyzed

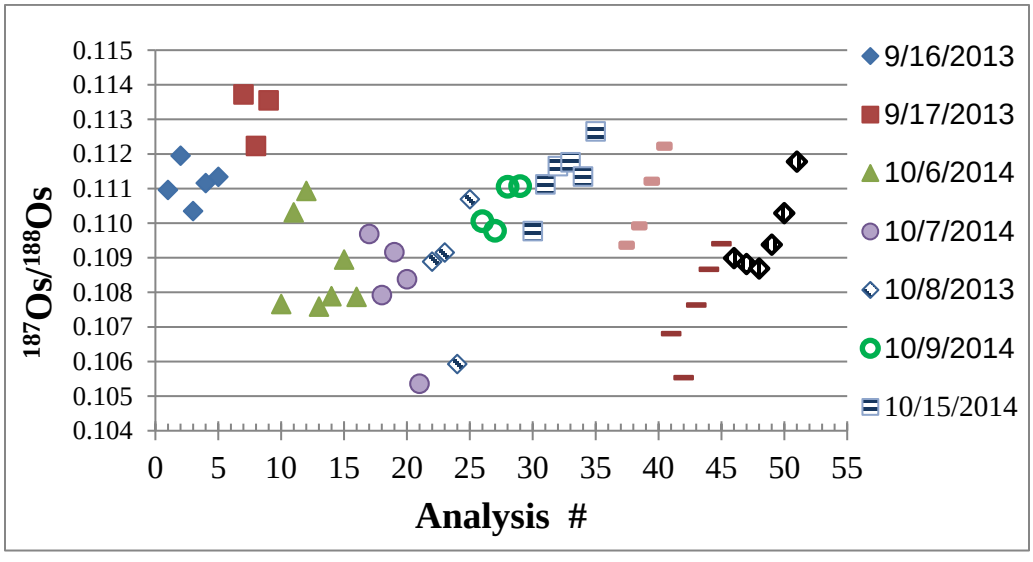

Figure A2.2. a) Duplicate Os analyses of USGS nodule standard A-. Analysis #s 15, 19, and 21 had no Os present. Analysis #'s 9,10,17, and 20 had an unknown contaminant on the ^{185}Re line. Dark points for those analyses are with the measured ^{185}Re and the light points for the same run are with a blank ^{185}Re value replacing the contaminated ^{185}Re. Error bars are instrumental error, most are too small to see. b) Larger view of the outlined region in figure a.

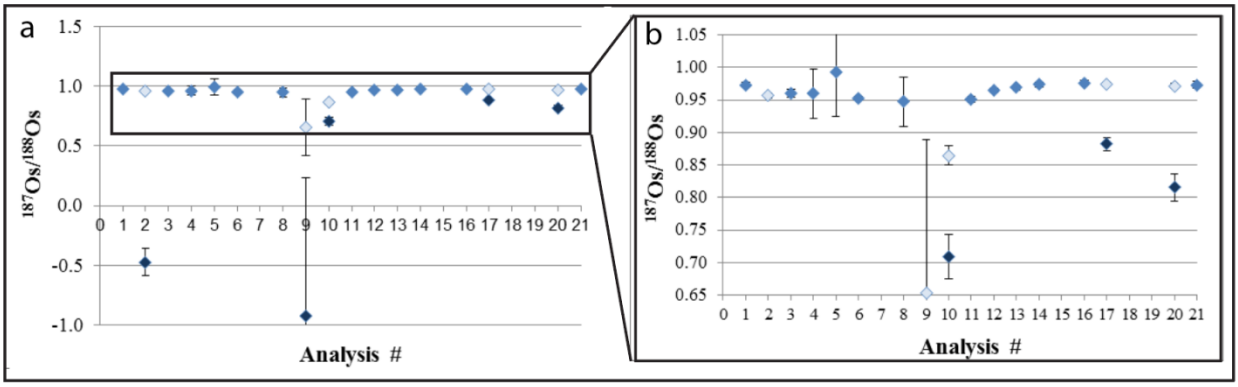

Figure A2.3. Plot of ℇNd from 4 Fe-Mn crusts compared to published data from central Pacific Fe-Mn crusts. Central Pacific D11-1 and CD29-2 from Ling et al., (1997).All lines are three point moving average trendlines.

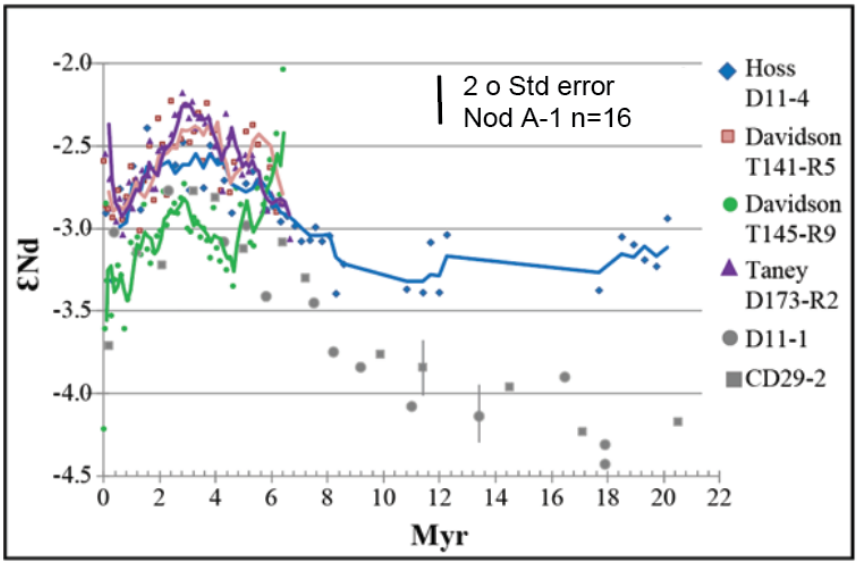

Figure A2.4 Ferromanganese crusts D11-4, T145-R9, D173-R2 and sets of 3 USGS nodule standards A-1 and P-1 pellets, packed in Crayola Air-Dry Clay in the ablation cell sample holder.

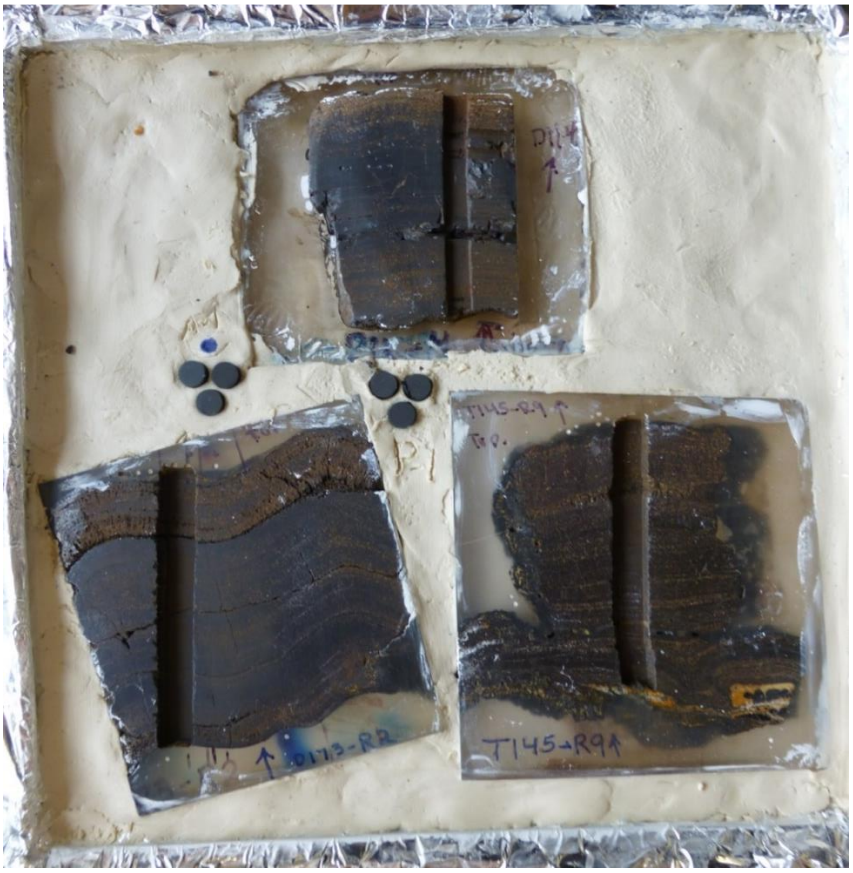

Figure A2.5 Plot of LA-MC-ICPMS data for $^{206}Pb/^{204}Pb$, $^{207}Pb/^{204}Pb$, $^{208}Pb/^{204}Pb$ compared to CD29-2 [Christensen, 1997; Nielsen et al., 2011]. Trend lines for CA Fe-Mn crusts (colored samples) are 3 point moving average trend lines.

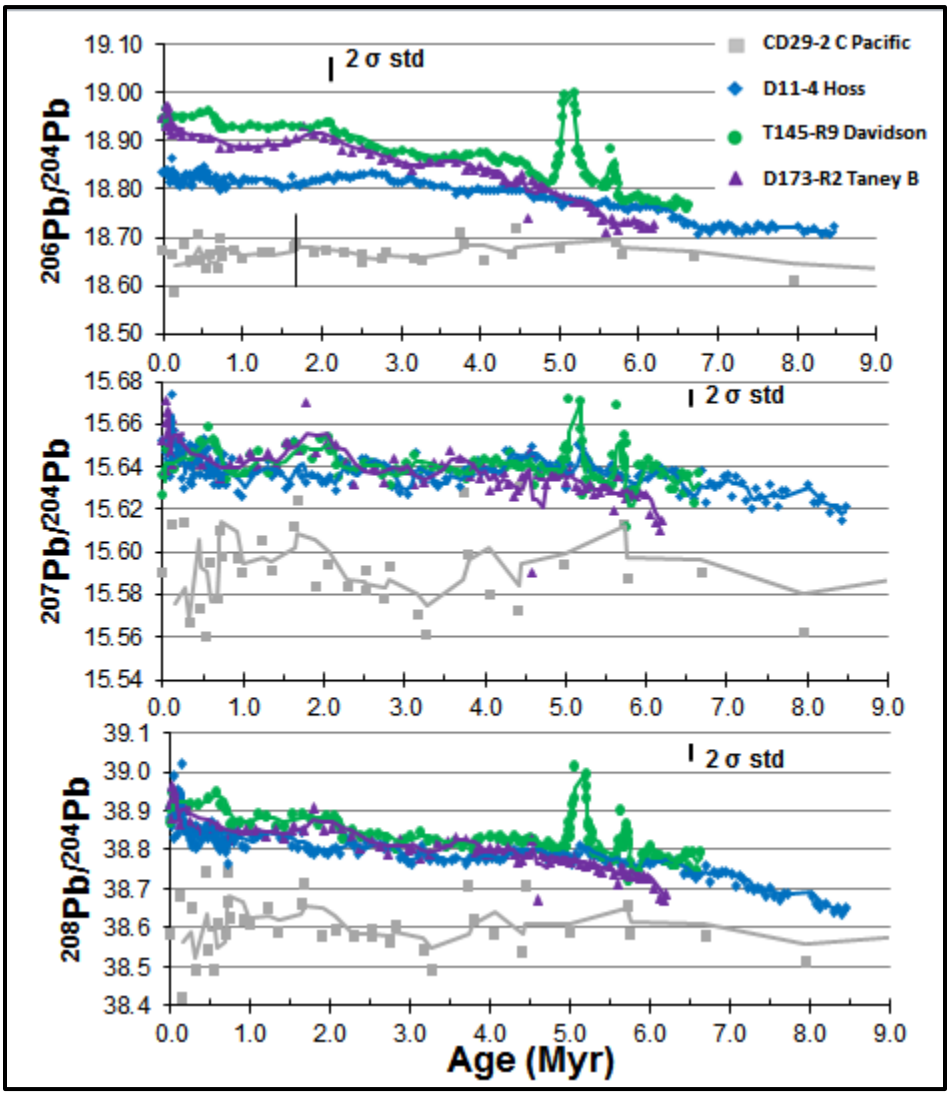

Table A2.1: USGS nodule standard values [*Foster and Vance,* 2006]

	USGS Nod-P1	**USGS Nod-A1**	**Delta A1-P1**
$^{206}Pb/^{204}Pb$	18.70	18.964	0.264
$^{207}Pb/^{204}Pb$	15.638	15.685	0.047
$^{208}Pb/^{204}Pb$	38.697	38.965	0.268
$\varepsilon^{205}Tl$	0.5	10.7	-
$^{205}Tl/^{203}Tl$	2.388	2.391	-

Table A 2.2 Water normalized chemical data for Fe-Mn crusts

Sample	D11-4	D11-11	T141 R-5A	T145 R-9A	D173-R2	T121 R-5B
Seamount	Hoss	Hoss	Davidson	Davidson	Taney B	Taney D
Cruise	F7-87-SC	F7-87-SC	M. 2000	M. 2003	M. 2010	M. 2000
Collection Method	Dredge	Dredge	ROV	ROV	ROV	ROV
Water Depth (m)	2,560-2,540	2,560-2,540	2388	3298	3178	3887
GR (mm/Myr)	3.72	2.53	9.80	17.1	6.06	22.1
Age (Ma)	9.7	15.8	3.3	2.6	8.3	2.1
Thickness (mm)	36	40	32	45	50	46
Fe (wt%)	21.5	20.3	29.0	25.2	21.0	25.5
Mn	18.1	18.7	22.7	16.4	15.5	20.2
Fe/Mn	1.19	1.09	1.28	1.53	1.35	1.26
Si	8.19	6.86	9.01	13.9	8.88	10.9
Al	1.29	1.29	1.66	2.42	1.15	1.97
Ca	2.04	2.14	2.45	1.83	1.73	2.01
Mg	0.95	0.95	1.19	0.97	0.86	1.18
Na	1.7	1.74	1.77	2.01	1.42	1.86
K	0.6	0.61	1.04	1.13	0.59	1.05
P	0.39	0.41	0.56	0.38	0.35	0.40
Ti	0.61	0.66	0.64	0.59	0.39	0.54
LOI	--	--	15.8	15.5	36.1	16.7
H2O-	23.1	24.2	21.1	17.5	17.9	17.9
Ag (ppm)	--	--	--	--	0.07	--
As	312	317	322	195	205	226
Ba	2211	1715	2041	1830	1981	1754
Be	--	--	2.79	3.15	5.66	2.46
Bi	--	--	21.5	17.0	10.8	11.3
Cd	1.80	1.70	3.30	2.42	2.67	4.17
Co	2861	3562	2091	1208	1981	1153
Cr	10.0	9.00	57.0	52.1	28.3	14.4
Cs	--	--	7.60	--	--	--
Cu	533	369	304	464	532	630
Ga	--	--	29.2	29.1	5.07	37.2
Hg (ppb)	--	--	7.60	6.06	--	15.4
Hf (ppm)	--	--	19.0	18.2	4.20	7.54

In	--	--	--	--	0.12	--
Li	--	--	6.34	4.85	8.25	14.0
Mo	585	554	534	322	479	437
Nb	--	--	40.6	40.0	26.9	27.6
Ni	2471	2507	2357	1236	1415	2410
Pb	1430	1451	1470	1045	1285	886
Rb	--	--	46.9	23.0	8.02	33.7
Sb	--	--	58.7	38.2	48.2	36.9
Sc	--	--	6.46	8.24	10.6	9.73
Se	--	--	--	--	0.94	6.79
Sn	--	--	--	--	2.36	--
Sr	1560	1451	1195	939	1344	997
Ta	--	--	--	2.42	0.41	0.98
Te	--	--	7.22	7.27	6.49	6.05
Th	--	--	38.3	41.0	23.7	40.0
Tl	--	--	61.3	15.6	13.2	25.6
U	--	--	11.5	7.88	10.9	8.37
V	741	686	678	533	636	582
W	--	--	87.5	44.8	95.2	44.6
Zn	702	594	598	555	627	676
Zr	--	--	798	897	37.1	792
La (ppm)	--	--	317	304	309	305
Ce	1143	1240	1508	1069	943	1087
Pr	79.2	--	64.9	73.3	72.1	79.9
Nd	321	369	286	320	291	336
Sm	68.5	--	59.8	67.0	66.4	76.1
Eu	16.1	20.0	16.5	17.8	15.9	19.8
Gd	68.7	--	60.7	64.7	65.9	68.4
Tb	11.1	--	11.0	11.4	10.4	12.38
Dy	66.7	--	64.9	63.6	62.4	72.1
Y	208	224	190	184	223	178
Ho	13.0	13.3	15.5	15.0	12.5	14.4
Er	35.0	36.3	36.2	34.4	33.0	32.4
Tm	5.33	5.30	4.94	4.61	4.88	4.45
Yb	32.9	34.2	30.9	27.5	31.0	26.2
Lu	4.56	4.71	5.04	5.07	4.52	4.09
Au (ppb)	--	--	--	--	--	1.40
Ru	--	--	10.1	--	--	5.91
Rh	7.00	7.30	6.34	--	--	3.94
Pd	2.90	3.30	--	--	--	2.95

Os	--	--	--	--	--	1.97
Pt	43.0	46.0	87.5	--	--	43.3

M. = Monterey Bay Aquarium Research Institute (MBARI)
-- no data

SUPPLEMENTAL FILES

Supplemental Files contain data tables that are too large to reasonably display in this thesis. The files are described here, and are available in digital format.

Chapter 1. Formation of Fe-Mn crusts within a continental margin environment

Table S1.1 Water-normalized California-continental margin bulk and mean bulk chemistry data

Table S1.2 Water-normalized layer chemistry for California-continental margin Fe-Mn crusts

Table S1.3 Surface-scrape water-normalized chemistry data for California-continental margin Fe-Mn crusts

Table S1.4 Water-normalized bulk chemistry statistics by seamount

Table S1.5 X-ray diffraction mineralogy major, minor, & accessory minerals for California-continental margin Fe-Mn Crusts. All samples have major δ MnO2 and FeOOH

Chapter 2. River sediment sources to the Monterey Canyon Submarine Canyon System- constraints from Fe-Mn crust Os, Nd, and Pb isotopes

S2.1 Anaconda Python code to create a sample list from file. Must be named read_exp to use.

S2.2 Anaconda Python code using Python launcher to provide a graphical interface for the user to designate sample and background on continuous laser ablation data. Must be named parse_exp to use.

S2.3 Anaconda Python code to process the Pb sample data using a background reduction and standard sample standard bracketing for data correction. Must be named process_exp to use.

Table S2.1 Data for $^{187}Os/^{188}Os$ for CCM Fe-Mn crusts, USGS standard Nod A-1, and standard LoOsStd

Table S2.2 Data for $^{143}Nd/^{144}Nd$ and ƐNd for Hoss D11-4, Taney D173-R2, Davidson T141-R5, T145-R9, USGS nodule standards A-1 and P-1, and Standard JNdi-1

Table S2.3 Data for $^{206}Pb/^{204}Pb$, $^{207}Pb/^{204}Pb$, $^{208}Pb/^{204}Pb$ and $^{207}Pb/^{206}Pb$ Hoss D11-4, Taney D173-R2, Davidson T145-R9 and USGS nodule standards A-1 and P-1.